

# PROCEEDINGS

---

of the

## 1<sup>st</sup> ONE-DAY WORKSHOP

on New Aspects and Perspectives in Nuclear Physics

DEPARTMENT OF PHYSICS  
THE UNIVERSITY OF IOANNINA

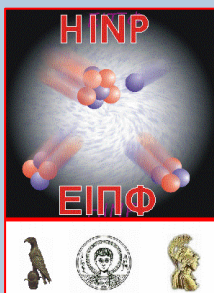
SEPTEMBER 8, 2012



University  
of Ioannina

### EDITORS

A. Pakou  
C. Papachristodoulou



---

HELLENIC INSTITUTE OF NUCLEAR PHYSICS

HELLENIC INSTITUTE OF NUCLEAR PHYSICS

## PROCEEDINGS

of the

### 1<sup>st</sup> ONE-DAY WORKSHOP

on New Aspects and Perspectives in Nuclear Physics



DEPARTMENT OF PHYSICS  
THE UNIVERSITY OF IOANNINA

SEPTEMBER 8, 2012

# HELLENIC INSTITUTE OF NUCLEAR PHYSICS

## **GOVERNING BOARD**

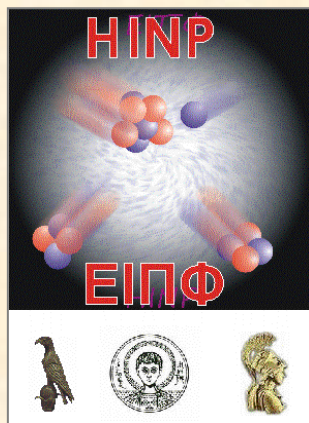
- A. Pakou (President)
- S. Massen (Vice President)
- G. Lalazissis (Secretary)
- E. Stiliaris (Treasurer)
- T. Kosmas (Member)

## **ORGANIZING COMMITTEE**

- A. Pakou (Chair)
- D. Bonatsos
- G. Lalazissis
- E. Stiliaris

## **EDITORS**

- A. Pakou
- C. Papachristodoulou



**HELLENIC  
INSTITUTE OF  
NUCLEAR  
PHYSICS**

# 1<sup>st</sup> one day Workshop

on

## New Aspects and Perspectives in Nuclear Physics

8<sup>th</sup> of September, 2012

Ioannina, Greece

**Session I:** Theory: Nuclear Structure and Nuclear Astrophysics

**Session II:** Experiment: Nuclear Reactions, Hadrons

**Session III:** Applications: Environment – Material Science – Medical – Dating

**Session IV:** Round Table Discussion: The Present and Future of Nuclear Physics in Greece



University  
of Ioannina

**Department of Physics  
Building Φ2, 3<sup>rd</sup> floor  
Conference room**

### Organizing committee

**A. Pakou  
D. Bonatsos  
G. Lalazissis  
E. Stiliaris**

<http://www.uoi.gr/HINP/News.htm>

e-mail: [apakou@cc.uoi.gr](mailto:apakou@cc.uoi.gr)

## **FOREWORD**

The 1<sup>st</sup> annual Workshop on new Aspects and Perspectives in Nuclear Physics, sponsored by the Hellenic Institute of Nuclear Physics (HINP), was held at the University of Ioannina – Department of Physics, on the 8<sup>th</sup> of September, 2012. The aim of the Workshop was to keep track of new aspects and perspectives in Nuclear Physics, as demonstrated by research carried out at the national and international level, to promote synergy between the various groups and to conclude the current status, challenges and future opportunities in Nuclear Physics research in a round table discussion.

There has been a very enthusiastic response to the Workshop in terms of the number of participants who all gave oral presentations, covering a wide range of novel aspects in the field of Nuclear Physics. Out of the 22 members of the Institute, 14 members were present together with 9 graduate students. Their paper contributions are included in this volume of Proceedings. Invited talks were not in the scope of the Workshop, as it was mainly organized to strengthen interaction between the members of the newly established virtual Institute.

We would like to thank the Department of Physics for hosting the Workshop, as well as the Rector's Office for providing free accommodation of participating students at the University of Ioannina "International Center of Hellenic Education, Culture & Vocational Training - Stavros Niarchos". We also thank the Dean of the School of Natural Sciences and the President of the Department of Physics for their kind presentations in the opening session. Finally, the support to technical aspects provided by the graduate students of the University of Ioannina is warmly acknowledged.

Athena Pakou  
on behalf of the Organizing Committee

Ioannina, October 2012

## Contents

<i>Covariant nuclear density functional theory</i> G. A. Lalazissis	1
<i>Proton-neutron interactions in heavy nuclei</i> D. Bonatsos	4
<i>Nuclear equation of state effects on the r-mode instability of neutron stars</i> Ch. C. Moustakidis, M. Papazoglou	7
<i>Semi-leptonic weak interactions in nuclei and their role to Astrophysics</i> T. S. Kosmas	10
<i>Parafermionic behavior of Bose-Einstein condensates</i> A. Martinou, D. Bonatsos	13
<i>Flavour Changing Neutral-Current Processes in Nuclei</i> D. K. Papoulias, T.S. Kosmas	16
<i>Realistic nuclear structure calculations for orbital e-capture by nuclei</i> P. G. Giannaka, T.S. Kosmas	19
<i>Model Independent Analysis of the <math>\gamma^*p \rightarrow \Delta</math> Transition with Polarized Electron Scattering Data</i> E. Stiliaris, C.N. Papanicolas	22
<i>Production of neutron-rich nuclei toward the r-process path in peripheral heavy-ion collisions at low energies</i> G. A. Souliotis	25
<i>Transfer Reactions at REX-ISOLDE: The <math>^{66}\text{Ni}(d,p)^{67}\text{Ni}</math> experiment</i> N. Patronis <i>et al.</i>	28
<i>Large Volume Spherical Proportional Counter: Development and Applications</i> I. Savvidis <i>et al.</i>	31
<i>CASTOR: A Calorimeter for Heavy Ions at LHC</i> X. Aslanoglou <i>et al.</i>	34
<i>Optical Potential and Relevant Reaction Mechanisms at near barrier energies</i> A. Pakou	37
<i>Fusion cross sections of <math>^8\text{B}+^{28}\text{Si}</math> at near barrier energies</i> A. Pakou <i>et al.</i>	40
<i>Elastic Backscattering measurements and optical potential analysis for the systems <math>^{6,7}\text{Li} + ^{208}\text{Pb}</math>, <math>^{116,120}\text{Sn}</math>, <math>^{58}\text{Ni}</math> at sub- and near-barrier energies</i> K. Zerva <i>et al.</i>	43
<i>Study of the reaction <math>^{20}\text{Ne}+^{28}\text{Si}</math>: Elastic scattering at near barrier energies</i> V. Soukeras <i>et al.</i>	46
<i>Study of the system <math>^{20}\text{Ne}+^{28}\text{Si}</math>: Transfer reactions at near barrier energies</i> O. Sgouros <i>et al.</i>	49

<i>Research in the years of the economic crisis: A short review of the recent research activity of the Radiochemical Laboratory of the Aristotle University of Thessaloniki</i> P. Misaelides, F. Noli	52
<i>Radionuclides in the environment and their applications</i> A. Ioannidou <i>et al.</i>	53
<i>Applications of Ion Beam and Radiochemical techniques in Materials Science and Environment</i> F. Noli	56
<i>An Introduction to selected Applied Nuclear Physics activities at Ioannina</i> K. Ioannides <i>et al.</i>	57
<i>Dating with TL-OSL for Geology and Archaeology</i> K. Stamoulis <i>et al.</i>	60
<i>The Compton Camera in the <math>\gamma</math>-Ray Imaging</i> M. Mikeli <i>et al.</i>	63
<i>Optical and Infrared Tomography in Medical Physics</i> A.-N. Rapsomanikis <i>et al.</i>	66
<i>Construction of a High-Resolution Mobile <math>\gamma</math>-Camera System for Mammography Study</i> M. Zioga <i>et al.</i>	69
<i>Round-table discussion: The Present and Future of Nuclear Physics in Greece</i> Coordinators: D. Bonatsos, P. Misaelides, A. Pakou	72

# Covariant Nuclear Density Functional Theory

Georgios A. Lalazissis

*Department of Theoretical Physics Aristotle University of Thessaloniki  
54124 Thessaloniki, Greece*

Density functional theory (DFT) plays an important role for the microscopic description of quantum mechanical many-body problem. In particular nuclear DFT is a universal and powerful tool for describing properties of finite nuclei all over the periodic table. Most practical applications of nuclear DFT use the effective single-particle Kohn-Sham (KS) equations [1]. The covariant form of nuclear density functional theory is based on the Relativistic mean field theory (RMF) with density dependent effective forces [2, 4]. It is based on Lorentz invariance, connecting in a consistent way the spin and spatial degrees of freedom of the nucleus, in other words the nuclear spin-orbit potential emerges automatically with the empirical strength in a covariant formulation. Additional advantages in using covariant DFT is the consistent treatment of large isoscalar, Lorentz scalar and vector self-energies, which provides a unique parametrization of time odd components of the nuclear mean -field, i.e nucleon currents, which is absent in the non-relativistic representation of nuclear DFT. Moreover, the empirical pseudospin symmetry in nuclear spectroscopy finds a natural explanation

The Lorentz invariance apart from the description of the spin-orbit coupling, puts stringent restrictions on the number of parameters in the corresponding functionals without, however, reducing the quality of the agreement with experiment. Therefore, a relatively small number of parameters is necessary, which are adjusted to reproduce a set of bulk properties of spherical nuclei. The resulting energy density functionals (EDF) are considered universal in the sense that they can be used for nuclei all over the chart of nuclides, where mean field is applicable, for ground state properties as well as for excited states.

The most successful EDF originate from the Relativistic Hartree Bogoliubov (RHB) model in which p-h and p-p channels are treated simultaneously in a self consistent manner [5]. A large variety of nuclear phenomena have been described over the years within this model, the equation of state of symmetric nuclear matter, ground state properties of finite spherical and deformed nuclei at and far away from the valley of stability. The model is able to describe very successfully exotic phenomena such as halo nuclei, weakening of shell effects away from stability line, superheavy nuclei.

In time dependent systems, the Runge – Gross (RG) theorem [6] provides the formal foundation of time-dependent density functional theory. It shows that the density can be used as the fundamental variable in describing quantum [many-body systems](#) in place of the wavefunction, and that all properties of the system are [functionals](#) of the density. Starting from RG theorem one is able to derive the time dependent KS equations and then using the adiabatic approximation can describe excited states such as rotational bands in normal deformed and superdeformed nuclei [7] and collective vibrations. Rotations are treated in the cranking approximation, which provides quasi-static description of the nuclear dynamics in a rotating frame. For the description of vibrations, a time-dependent mean field approximation is used by assuming independent particle motion in time dependent average fields. In the small amplitude

limit, one obtains the relativistic Random Phase Approximation (RRPA) and for open shell nuclei the corresponding relativistic quasiparticle random phase approximation (QRPA) [8].

This method provides a natural framework to investigate collective and non-collective excitations of p-h character. It is successful, in particular, for understanding the position of giant resonances and spin-or/and isospin excitations such as the Gamow-Teller Resonance (GTR) or the isobaric Analog Resonances (IAR) [9]. The corresponding eigenmodes can be determined either by diagonalizing the RRPA / RQRPA equations in an appropriate basis [8] or by solving the linear response equations in time-dependent external field [10]. The two methods lead, in principle, to exactly identical results. It should be noted however, that the second method provides a more consistent treatment of the coupling to the continuum.

Recently, RRPA/ RQRPA has also been used for a theoretical interpretation of the low-lying E1-strength observed in neutron rich isotopes, the so called ``pygmy modes`` [11-12] and for low-lying collective quadrupole excitations [13].

It should be noted, however, that nuclear DFT based on the mean field framework cannot provide an exact treatment of the full nuclear dynamics. It is known to break down in transitional nuclei, where one has to include correlations going beyond the mean field approximation by treating quantum fluctuations through a superposition of several mean field solutions as for instance in the generator coordinate method (GCM) [14]. It is also known that even in ideal shell model nuclei such as in  $^{208}\text{Pb}$ , with closed proton and neutron shells, one finds in self consistent mean field calculations usually a single particle spectrum with a considerable enhanced Hartree-Fock gap in the spectrum and a reduced level density at the Fermi surface as compared with experiment. The situation is considerably improved by taking into account the energy dependent part of the self energy and treating it in terms of the particle-vibration coupling model.

Indeed, using the quasi-particle concept of the Landau theory [15] and Green functions techniques one can derive a one-body equation for the single particle Green function, which is in principle exactly the Dyson equation. It contains the non-local and energy dependent part of the self energy (known also as mass operator). The most important origin of energy dependence is given by the coupling of the single particle motion to the low-lying collective vibrations, these are taken into account by extending the self-consistent RQRPA by the particle vibration coupling (PVC) model using the quasiparticle blocking approximation [16-17]. The inclusion of low-lying collective vibrations improves considerably the agreement of the calculated single particle level scheme with experiment. Moreover, we get accurate information not only for the position of the giant resonances but also for their widths. The additional correlations cause fragmentation of the resonances which is fully in agreement with the experimental observations [18].

The GCM model, mentioned above, is a very nice tool for extending the relativistic energy density functionals ``beyond mean field``. In this way, spectra, transitions probabilities e.t.c can also be calculated. This, however, makes necessary the inclusion of collective correlations. These correlations arise from symmetry restoration and fluctuations around the mean field minimum. They are taken into consideration by mixing angular momentum and particle number projected states corresponding to different quadrupole moments within the GCM model.

Such a procedure has been frequently used in axially deformed configuration [19], it becomes, however, very complicated for heavy nuclei, calculated in three dimensions. An alternative approach is a collective Bohr Hamiltonian formulated with deformation dependent parameters determined by microscopic self-consistent relativistic Hartree Bogoliubov calculations. The method has been very successfully applied to the study of nuclear quantum phase transitions [20] and superheavy nuclei [21].

In conclusion, nuclear DFT provides a very successful and microscopic description for ground

states and excited states in nuclei. Most of the successful functionals are at present phenomenological. On the mean field level there is no energy dependence of the self-energy, no fluctuations and symmetry violations.

The energy dependence of the self energy can be treated by means of the particle vibration model, while the symmetries and fluctuations can be considered by projections and the GCM method. The concept of a Bohr-Hamiltonian simplifies considerably the calculations. Many things should be further done. On the static part: We are still far from a microscopic derivation of the model. We have to improve the functionals both in p-h and p-p channels. On the dynamical part : PVC model is so far restricted to spherical systems. GCM is restricted to very few degrees of freedom.

- [1] W. Kohn, L.J Sham, **Phys . Rev.** **140**, A1133 (1963)
- [2] B. D. Serot and J. D. Walecka, **Adv. Nucl. Phys.** **16** , 1 (1986) .
- [3] J. Boguta and A. R. Bodmer, **Nucl. Phys.** **A292**, 43 (1997) .
- [4] G. A. Lalazissis, P. Ring, and D. Vretenar (Eds.), *Extended Density Functionals in Nuclear Structure Physics , Lecture Notes in Physics 641*, (Springer, Berlin Heidelberg 2004).
- [5] D. Vretenar, A.V. Afanasjev, G.A. Lalazissis, P. Ring, **Phys. Rep.** **409**, 101 (2005).
- [6] E. Runge and E.KU. Gross, **Phys. Rev. Lett.** **52**, 997 (1984).
- [7] A. V. Afanasjev, G. A. Lalzissis and P. Ring, **Nucl. Phys. A** **634**, 395 (1998).
- [8] N. Paar, P. Ring, T. Niksic, D. Vretenar, **Phys. Rev. C** **67**, 034312 (2003).
- [9] N. Paar, T. Niksic, D. Vretenar, P. Ring **Phys. Rev. C** **69**, 054303 (2004).
- [10] I. Dautidis and P. Ring, **Phys. Rev. C** **83**, 044303 (2011) .
- [11] D. Vretenar, N. Paar, P. Ring G.A. Lalazissis, **Phys. Rev C** **63**, 047301 (2001).
- [12] D. Vretenar, N. Paar, P. Ring G.A. Lalazissis, **Nucl. Phys. A** **692**, 496 (2001).
- [13] A. Ansari and P. Ring, **Phys. Rev. C** **74**, 05313 (2006).
- [14] T. Niksic, D. Vretenar, P. Ring, **Prog. Part. Nucl. Phys.** **66**, 519 (2011) .
- [15] A.B. Migdal, *Theory of Finite Fermi Ssytems: Applications to Atomic Nuclei*, Wilson Interscience, New York 1967.
- [16] E. Litvinova, P. Ring and V. Tselyaev, **Phys. Rev. C** **73**, 044328 (2006).
- [17] E. Litvinova, P. Ring and V. Tselyaev, **Phys. Rev. C** **75**, 064308 (2007).
- [18] E. Litvinova, P. Ring and V. Tselyaev, **Phys. Rev. C** **78**, 014312 (2008).
- [19] T. Niksic, D. Vretenar, G.A. Lalazissis, P. Ring, **Phys. Rev. Lett.** **99**, 092502 (2007).
- [20] Z. P Li, T, Niksic, D. Vretenar, J. Meng, G.A Lalazissis, P. Ring, **Phys. Rev. C** **79**, 054301 (2009).
- [21] V. Prassa, T. Niksic, G. A. Lalazissis, D. Vretenar, **Phsy. Rev. C** **86**, 024318 (2012).

## Proton-neutron interactions in heavy nuclei

D. Bonatsos

*Institute of Nuclear and Particle Physics, National Centre for Scientific Research "Demokritos",  
GR-15310 Aghia Paraskevi, Attiki, Greece  
[bonat@inp.demokritos.gr](mailto:bonat@inp.demokritos.gr)*

### Abstract

*$\delta V_{pn}$  is a particular double difference of nuclear binding energies serving as a filter isolating the valence proton-neutron interaction.  $\delta V_{pn}$  is known to exhibit spikes in light nuclei at  $N=Z$ , explained by the  $SU(4)$  Wigner supermultiplet. Recently, it has been found that  $\delta V_{pn}$  values in the rare earth region show similar peaks, occurring at  $N_{val} \sim Z_{val}$ . These peaks, evident for both even and odd  $Z$  values, are interpreted in terms of large spatial overlaps of respective proton and neutron wave functions whose Nilsson quantum numbers are related by  $\Delta K[\Delta N, \Delta n_z, \Delta \Lambda] = 0[110]$ , i.e., the wave functions differ only by a single oscillator quantum in the  $z$ -direction. The implications of this for the development of collectivity and deformation in heavy nuclei, and the locus of this development, are discussed.*

The double difference of binding energies

$$\delta V_{pn}(Z,N)=[B(Z,N)+B(Z-2,N-2)-B(Z,N-2)-B(Z-2,N)]/4 \quad (1)$$

is known [1] to be a measure of the average interaction between the last two protons with the last two neutrons in a given nucleus having  $Z$  protons and  $N$  neutrons.

$\delta V_{pn}$  is known [1] to exhibit spikes in light nuclei with  $N=Z$ , shown in Fig. 1. These spikes are justified [2] by the existence of the  $SU(4)$  Wigner supermultiplet in this region.

Recently, it has been shown [1] that  $\delta V_{pn}$  also exhibits similar spikes in rare earth nuclei with equal numbers of valence neutrons and valence protons,  $N_{val}=Z_{val}$ , shown in Fig. 2. Since the  $SU(4)$  Wigner supermultiplet is not present in this region, destroyed by the strong spin-orbit interaction, an alternative justification has to be found.

A detailed study of the orbitals occupied by the last two neutrons and the last two protons in the rare earths exhibiting the spikes, reveals [1] that they are Nilsson orbitals differing by  $\Delta K[\Delta N, \Delta n_z, \Delta \Lambda] = 0[110]$ , as shown in the upper part of Fig. 3. These orbitals show similar evolution as functions of the nuclear deformation, as shown in the lower part of Fig. 3. They are expected to have maximal spatial overlaps, thus leading to enhanced proton-neutron interactions, in a situation reminiscent of the Federman-Pittel mechanism [3].

A more careful look at these orbitals reveals that they correspond to proton-neutron pairs with  $S=1, T=0$ . When plotted in the nuclear chart vs.  $Z$  and  $N$ , the spike-exhibiting nuclei appear on a straight line bordering the plateau of high deformation.

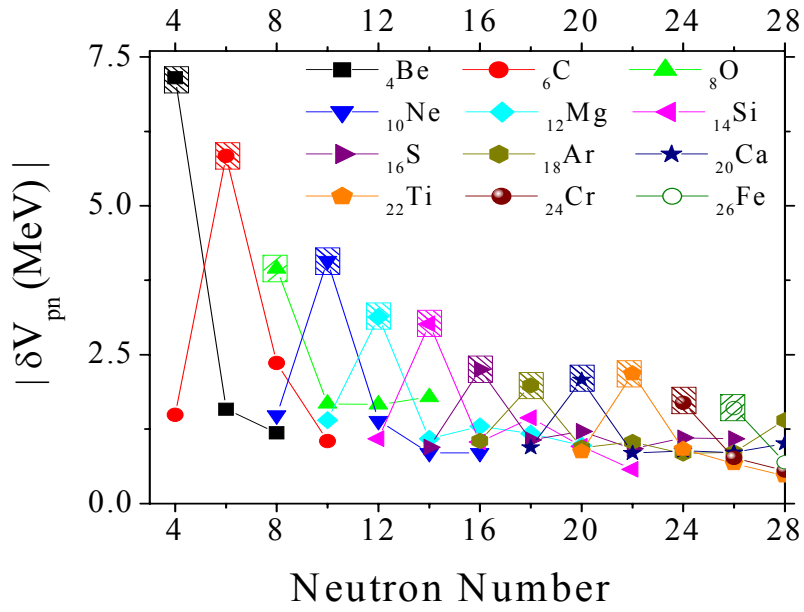


Figure 1:  $\delta V_{pn}$  for light nuclei, exhibiting spikes at  $N=Z$  [1].

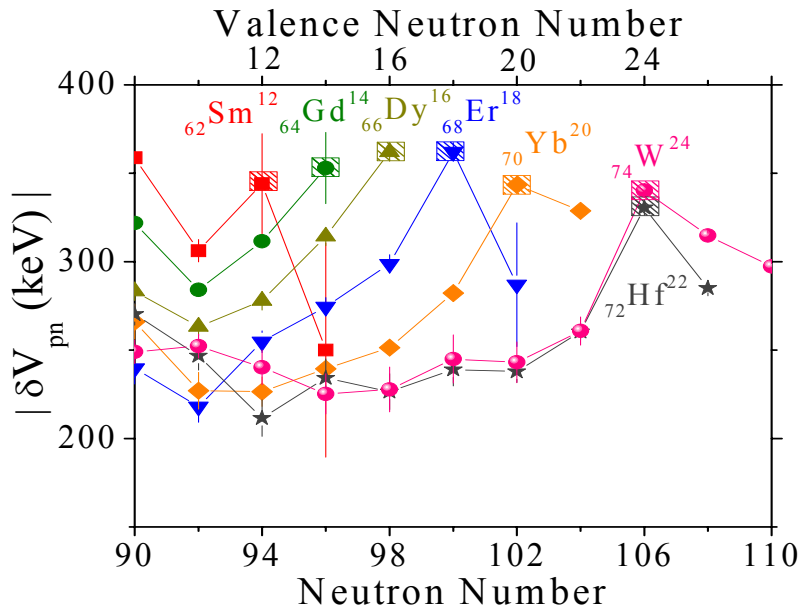


Figure 2:  $\delta V_{pn}$  for rare earth nuclei, exhibiting spikes at  $N_{val}=Z_{val}$  [1].

168 Er: p 7/2 [523]; n 7/2 [633]

172 Yb: p 1/2 [411]; n 1/2 [521]

178 Hf: p 7/2 [404]; n 7/2 [514]

180 W: p 7/2 [404]; n 7/2 [514]

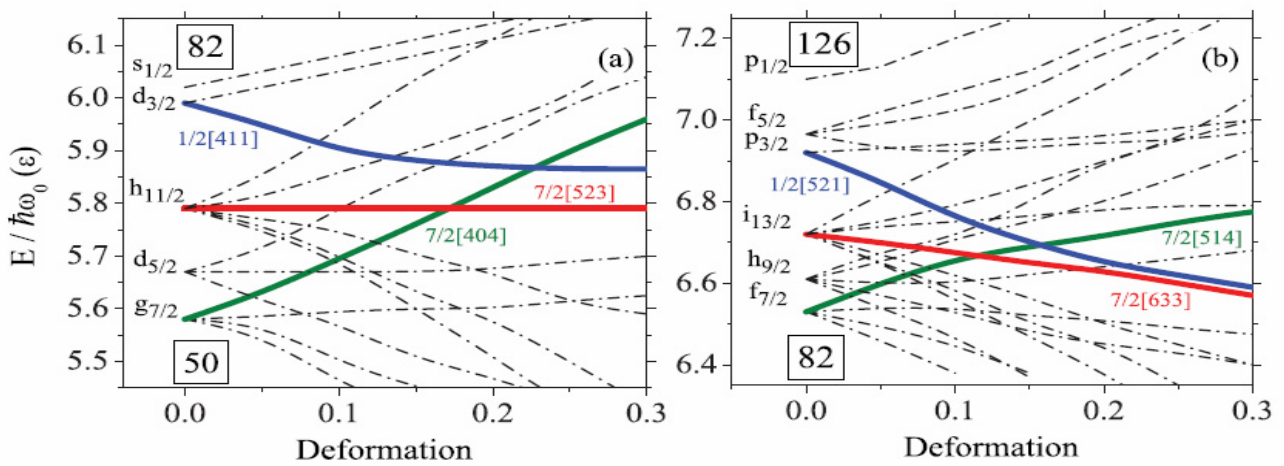


Figure 3: Nilsson orbitals occupied by the last two protons and the last two neutrons in rare earths exhibiting  $\delta V_{pn}$  spikes (upper part) [1] and their dependence on nuclear deformation (lower part).

Up to now, symmetry based calculations for heavy deformed nuclei have been based on the pseudo-SU(3) coupling scheme [4]. The present findings are suggestive of a new coupling scheme for deformed nuclei, on which work is in progress [5].

1. R. B. Cakirli, K. Blaum, and R. F. Casten, **Phys. Rev. C** **82**, 061304 (R) (2010).
2. P. Van Isacker, D. D. Warner, and D. S. Brenner, **Phys. Rev. Lett.** **74**, 4607 (1995).
3. P. Federman and S. Pittel, **Phys. Rev. C** **20**, 820 (1979).
4. R. D. Ratna Raju, J. P. Draayer, and K. T. Hecht, **Nucl. Phys. A** **202**, 433 (1973).
5. D. Bonatsos, R. F. Casten, S. Karampagia, R. B. Cakirli, and K. Blaum, in preparation.

# Nuclear equation of state effects on the r-mode instability of neutron stars

Ch.C. Moustakidis<sup>1,2</sup> and M. Papazoglou<sup>1</sup>

<sup>1</sup>*Department of Theoretical Physics, Aristotle University of Thessaloniki, Thessaloniki, Greece*

<sup>2</sup>*Theoretical Astrophysics, University of Tuebingen IAAT, Tuebingen, Germany*

## Abstract

*The effects of the density dependence of the nuclear symmetry energy on r-mode instability properties are presented and analyzed. A comparison of theoretical predictions with observed neutron stars in low-mass x-ray binaries is also performed and analyzed.*

The oscillations and instabilities of relativistic stars gained a lot of interest in the last decades because of the possible detection of their gravitational waves [1, 2]. Especially neutron stars may suffer a number of instabilities which come in different flavors but they have a general feature in common, they can be directly associated with unstable modes of oscillation. The r-modes are oscillations of rotating stars whose restoring force is the Coriolis force. The gravitational radiation-driven instability of these modes has been proposed as an explanation for the observed relatively low spin frequencies of young neutron stars and of accreting neutron stars in low-mass X-ray binaries as well [1]. This instability can only occur when the gravitational-radiation driving time scale of the r-mode is shorter than the time scales of the various dissipation mechanisms that may occur in the interior of the neutron star.

The motivation of the present work is to study extensively the nuclear equation of state (EOS) effect on the r-mode instability of neutron stars with a perfectly rigid crust [1]. Actually EOS affects the time scales associated with the r-mode, in two different ways. Firstly, EOS defines the radial dependence of the mass density distribution  $\rho(\mathbf{r})$ , which is the basic ingredient of the relevant integrals. Secondly, it defines the core-crust transition density  $\rho_c$  and also the core radius  $R_c$  which is the upper limit of the mentioned integrals.

The r-modes evolve with time dependence  $e^{i\omega t - t/\tau}$  as a consequence of ordinary hydrodynamics and the influence of the various dissipative processes. The real part of the frequency of these modes,  $\omega$ , is given by  $\omega = -[(m-1)(m+3)/(m+1)]\Omega$ , where  $\Omega$  is the angular velocity of the unperturbed star. The imaginary part  $1/\tau$  is determined by the effects of gravitational radiation, viscosity, etc. [1, 2]. In the small-amplitude limit, a mode is a driven, damped harmonic oscillator with an exponential damping time scale

$$\frac{1}{\tau(\Omega, l)} = \frac{1}{\tau_{GR}(\Omega)} + \frac{1}{\tau_{bv}(\Omega, l)} + \frac{1}{\tau_v(\Omega, l)},$$

where  $\tau_{GR}$ ,  $\tau_{bv}$ ,  $\tau_v$  are gravitational radiation, bulk viscosity and shear viscosity times scales. Gravitational radiation tends to drive the r-modes unstable, while viscosity suppresses the instability. More precisely dissipative effects cause the mode to decay exponentially as  $e^{-t/\tau}$  (i.e., the mode is stable) as long as  $\tau > 0$  [1]. The damping time scale due to viscous dissipation at the boundary layer of the perfectly rigid crust and fluid core is given by [1]

$$\tau_v = \frac{1}{2\Omega} \frac{2^{2m+1/2}(m-1)!}{m!(2m+1)!!m} \sqrt{\frac{2\Omega R_c^3 \rho_c}{\eta_c}} \int_0^{R_c} \frac{\rho(r)}{\rho_c} \left(\frac{r}{R_c}\right)^{2m+2} \frac{dr}{R_c},$$

where the quantities  $R_c$ ,  $\rho_c$  and  $\eta_c$  are the radius, density and viscosity of the fluid at the outer edge of the core. The fiducial viscous time scale  $\tau_v$  is defined as

$\tau_v = \tau_v (\Omega_c / \Omega)^{1/2} (T / 10^8 K)$ , where  $\Omega_0 = \sqrt{\pi G \bar{\rho}}$  and  $\bar{\rho} = 3M / 4\pi R^3$  is the mean density of the star. The gravitational radiation time scale is given by [1]

$$\frac{1}{\tau_{GR}} = \frac{32\pi G M^{4m+2}}{c^{2m+3}} \frac{(m-1)^{2m}}{[(2m+1)!!]^2} \left(\frac{\pi c}{\Omega}\right)^{2m+2} \int_0^{R_c} \rho(r) r^{2m+2} dr,$$

while the fiducial gravitational radiation time scale  $\tau_{GM}$  is defined as  $\tau_{GM} = \tau_{GR} \left(\frac{\Omega_c}{\Omega}\right)^{2m+2}$ . The critical angular velocity  $\Omega_c$ , above which the  $r$ -mode is unstable, is defined by the condition  $\tau_{GM} = \tau_v$  and given, for  $m = 2$ , by [1]

$$\frac{\Omega_c}{\Omega_0} = \left(\frac{\tau_{GR}}{\tau_v}\right)^{2/11} \left(\frac{10^8 K}{T}\right)^{2/11}.$$

In the present work we employ a phenomenological model for the energy per baryon of the asymmetric nuclear matter having the advantage of an analytical form [3]. By suitably choosing the parameterization of the model we obtain different forms from the density dependence of the nuclear symmetry energy by varying the slope parameter  $L$ . The nuclear symmetry energy  $E_{sym}(n)$  and the slope of the symmetry energy  $L$  at nuclear saturation density  $n_0$  are defined as following

$$E_{sym}(n) = E_{sym,2}(n) = \frac{1}{2!} \frac{\partial^2 E_b(n, I)}{\partial I^2} \Big|_{I=0}, \quad L = 3n_0 \frac{\partial E_{sym}(n)}{\partial n} \Big|_{n=n_0},$$

where  $E_b(n, I)$  is the energy per baryon in asymmetric nuclear matter and  $I$  is the asymmetry parameter. By suitably choosing the parameterization it is possible to obtain different forms for the density dependence of the symmetry energy  $E_{sym}(n)$  as well as on the value of the slope parameter  $L$ . We take as a range of  $L$   $50 \text{ MeV} \leq L \leq 110 \text{ MeV}$  where the value of the symmetry energy at saturation density is fixed to be  $E_{sym}(n_0) = 30 \text{ MeV}$ .

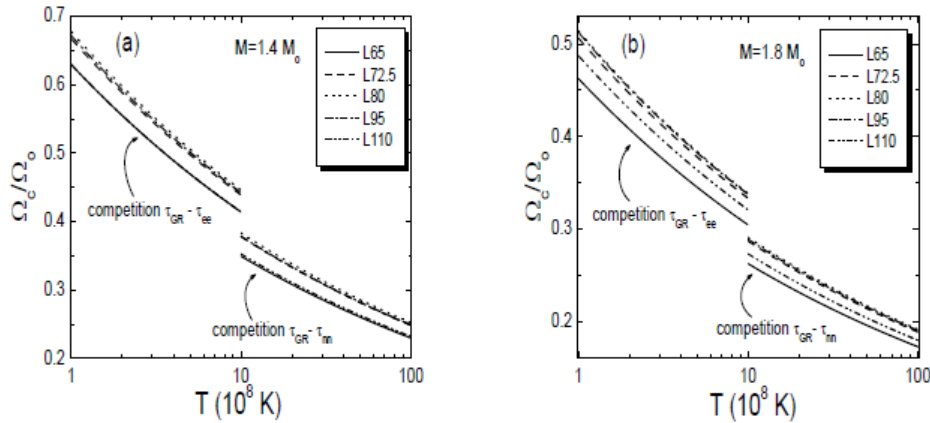


Figure 1: Temperature dependence of the critical angular velocity ratio  $\Omega_c/\Omega_0$  for a neutron star with mass  $M = 1.4M_\odot$  (a) and  $M = 1.8M_\odot$  (b) constructed for the selected EOSs.

In Fig. 1 are displayed the  $r$ -mode instability windows for neutron stars with mass  $1.4M_\odot$  (a) and  $1.8M_\odot$  (b) for the selected equations of state as a function of the temperature. For low values of temperature ( $T \leq 10^8 K$ ) and for high values ( $T \geq 10^9 K$ ) of temperature we plot the ratios respectively

$$\frac{\Omega_c}{\Omega_o} = \left( \frac{\tau_{GR}}{\tau_{GR}} \right)^{2/11} \left( \frac{10^8 K}{T} \right)^{2/11}, \quad \frac{\Omega_c}{\Omega_o} = \left( \frac{\tau_{GR}}{\tau_{GR}} \right)^{2/11} \left( \frac{10^8 K}{T} \right)^{2/11}$$

The most striking feature is the location of the ratio  $\Omega_c/\Omega_o$  in a narrow interval (mainly in the case of neutron star with mass  $1.4M_\odot$ ). Actually, the ratio  $\Omega_c/\Omega_o$  increases around 7% (for  $T \leq 10^8 K$ ) and around 9% (for  $T \geq 10^8 K$ ) with the lower values corresponding to the case of  $L = 65 MeV$  and the higher to the case  $L = 80 MeV$ . It is concluded that the values of the ratio saturate for  $L$  close to the value  $80 MeV$ . In the case of a neutron star with mass  $1.8M_\odot$  the ratio  $\Omega_c/\Omega_o$  increases around 10% both for  $T \leq 10^8 K$  and for  $T \geq 10^8 K$  with the lower values corresponding to the case of  $L = 65 MeV$  and the higher to the case  $L = 80 MeV$ .

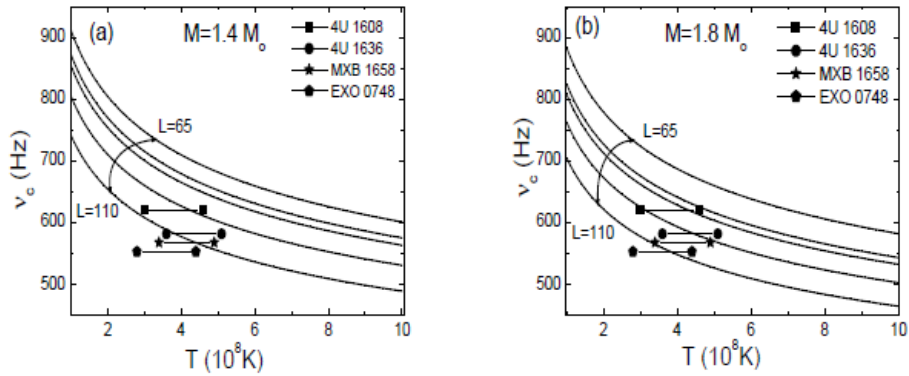


Figure 2: The critical frequency temperature dependence for a neutron star with mass  $M = 1.4M_\odot$  (a) and  $M = 1.8M_\odot$  (b) constructed for the selected EOSs. In addition, the location of the observed short-recurrence time LMXBs [4, 5]

In Fig. 2 we compare the r-mode instability window for the selected equation of states with those of the observed neutron stars in low-mass x-ray binaries (LMXBs) for  $1.4M_\odot$  and  $1.8M_\odot$ . Firstly, we found that the instability window drops by  $\approx 20 - 40 Hz$  when the mass is raised from  $1.4M_\odot$  to  $1.8M_\odot$ . We examine four cases of LMXBs that is the 4U 1608-522 at 620 Hz, 4U 1636-536 at 581 Hz, MXB 1658-298 at 567 Hz and EXO 0748-676 at 552 Hz [4,5]. The masses of the mentioned stars are not measured accurately but the core temperature  $T$  is derived from their observed accretion luminosity. It is obvious from Fig. 2 that for a  $1.8M_\odot$  all the considered LMXBs lie inside instability window. The case is similar for a  $1.4M_\odot$  where the only exception the EXO 0748-676. The LMXBs should be out of the instability window. Consequently, one can presume that either the LMXBs masses are even lower than  $1.4M_\odot$  or the softer equation of state is more preferred. However, additional theoretical and observation work must be dedicated before a definite conclusion.

## References

1. L. Lindblom, B.J. Owen, and G. Ushomirsky, **Phys. Rev. D** **62**, 084030 (2001).
2. N. Andersson and K.D. Kokkotas, **Int. J. Mod. Phys. D** **10**, 381 (2001).
3. Ch.C. Moustakidis, **Phys. Rev. C** **76**, 025805 (2007); Ch.C. Moustakidis, **Phys. Rev. C** **78**, 054323 (2008) ; Ch.C. Moustakidis and C.P. Panos, **Phys. Rev. C** **79**, 045806 (2009) .
4. A.L. Watts, B. Krishnam, L. Bildsten, and B.F. Schutz, **Mon. Not. R. Astron. Soc.** **389**, 839 (2008).
5. L. Keek, D.K. Galloway, J.J.M. Zand, and Heger, **Astrophys. J.** **718**, 292 (2010) .

# Neutral-current neutrino-nucleus reactions and their impact to supernova physics

T S Kosmas

*Department of Physics, The University of Ioannina, and HINP, GR-45110, Ioannina, Greece*

## Abstract

*We study neutral-current neutrino-nucleus reactions in nuclei that are relevant for supernova physics and for terrestrial experiments aiming at neutrino astrophysics as well as neutrino-nucleus scattering cross sections measurements. Such studies allow us to improve estimates of nuclear responses to low energy neutrinos in light of the operation of nuclear neutrino-detectors with very-low threshold and very high sensitivity. The adopted neutrino energy range is extended up to 100 MeV so as to consider allowed and forbidden multipole contributions to cross sections. Both contributions are calculated within the quasi-particle random phase approximation by using realistic two-body forces (Bonn CD potential).*

## 1. Introduction

Neutrinos are neutral particles (without electric charge and magnetic moment) having very small masses (according to the recent experimental evidences). Since they are not deflected from electromagnetic fields and interact very weakly gravitationally, they can travel cosmological large distances without interaction, so as they may escape the very dense surrounding deepest in the interior of massive stars [1]. This property makes them almost ideal messenger-particles of distant stars, a feature that allows us to look into the innermost part of the stars. However, the very low neutrino interaction cross-section is simultaneously the biggest disadvantage for their detection that can be probed through measuring Cherenkov light from secondary particles or through the de-excitation products of neutrino-induced excitations of nuclear  $\nu$ -detectors in extremely sensitive (mostly underground) experiments. Such probes, however, need significant event rates and, therefore, huge volume detectors have to be constructed [2,3,4].

On the other hand, from supernova (SN) physics it is known that, the death of massive (with mass  $M > 8-10M$  solar masses) stars is marked through very energetic explosions known as core-collapse supernovae. In a typical SN, energy of about  $10^{53}$  erg is released (within 10 seconds after the explosion) in the form of neutrinos which (except their oscillation on propagation) travel to Earth undistorted. In the present work, we explore the role of neutrino-nucleus reactions in understanding open questions relevant to SN physics.

Our strategy in this research plan is as follows. First, we consider neutral-current (NC) neutrino-nucleus scattering, assuming that the nuclear target is at zero temperature, for some isotopes contents of promising neutrino detection materials that are quite advantageous (i) for measuring rare events (double-beta decay, etc.) and (ii) for potential use in studying neutrino physics issues [2,3,4]. Second, we treat charged-current (CC) interactions of neutrinos with the above nuclear isotopes. The relevant cross sections are by about an order of magnitude larger than the corresponding for NC ones. Third, we consider nuclear responses to SN-neutrinos focusing on the possibility of including in these estimations contributions coming from particle decays of neutrino-induced excited final states lying above the separation energies for protons and neutrons. In studying detector responses to SN neutrinos, particle decays cause extra signals which are important to be included in the study. Fourth, we study thermal effects on the NC inelastic neutrino-nucleus scattering under SN conditions (hot nuclei) fo-

cusing on the iron group isotopes which play a significant role in SN physics involving neutrinos.

## 2. Neutrino-nucleus cross sections at zero temperature

By applying the Donnelly-Walecka multipole decomposition method [2], the double differential cross section of NC  $\nu$ -nucleus scattering reads

$$\frac{d^2\sigma_{i\rightarrow f}}{d\Omega d\omega}(\varphi, \theta, \omega, \varepsilon_\nu) = \frac{2G^2\varepsilon_f^2 \cos^2(\theta)}{\pi(2J_i+1)} [C_V + C_A - C_{VA}]$$

where  $\omega = \varepsilon_\nu - \varepsilon_f \approx E_f - E_i$  is the excitation energy of the nucleus,  $E_i$  and  $E_f$  represent the energy of the initial (ground) and final states of the studied nucleus, respectively. The term  $C_V$  ( $C_A$ ) in Eq. (1) is a summation over the contributions coming from the polar-vector (axial-vector) operators written in terms of the matrix elements of the eight multipole operators  $M_J^{(5)}, L_J^{(5)}, T_J^{el(5)}$  and  $T_J^{mag(5)}$ , (the superscript '5' refers to the axial-vector components). The interference term  $C_{VA}$  in Eq. (1) contains the product of transverse polar-vector and transverse axial-vector matrix elements [2]. For normal parity transitions,  $C_{VA}$  contains contributions of  $T_J^{el}$  and  $T_J^{mag5}$  operators while for abnormal parity ones  $C_{VA}$  contains matrix elements of  $T_J^{mag}$  and  $T_J^{el5}$ . Total cross sections,  $\sigma$ , are subsequently calculated by integrating (numerically) Eq. (1) as is described below.

## 3. Neutrino-nucleus cross sections at finite temperature

In order to treat nuclear excitations at finite temperature, we adopt the approach of Thermo Field Dynamics (TFD) based on two main ingredients: the thermal vacuum,  $|0(T)\rangle$ , of the TFD, and the thermal Hamiltonian  $H$  [5,6]. The thermal vacuum describes equilibrium properties of the system while the eigenstates of the thermal Hamiltonian  $H$  correspond to excited states of the system at finite temperature.  $H$  is defined as a difference between the system's Hamiltonian and the so-called tilde Hamiltonian, i.e.,  $H = H_s - \tilde{H}$ . The tilde Hamiltonian has the same eigenvalues as  $H$  and is obtained from  $H$  in accordance with properly formulated tilde conjugation rules [5]. The thermal vacuum is the zero-energy eigenstate of the the Hamiltonian  $H$  and for an arbitrary operator  $A$  it satisfies the thermal state condition [5]

$$A|0(T)\rangle = \sigma e^{H/2T} \tilde{A}^\dagger |0(T)\rangle,$$

( $\sigma=1$  if  $A$  is bosonic and  $\sigma=i$  if  $A$  is fermionic operator). As it follows from this definition, each of the eigenstates of  $H$  with positive energy has the counterpart (the tilde-conjugate eigenstate) with negative but the same absolute energy value. Transitions from the thermal vacuum to positive energy states correspond to excitation of the system, while transitions to negative energy states describe de-excitation of thermally excited states. Application of the TFD formalism to a hot nucleus [5] determines the thermal behaviour of the studied nucleus. Thus, for example, in the context of the thermal QRPA method [5] one should diagonalize the thermal Hamiltonian  $H_{QRPA} = H_{SQRPA} - \tilde{H}_{QRPA}$  and find the corresponding thermal vacuum state. This can be done in two steps. Initially, the sum of single-particle,  $H_{sp}$ , and pairing,  $H_{pair}$ , parts of  $H_{QRPA}$  (BCS level), i.e.,  $H_{BCS} = H_{sp} + H_{pair}$ , is diagonalized. At the second step of the diagonalization of  $H_{QRPA}$ , long-range correlations (due to the particle-hole interaction) are taken into account within the thermal QRPA (TQRPA). Temperature dependent total cross section  $\sigma(\varepsilon_\nu, T)$  are, then, obtained from the double differential cross sections by summing over all possible (thermal) one-phonon states of different multipolarities and by numeri-

cal integration over scattering angles. The total cross section at finite temperature may be separated into two parts as [5]

$$\sigma(\varepsilon_\nu, T) = \sigma_d(\varepsilon_\nu, T) + \sigma_u(\varepsilon_\nu, T)$$

Where  $\sigma_d(\varepsilon_\nu, T)$  ( $\sigma_u(\varepsilon_\nu, T)$ ) describes neutrino down (up)-scattering  $\varepsilon_\nu \geq \varepsilon_f$  ( $\varepsilon_f \geq \varepsilon_\nu$ ). Here  $\varepsilon_f$  is a neutrino energy in the final states. The down-scattering processes are responsible for nuclear excitation, i.e., they increase the entropy of the collapse environment. In contrast, the up-scattering processes reduce the entropy as they correspond to nuclear de-excitation. Since we do not apply Brink's hypothesis for the down-scattering part, both  $\sigma_d(\varepsilon_\nu, T)$  and  $\sigma_u(\varepsilon_\nu, T)$  depend on temperature. Such cross sections results will be published in Ref. [6].

#### 4. Results and Discussion

As a first step towards the above purposes, we have applied the method to the nucleus  $^{56}\text{Fe}$  starting from the study of the behavior of the cross section  $\sigma(\omega, \varepsilon_\nu = \text{const}, T=0)$  in various leading sets of multipole states (up to  $J^\pi = 6^+$ ). The results of original *QRPA* calculations have shown that the most important multiplicities are the positive parity transitions  $0^+$ ,  $1^+$  and  $2^+$  the negative parity transitions  $1^-$ . In general, for inelastic scattering of low-energy neutrinos, the leading multipoles that yield the most significant cross sections, are the  $J^\pi = 1^+$  and  $J^\pi = 1^-$ . In the case of the  $1^+$  multipole the axial-vector pieces  $L_1^5$  and  $T_1^{el\ 5}$  dominate over the vector piece  $T_1^{mag}$ . Since the momentum transfer for low-energy neutrino scattering is rather small, the axial-vector matrix elements dominate over the vector ones (even by an order of magnitude or more). The variation of  $\sigma(\omega, \varepsilon_\nu = \text{const}, T=0)$  in the case of the reaction  $^{56}\text{Fe}(\nu, \nu')^{56}\text{Fe}^*$  presents some characteristic clearly pronounced peaks at various excitation energies  $\omega$  and specifically for the transitions  $J^\pi = 1^+, 1^-$  but also for  $J^\pi = 0^+, 2^+$  ones. We have chosen to show  $\sigma(\omega, \varepsilon_\nu = \text{const})$  for  $\varepsilon_\nu$  close to the mean energies of supernova neutrinos and anti-neutrinos guided by recent SN neutrino simulations suggesting the mean energies  $\langle \varepsilon_\nu \rangle = \langle \varepsilon_{\bar{\nu}_e} \rangle = 22 - 25 \text{ MeV}$  [3]. From this study we found that, in the reaction  $^{56}\text{Fe}(\nu, \nu')^{56}\text{Fe}^*$  the maximum peak corresponds to a  $J^\pi = 1^+$ , transition at  $\omega$  around  $10 \text{ MeV}$  and a second one corresponds to a  $1^-$  state with energy  $\omega = 13 \text{ MeV}$  (ground state transitions). Temperature dependent cross sections will be published elsewhere [6].

#### 5. Summary and Conclusions

Neutral-current neutrino-nucleus reactions cross sections in nuclei that are important for supernova simulations and for terrestrial experiments aiming at astrophysical neutrino detection, are required. On the other hand, a great number of open issues in supernova physics may be unraveled by future galactic (or extragalactic) supernova explosions which nowadays may well be analyzed with very high statistics by Earth neutrino detection experiments. Thermal effects on NC neutrino nucleus cross sections especially for Fe group isotopes are important to understand SN dynamics.

#### References:

1. K. Langanke and G. Martinez-Pinedo, **Rev. Mod. Phys.** **75**, 819 (2003)
2. V. Tsakstara and T.S. Kosmas, **Phys. Rev. C** **83**, 054612 (2011) and references therein.
3. V. Tsakstara and T.S. Kosmas, **Phys. Rev. C** **84**, 064620 (2011).
4. V. Tsakstara and T.S. Kosmas, **Phys. Rev. C**, (2012), in press.
5. A. A. Dzhiyev et. al, **Phys. Rev. C** **81**, 015804 (2010).
6. A.A. Dzhiyev, V. Tsakstara, T.S. Kosmas, A.I. Vdovin, **Phys. Rev. C**, to be submitted.

# Parafermionic Behavior of Bose-Einstein Condensates

Andriana Martinou<sup>1</sup>, Dennis Bonatsos<sup>2</sup>

<sup>1</sup>*School of Applied Mathematical and Physical Sciences, National Technical University of Athens, GR-15780 Zografou Campus, Athens, Greece*

<sup>2</sup>*Institute of Nuclear and Particle Physics, National Centre for Scientific Research "Demokritos", GR-15310 Aghia Paraskevi, Attiki, Greece*

## Abstract

*The aim of this study is to explain the transition from the bosonic to the fermionic behavior of the atoms in Bose-Einstein Condensates (BECs) that were created in an experiment in Rice University. A BEC consists of a number of atoms which are trapped in a small space area and cooled down to almost zero temperature. These individual atoms exhibit a bosonic behavior. The paradox is that the BEC, although it is a collection of bosonic particles, exhibits a fermionic behavior. This paradox has been explained by means of the Gross-Pitaevskii equation and the theory of Generalised Parafermionic Oscillators. The theory introduces a quantity called the order of the parafermion, which measures the divergence from the bosonic behavior. It is proved that the nonlinearity of the BEC's energy  $E(N)$ , where  $N$  is the number of atoms, signifies the divergence from the bosonic behavior. A link with the Tonks-Girardeau gas is being given.*

The trigger for this study was an experiment in Rice University. A precise description of the experiment and its results can be found at [1]. A collection of  ${}^7_3\text{Li}$  atoms has been used for the purposes of the experiment. Every atom of each BEC is under the influence of two types of potentials:

a) The potential of the magneto-optical trap

$$V_{\text{ext}} = \frac{1}{2}m\omega_r^2 r^2 + \frac{1}{2}m\omega_z^2 r^2, \quad (1)$$

b) The mean field potential caused by the atoms interaction.

$$V_{\text{int}} = g |\Psi(\vec{r}, t)|^2, \quad (2)$$

where  $g$  is the coupling constant of their mutual interaction and  $\Psi(\vec{r}, t)$  is the wavefunction of the BEC. A picture of the resulting BECs is Fig.(1). The atoms and the BEC are expected to have a boson-like behavior because they contain an even number of fermions [2]. But a gap between the BECs indicates that they collide in a fermionic manner.

We know that ideal fermions or bosons can be alone the elementary particles. A combination of them them is neither an ideal fermion nor an ideal boson, but something in the middle. *A parafermion is any kind of (non-elementary) particle characterized by a parameter  $\rho$  which is called the "order of the parafermion".* This parameter is proportional to the number of the parafermions that can occupy the same state. Thus, if  $\rho \rightarrow 1$  the parafermion exhibits a fermionic behavior. On the other hand, if  $\rho \gg 1$ , its behavior is bosonic.

Systems of parafermions can be studied within the mathematical framework of the *generalized deformed oscillator*, which is defined as the algebra generated by the operators  $\{1, a, a^+, N\}$  and a structure function  $\Phi(N)$ , satisfying the commutation relations [3,4]

$$\begin{aligned} [\alpha, \alpha^+] &= \Phi(N+1) - \Phi(N), \\ \{\alpha, \alpha^+\} &= \Phi(N+1) + \Phi(N), \end{aligned} \quad (3)$$

where  $N$  is the number operator. The structure function is characteristic to the deformation scheme. In Ref.[5] one can find the structure functions corresponding to different deformed oscillators. It has been proved that any *generalized deformed parafermionic algebra* can be written as a generalized oscillator with structure function

$$\Phi(N) = N(\rho + 1 - N)(\lambda + \mu N + \nu N^2 + \dots) \quad (4)$$

The building blocks of a BEC are the Lithium atoms, which are treated as a system of parafermions. The appropriate Hamiltonian for this parafermionic system is the Bose-like Hamiltonian [6]

$$H_B = \frac{1}{2} \{a, a^+\}, \quad (5)$$

possessing the energy eigenvalues

$$E(N) = \frac{1}{2} (\Phi(N) + \Phi(N+1)). \quad (6)$$

Using Eq.(4) and keeping up to  $N^4$  terms, the energy eigenvalues are written as

$$E(N) = -(\lambda + \mu + \nu)\rho - ((2\mu + 3\nu)\rho - 2\lambda - \mu - \nu)N - (3\nu\rho - 3\mu - 3\nu)N^2 + 4\nu N^3. \quad (7)$$

We can obtain a second calculation of the BEC's energy through Quantum Field Theory. The nonlinear Schrödinger equation derived by this theory is the so called Gross-Pitaevskii (GP) equation. By assuming that the mean field potential acts only on the symmetry axis of the cylindrical trap and that the BEC is in the ground state the GP equation is [7]

$$i\hbar \frac{\partial U(z,t)}{\partial t} + \frac{\hbar^2}{2m} \frac{\partial^2 U(z,t)}{\partial z^2} - g |U(z,t)|^2 U(z,t) = 0. \quad (8)$$

A solution of this equation which respects the boundary conditions is

$$U(z,t) = A \operatorname{sech}[\eta(z - vt)] e^{i(kz - \omega t)}. \quad (9)$$

The number of atoms in each BEC is given as

$$N = \int_{-\infty}^{+\infty} |U(z,t)|^2 dz = \frac{2|A|^2}{\eta}, \quad (10)$$

while the energy of the BEC is [7]

$$E = i\hbar \int_{-\infty}^{+\infty} h(U^*, U, t) dz = \frac{1}{2} \int_{-\infty}^{+\infty} \left( \frac{\hbar^2}{m} \left| \frac{\partial U}{\partial z} \right|^2 + g |U|^4 \right) dz = \frac{\hbar^2}{2m} \left( k^2 + \frac{\eta^2}{3} \right) N + \frac{g\eta}{6} N^2, \quad (11)$$

leading to

$$E = c_1 N + c_2 N,$$

with  $h(U^*, U, t)$  being the energy functional . We can calculate the order of the parafermion by equating Eq. (7) with Eq. (11 ). The parameter  $\rho$  is

$$\rho = \frac{3\hbar^2}{|g| m \eta} \left( k^2 + \frac{\eta^2}{3} \right) = \frac{c_1}{|c_2|}. \quad (12)$$

The order of the parafermion may be of value for the study of a Tonks-Girardeau gas. In such a gas a collection of bosonic particles is confined in one dimension. As soon as the particles enter the Tonks-Girardeau region, they start to collide in a fermionic way. The quantity used to check whether the particles have entered the Tonks-Girardeau region is the ratio of the interaction energy to the kinetic one,  $\gamma = I / K$ . *If the gas is homogenous*, then this ratio is  $\gamma = mg / n\hbar^2$ , where  $n$  is the concentration of particles [8]. Supposing that  $n \approx |A|^2$ , which implies  $\eta \approx nN$ , one can prove that the order of the parafermion is inversely propotional to the ratio  $\gamma$ :

$$\rho \propto \frac{1}{\gamma}. \quad (13)$$

We conclude that *the non linear term of the energy, of an ultracold gas, signifies the divergence from the bosonic behavior .*

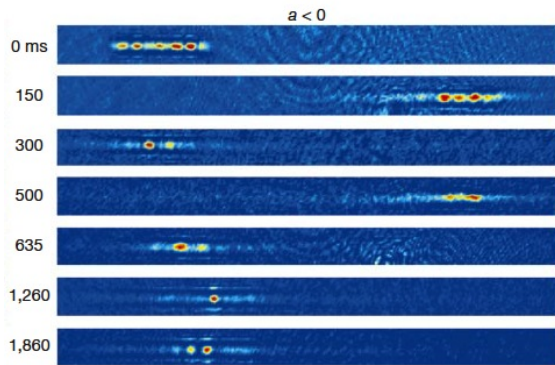


*Fig. (1) The Lithium atoms were tunned to attract each other. This resulted in the creation of four BECs. A gap between them at  $t=0$  ms indicates a fermionic behavior. [1]*

1. K. E. Strecker, G. B. Partridge, A.G. Truscott, R. G. Hulet, **Nature** **417**, 150 (2002).
2. R. P. Feynman, R. B. Leighton, and M. Sands, *The Feynman Lectures on Physics* (Addison-Wesley, Reading, 1965) Vol. 3, Chap. 4.
3. C. Daskaloyannis, **J. Phys. A** **24**, L789(1991).
4. C. Daskaloyannis and K. Ypsilantis, **J. Phys. A** **25**, 4157 (1992).
5. D.Bonatsos and C. Daskaloyannis, **Prog. Part. Nucl. Phys.** **43**, 537 (1999).
6. C. Quesne, **Phys. Lett. A** **193**, 245 (1994).
7. D. Frantzeskakis, in *Order and Chaos in Nonlinear Dynamical Systems* (in Greek), ed. T. Bountis and S. Pnevmatikos (G. A. Pnevmatikos, Athens, 2000) Vol. 6, p. 167, 181.
8. B.Paredes and A. Widera and V. Murg and O. Mandel and S. Fölling and I. Cirac and G. V. Shlyapnikov and T. W. Hänsch and I. Bloch, **Nature** **429**, 277 (2004)

# Flavour Changing Neutral Processes in Nuclei

D.K. Papoulias<sup>1</sup> and T.S. Kosmas<sup>1</sup>

<sup>1</sup>*Department of Physics and HINP, The University of Ioannina, Ioannina, Greece*

[dimpap@cc.uoi.gr](mailto:dimpap@cc.uoi.gr)

[hkosmas@cc.uoi.gr](mailto:hkosmas@cc.uoi.gr)

## Abstract

*The Flavour Changing Neutral Current (FCNC) reactions taking place in the presence of nuclei are investigated. Specifically, we focus on  $\nu$ -nucleus FCNC reactions of the form  $(A, Z)(\nu_\alpha \nu_\beta)(A, Z)^*$ , and  $(A, Z)(\tilde{\nu}_\alpha \tilde{\nu}_\beta)(A, Z)^*$ , with  $\alpha \neq \beta$ . We adopt the Seesaw mechanism, which extends the Standard Model and predicts such exotic processes by adding a heavy right-handed neutrino singlet  $N_r$  per neutrino generation. In this description we have been inspired by the successful application of the Seesaw model in other lepton flavour violating (LFV) processes studied in detail previously, like the  $\mu^- \rightarrow e^-$  conversion in nuclei.*

*FCNC  $\nu$ -nucleus reactions have a great impact to neutrino Astrophysics and hence a comprehensive study of such processes is of significant importance. From a nuclear theory point of view, the projection method of Donnelly-Walecka is employed for  $\nu$ -nucleus cross sections calculations. The single-particle transition matrix elements are evaluated with the use of an in house Mathematica code constructed for this purpose using the compact formalism developed by our group recently. Results for differential cross sections on some concrete nuclear systems are expected to be obtained soon.*

## Introduction

Since their invention, neutrinos are still of great theoretical and experimental interest. Neutrinos appear to be excellent probes to investigate open issues in Astrophysics such as the interior of the Sun and distant massive stars, Supernova physics, etc. From a Cosmological point of view, in Leptogenesis theories heavy right-handed Majorana neutrinos provide a very promising explanation of the early stages of the Universe and the matter-antimatter asymmetry as well. On the other hand, from a nuclear physics point of view, neutrinos may be the best candidates to provide us a deeper understanding of the nuclear structure and the fundamental electroweak interactions in nucleus and nuclei.

Except the Standard Model (SM) theories, there are many theories beyond the SM involving neutrinos, like  $\mu^- \rightarrow e^-$  conversion in nuclei [1,2,3,4], which is a Lepton Flavour Violating (LFV) process and the Flavour-Changing Neutral-Current (FCNC) neutrino-nucleus reactions [5,6]. Our aim is to study in detail such reactions by performing realistic nuclear structure calculations within the framework of a nuclear structure model (Shell-model, RPA, QRPA, etc.).

## Brief Description of the Formalism

The FCNC (anti)neutrino reactions in the presence of nuclei are described by:

$$\nu_\alpha(\tilde{\nu}_\alpha) + (A, Z) \rightarrow \nu_\beta(\tilde{\nu}_\beta) + (A, Z)^*, \quad (1)$$

where  $\alpha, \beta = e, \mu, \tau$  denote the flavour indices and  $A, Z$  are the mass and atomic number of the nucleus, respectively. A tree-level Feynman diagram of the aforementioned processes is illustrated in Fig. 1.

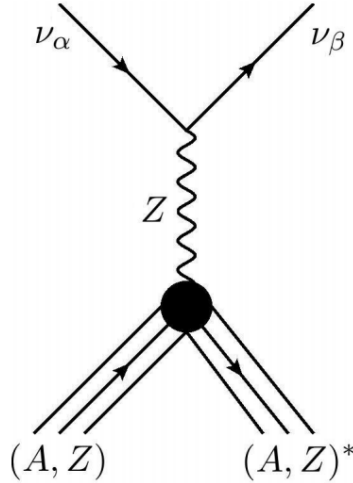


Figure 1: Tree-level Feynman diagram contributing to FCNC  $\nu$ -nucleus processes.

For the purposes of the present work, we follow the research made in Ref. [1,2,3] for the study of  $\mu^- \rightarrow e^-$  conversion in nuclei where the authors adopted the Seesaw mechanism [4] as reference model. The LFV parameters of the quark-level interaction Lagrangian enter in the nucleon-level Hamiltonian which can be written as that of Ref. [1]. These parameters can be constrained by experiments searching for  $\mu^- \rightarrow e^-$  conversion at sensitivity  $10^{-16} - 10^{-19}$ , like the mu2e and Project X at Fermilab and the COMET at J-PARC, Japan.

Eventually, at nuclear-level the interaction Hamiltonian can be cast in the form:

$$H_{\text{eff}} = \frac{G_F}{\sqrt{2}} \int j_{\mu}^{\text{lept}}(x) J^{\mu}(x) dx, \quad (2)$$

where  $j_{\mu}^{\text{lept}}$  is the leptonic current and  $J^{\mu}$  the hadronic nuclear current (current-current interaction hypothesis). At this point, it should be mentioned that the matrix elements (ME) of Eq. (2) between initial and final nuclear states are needed for calculating partial transition rates. These ME read:

$$\langle f | H_{\text{eff}} | i \rangle = \frac{G_F}{\sqrt{2}} l^{\mu} \int dx e^{-iq \cdot x} \langle f | J_{\mu}(x) | i \rangle, \quad (3)$$

where  $q$  stands for the magnitude of the three momentum-transfer given by:

$$q = \left[ \omega^2 + 2\varepsilon_i (\varepsilon_i - \omega) (1 - \cos \mathcal{G}) \right]^{1/2}. \quad (4)$$

In the latter expression  $\varepsilon_i$  denotes the energy of the incoming lepton  $\omega$  represents the excitation energy of the nucleus and  $\mathcal{G}$  is the scattering angle (laboratory frame). Thus, the nuclear calculations are based on the ME of the hadronic current for the evaluation of which we employ the Donnelly-Walecka (D-W) model [8,9]. Accordingly, the multipole expansion of the hadronic current leads to the seven basic nuclear operators,  $T_i^J$ ,  $i = 1, \dots, 7$ , as defined in Ref. [8]. The corresponding symbols in D-W method are:  $M_{JM}^{\text{Coul}}$ ,  $\Delta_{JM}$ ,  $\Delta'_{JM}$ ,  $\Omega_M^J$ ,  $\Sigma_M^J$  and  $\Sigma_M^{\prime J}$ . The cross section of any semi-leptonic process in nuclei is proportional to the ME squared of  $T_i^J$  and to this purpose a compact formalism for their evaluation has been developed in the harmonic oscillator basis which reads [8]:

$$\langle j_1 || T_i^J || j_2 \rangle = e^{-y} y^{\beta/2} \sum_{\mu=0}^{n_{\max}} \wp_M^J y^\mu, \quad (5)$$

where  $n_{\max} = (N_1 + N_2 - \beta)/2$  with  $N_i = 2n_i + \ell_i$  representing the harmonic oscillator quanta of the  $i$ -th level. In our notation the well defined quantum numbers are:  $|j_1\rangle \equiv |(n_1, \ell_1) j_1\rangle$ .

### Results and Discussion:

For the purposes of our research an in house Mathematica code has been constructed to evaluate the single-particle reduced transition ME of Eq. (5), for any operator  $T_i^J$ . In Table 1, we list some of the results for the coefficients  $\wp_M^J$  giving the ME of  $T_1^J \equiv M_{JM}^{Coul}$ . Our code provides the ME of Eq. (5) for any configuration  $(j_1 j_2) J$ . We mention that in Ref. [7], only those configurations for which  $N_1 - N_2 \leq 3$  are included.

$(n_1 \ell_1)_{j_1} - (n_2 \ell_2)_{j_2}$	$J$	$\mu = 0$	$\mu = 1$	$\mu = 2$	$\mu = 3$
$0s_{1/2} - 0f_{5/2}$	3	$-\frac{4}{\sqrt{35}}$			
$0s_{1/2} - 1p_{3/2}$	1	0	$-\frac{4}{\sqrt{15}}$		
$1p_{3/2} - 1p_{3/2}$	2	$-\frac{12}{5}$	$\frac{32}{15}$	$-\frac{8}{15}$	
$0d_{3/2} - 0f_{5/2}$	1	$-2\sqrt{\frac{14}{5}}$	$8\sqrt{\frac{14}{5}}$	$-\frac{8}{5}\sqrt{\frac{2}{35}}$	
$0f_{7/2} - 0f_{7/2}$	0	$2\sqrt{2}$	$-4\sqrt{2}$	$\frac{8}{5}\sqrt{2}$	$-\frac{16}{105}\sqrt{2}$

Table 1: The  $\wp_M^J$  coefficients single particle transition ME of  $T_1^J$ .

We note that  $\wp_M^J$  are simple rational (square roots of) numbers for the diagonal (non-diagonal) elements. The double differential cross-section of any semi-leptonic process in nuclei is  $\propto \langle j_1 || T_i^J || j_2 \rangle^2$  and the results of our realistic nuclear structure calculations are going to appear in future work.

### References:

1. T.S. Kosmas, S. Kovalenko and I. Schmidt **Phys. Lett. B** **511**,203 (2001) ; **B** **519**,78 (2001).
2. A. Faessler, T.S. Kosmas, S. Kovalenko and J.D. Vergados 2000 **Nucl. Phys. B** **587**, 25 (2000).
3. T.S. Kosmas **Nucl. Phys. A** **683**, 443 (2001).
4. F. Deppisch, T.S. Kosmas and J.W.F. Valle **Nucl. Phys. B** **752**, 80 (2006).
5. P. S. Amanik and G. M. Fuller **Phys. Rev. D** **75**, 083008 (2007).
6. P. S. Amanik, G. M. Fuller and B. Grinstein **Astropart. Phys.** **24**, 160 (2005).
7. T.W. Donnelly and W.C. Haxton, **At. Data Nucl. Data Tables** **23**, 103 (1979).
8. V. Ch. Chasioti and T. S. Kosmas **Nucl. Phys. A** **829**, 234 (2009).
9. V. Tsakstara and T.S. Kosmas **Phys. Rev. C** **83**, 054612 (2011); **C** **84**, 064620 (2011).

# Realistic nuclear structure calculations for orbital e-capture by nuclei

P.G. Giannaka and T.S. Kosmas

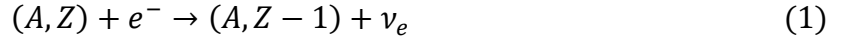
Theoretical Physics Section, University of Ioannina, GR 45110 Ioannina, Greece

## Abstract

*The orbital electron capture process on nuclei is revisited. We focus on the e-capture by nuclei of the “iron group peaked isotopes” that are important for searching the explosive nucleosynthesis. Towards this purpose, we improve our method: 1) In the level where use of compact analytical expressions for the required reduced matrix elements of all basic multipole operators is made. 2) In the level of constructing the nuclear Hamiltonian where the Bonn C-D potential (instead of the Bonn C used up to now) for the realistic two-body nuclear forces is employed. The ground state of the nuclear isotopes chosen is computed by solving iteratively the BCS equations while the excitation spectrum of the studied isotope is calculated by solving the QRPA equations. Results for the relevant cross sections are expected to be obtained soon.*

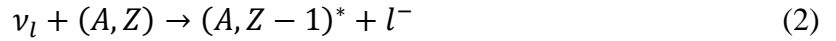
## Introduction

In this work, we study the orbital electron-capture which is represented by the reaction



Even though the investigation of this process started decades ago, more accurate transition rates are needed due to its significant importance in core-collapse supernova dynamics and other astrophysical phenomena [1,2,3,4]. For this aim, in the present work we have chosen to study comprehensively this process in a set of nuclei that are important from an astrophysical point of view (they belong to the “iron group peaked nuclei”) [4,5].

Electron-capture is a particle conjugate process of the corresponding charged-current neutrino-nucleus reaction, i.e.



This means that theoretically these two processes can be studied with the same nuclear methods as we adopt in the present paper.

## The nuclear Hamiltonian

The nuclear calculations start by writing down the weak interaction Hamiltonian  $\hat{H}_w$  which is formulated in a current-current form for all the semi-leptonic processes. By denoting the leptonic current as  $j_\mu^{lept}$  and the hadronic current as  $\hat{J}_\mu$ ,  $\hat{H}_w$  is written as

$$\hat{H}_w = \frac{G \cos \theta_c}{\sqrt{2}} j_\mu^{lept}(x) \hat{J}_\mu(x) \quad (3)$$

The hadronic current,  $\hat{J}_\mu$ , which is of interest from a nuclear theory point of view, consists of the polar-vector and the axial-vector components.

$$\hat{J}_\mu = g_V \hat{J}_\mu^V - g_A \hat{J}_\mu^A \quad (4)$$

These components are written by using isovector, axial-vector and pseudoscalar form factors that depend on the four-momentum transfer ( $q_\mu^2$ ), [9,10,12]. In Eq. (4)  $g_V$  ( $g_A$ ) represent the coupling of the polar (axial) vector interaction.

One of the main goals of this work is to construct an effective and advantageous code for calculating electron-capture rates for even-even nuclear isotopes within the context of quasi-particle random phase approximation (QRPA).

### Evaluation of the nuclear wave functions within QRPA.

As it is well known, the nucleus consists of protons and neutrons which, in a rather rough approximation, can be considered as independent particles attracted by the nuclear center through central strong forces. This attraction can be described by a mean field, as for example the Woods-Saxon type. In our case a Woods-Saxon potential that includes Coulomb corrections and a spin orbit part, is used.

The two-nucleons correlations, also known as the residual interaction of the nuclear Hamiltonian, are necessary to be included. In our case they are described by the Bonn C-D potential. The initially evaluated bare two-body matrix-elements of the latter interaction refer to an isotope of mass number  $A$ . In the specific isotope studied,  $(A,Z)$ , a renormalization of the two-body interaction is required. Toward this purpose we use four multiplicative parameters that renormalize the bare residual interaction (the first two, known as pairing parameters for protons and neutrons, renormalize the monopole interaction, the third tunes the particle-particle channel and the fourth the particle-hole two-nucleon interaction).

The ground state of the studied nucleus is obtained in the context of the BCS method. The solution of the relevant BCS equations gives the probability amplitudes  $V$  and  $U$  for each single particle level to be occupied or unoccupied, respectively and the single quasi-particle energies. Subsequently, we construct the excited states of the studied isotope by solving the QRPA equations. Their solution is an eigenvalue problem, which gives the  $X$  and  $Y$  amplitudes for forward and backward scattering as well as the QRPA excitation energies [7]. In the Donnelly-Walecka method the solution of the QRPA equations is obtained separately for each multipole set of states  $|J^\pi\rangle$ . [6,7,8,9].

In Tables 1 and 2 the values of the model parameters are listed through which we construct the wave functions for the initial (ground) and the final excited states of the isotope in question.

	<b>b</b> (h.o.)	$g_{pair}^n$	$g_{pair}^p$	$S_n$ (MeV)	$S_p$ (MeV)	$\Delta_n^{exp}$ (MeV)	$\Delta_n^{theo}$ (MeV)	$\Delta_p^{exp}$ (MeV)	$\Delta_p^{theo}$ (MeV)
<sup>96</sup> Ru	2,158	0,987	0,835	10,694	7,344	1,0824	1,0821	1,4955	1,4954
<sup>98</sup> Ru	2,165	0,978	0,889	10,183	8,293	1,1971	1,1975	1,5567	1,5535
<sup>106</sup> Cd	2,190	0,886	0,872	10,874	7,353	1,3492	1,3497	1,5057	1,5057
<sup>108</sup> Cd	2,196	0,927	0,965	10,339	8,140	1,3567	1,3574	1,4917	1,4924
<sup>84</sup> Sr	2,116	1,027	0,861	11,923	8,867	1,6137	1,6142	1,8685	1,8698
<sup>78</sup> Kr	2,094	0,979	0,812	12,081	8,234	1,6360	1,6354	1,8177	1,8172
<sup>74</sup> Se	2,078	0,963	0,823	12,066	8,545	1,9279	1,9272	1,8037	1,8036
<sup>102</sup> Pd	2,178	0,978	0,958	10,568	7,806	1,3094	1,3085	1,4947	1,4938
<sup>92</sup> Mo	2,145	1,135	0,637	12,673	7,457	1,7923	1,7920	1,4171	1,4162
<sup>94</sup> Mo	2,152	0,908	0,870	9,678	8,490	0,9793	0,9781	1,5105	1,5094

Table 1: Parameters determining the interaction of proton pairs,  $g_{pair}^p$ , and neutron pairs,  $g_{pair}^n$ . They are adjusted in such way that the corresponding experimental gaps,  $\Delta_p^{exp}$  and  $\Delta_n^{exp}$ , to be reproduced.

State	<sup>96</sup> Ru		State	<sup>102</sup> Pd	
	$g_{ph}$	$g_{pp}$		$g_{ph}$	$g_{pp}$
0 <sup>+</sup>	0,403	0,781	0 <sup>+</sup>	0,377	0,907
2 <sup>+</sup>	0,579	1,189	2 <sup>+</sup>	0,671	1,350
4 <sup>+</sup>	0,905	0,546	4 <sup>+</sup>	1,040	0,322
6 <sup>+</sup>	1,085	1,195	6 <sup>+</sup>	1,108	0,247
3 <sup>+</sup>	1,000	1,000	3 <sup>+</sup>	1,000	1,000
1 <sup>+</sup>	1,000	1,000	5 <sup>+</sup>	1,000	1,000

Table 2: Strength parameters renormalizing the bare interaction for the particle-particle ( $g_{pp}$ ) and particle-hole ( $g_{ph}$ ) interaction (in our method this is done separately for each multipolarity).

After the determining of the particle-particle and particle-hole parameters we proceed with checking the reproducibility of the low-lying energy spectrum. In the final step the results for the cross-sections of the process which, as is known, are proportional to the square of the relevant matrix elements [6,7,11] are obtained. Such results are expected to be published elsewhere.

### Summary

In this work, we study the orbital electron-capture on a set of nuclear isotopes which are promising for understanding the explosive nucleosynthesis, the chemical-element evolution in stars, etc. Up to now, we have constructed the ground state and the excited states of the isotopes of interest by using BCS and QRPA methods, respectively.

### Acknowledgments

This research has been co-nanced by the European Union (European Social Fund ESF) and Greek national funds through the Operational Program Education and Lifelong Learning" of the National Strategic Reference Framework (NSRF) - Research Funding Program: Heracleitus II. Investing in knowledge society through the European Social Fund.

### References

1. K. Langanke, G. Martinez-Pinedo et al, **Phys. Rev. Lett.** **90**, 241102 (2003).
2. A. Juodagalvis, K Langanke et al, **Nucl. Phys. A** **747**, 87 (2005).
3. H.A. Bethe, **Rev. Mod. Phys.** **747**, 801 (1990).
4. D.J. Dean, K. Langanke et al, **Phys. Rev. C** **58**, 1 (1998).
5. C.Frohlich,G.Martinez-Pinedo, et al, **Phys. Rev. Lett.** **96**, 142502 (2006).
6. V.C. Chasioti and T.S. Kosmas **Nucl. Phys. A** **829**, 234 (2009).
7. V. Tsakstara and T.S. Kosmas, **Phys. Rev. C** **83**, 054612 (2011).
8. T.W. Donnelly and R.D. Peccei, **Phys. Rep.** **50**, 1 (1979).
9. K.G. Balasi, E. Ydrefors and Kosmas, **Nucl.Phys. A** **868**, 82 (2011).
10. M. S. Athar, S.Ahmad and S.K. Singh , **Phys. Rev. C** **71**, 045501 (2005).
11. E. Kolbe **Phys. Rev. C** **54**, 4 (1996).
12. W.M. Alberico, S.M. Bilenky, et al, **Phys. Rev. C** **79**, 065204 (2009).

# Model Independent Analysis of the $\gamma^*p \rightarrow \Delta$ Transition with Polarized Electron Scattering Data

E. Stiliaris<sup>1</sup> and C.N. Papanicolas<sup>1,2</sup>

<sup>1</sup> *Department of Physics, National and Kapodistrian University of Athens, Athens, GREECE*  
stiliaris@phys.uoa.gr

<sup>2</sup> *The Cyprus Institute, Nicosia, CYPRUS*

## Abstract

*A novel method for extracting physical parameters from experimental and simulation data is presented. The method is based on statistical concepts and it relies on Monte Carlo simulation techniques. It identifies and determines with maximal precision parameters that are sensitive to the data. The method has been extensively studied and it is shown to produce unbiased results. It is applicable to a wide range of scientific and engineering problems. It has been successfully applied in the analysis of experimental data in hadronic physics and of lattice QCD correlators. In the current project, this method is being applied to recently obtained data in pion electroproduction. Response functions extracted from angular distributions of differential cross sections for polarised electron scattering at  $Q^2=0.127$  (GeV/c)<sup>2</sup> (Bates Data),  $Q^2=0.060, 0.200$  (GeV/c)<sup>2</sup> (Mainz Data) and  $Q^2=1.000$  (GeV/c)<sup>2</sup> (JLab Data) at  $W$  values across the  $\Delta$  Resonance are extensively analyzed in the framework of this model.*

## Introduction

A significant component of hadronic physics research focuses on the understanding of the excitation spectrum of the proton, the only stable hadron. Impressive progress has been achieved in the last decade largely driven by the advances in accelerator and instrumentation technologies. The high quality of data that have emerged and substantial progress in theory have brought a new level of sophistication to the field. Conjectures, such as the deformation of the nucleon have been confirmed [1] and transformed into an extensive program examining not its existence but rather the mechanisms that generate it.

A most fertile ground of research has been the identification of the nucleon resonances, the isolation and interpretation of the contributing multipoles to their excitation spectrum. Progress has been substantial but slow, due to the large width of the resonances, their overlapping nature and the incompleteness of the data base in terms of observables. Extensive work concerns the investigation of the  $\Delta^+(1232)$ , the first excited and only isolated state of the proton, through the  $N \rightarrow \Delta$  reaction.

## Resonance Multipole Extraction and the AMIAS Method

It has been assumed up to now that to extract multipole information model independently from nucleon resonance data (cross sections and polarization asymmetries), a complete set of experimental observables is required. Current experiments which measure an incomplete set of observables typically rely on model extraction. Multipoles have been presented in the literature extracted by employing one of the following two approaches: a) The Truncated Multipole Expansion (TME) approximation where most or all of the non resonant multipoles are neglected assuming that at the peak of the resonance only resonant amplitudes contribute significantly and b) The Model Dependent Extraction (MDE) method where certain multipole amplitudes, often the resonant amplitudes, within a phenomenological model description are adjusted to best describe the data. The second method, MDE, is obviously superior to TME,

for it assumes that multipoles that cannot be determined from the data are fixed through a model and not simply ignored. However it suffers from the fact that the extracted values are biased by the model and therefore characterized by a hard to evaluate systematic model uncertainty.

A Model Independent Analysis Scheme, "AMIAS", which is proposed in [2, 3], addresses most of the above mentioned limitations. The method is based on statistical concepts and it relies on Monte Carlo simulation techniques. Although it is presented in this paper for the case of the  $N \rightarrow \Delta$  transition, it provides a framework and a methodology of analysis which is applicable to all nucleon resonances. In applying AMIAS to the problem of multipole extraction in the  $N \rightarrow \Delta$  transition the parameters to be extracted,  $A_i^j$ , in the general formulation, are the multipole amplitudes  $M_{L\pm}$ , and if the data allow, the isospin separated amplitudes  $M_{L\pm}^{1/2}$ ,  $M_{L\pm}^{3/2}$ . The experimental observables  $\{O_i\}$  are typically cross section and polarization asymmetries. Furthermore, the parameters of our problem, the multipole amplitudes, are subjected to the constraint of unitarization, by imposing the Fermi Watson theorem. The linkage of observables to multipoles in the case of nucleon resonances is described through the Chew-Goldberger-Low-Nambu (CGLN) prominent work [4]. In the demonstration case with the Bates data shown here, the multipoles refer to the  $\pi^0$  charge channel and they are connected to the  $(A_p^{1/2}, A_n^{1/2}, A^{3/2})$  isospin-set through the relation  $A_{\pi^0 p} = A_p^{1/2} + 2/3 A^{3/2}$ . The AMIAS method produces numerical results, i.e. determines the multipole amplitudes and the associated uncertainties, from the experimental data by examining the properties of the ensemble of solutions, canonical or microcanonical.

Multipole	Extracted Value	Relative Error	MAID-2003	Sato & Lee	DMT
$M_{1+}$	$27.24 \pm 0.20$	0.73 %	27.464	27.661	27.489
$L_{1+}$	$0.82^{+0.20}_{-0.09}$	17.7 %	1.000	0.672	0.986
$L_{0+}$	$2.23 \pm 0.41$	18.4 %	2.345	1.008	1.994
$E_{0+}$	$3.44 \pm 0.70$	20.3 %	2.873	2.213	3.206
$E_{1+}$	$1.16^{+0.32}_{-0.24}$	24.1 %	1.294	1.288	1.401

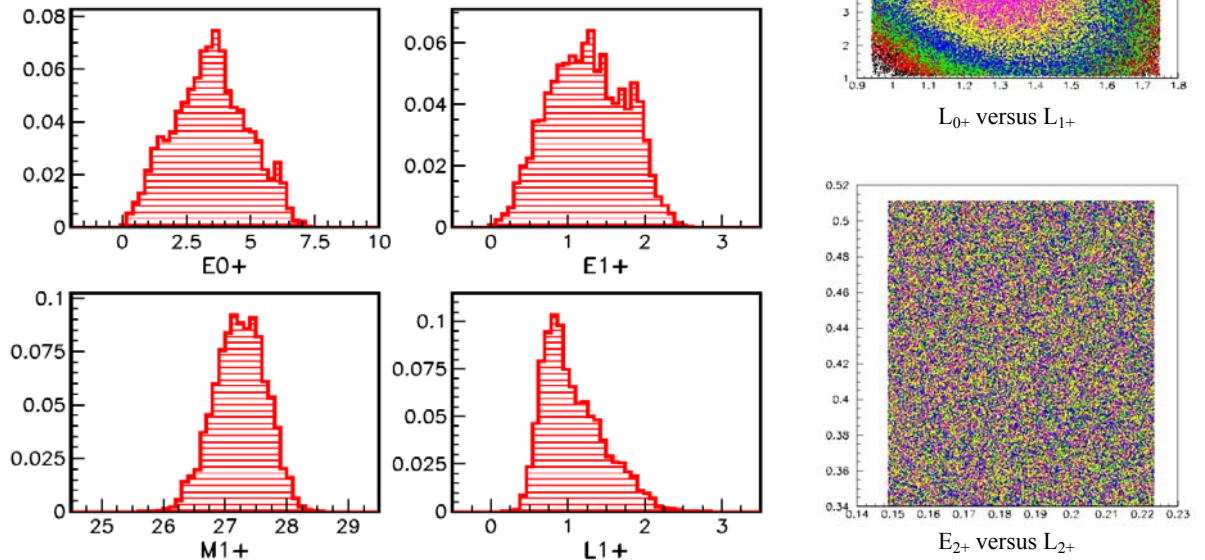


**Figure 1:** AMIAS extracted values compared to various model predictions (table) and probability distributions for some of the most sensitive amplitudes of the analyzed Bates/Mainz data set. Possible multipole correlations are represented by two-dimensional scatter plots.

The capabilities of the method are demonstrated in the re-analysis of the  $H(e,e'p)\pi^0$  measurements performed at  $Q^2=0.127 \text{ GeV}^2/c^2$  and  $W = 1232 \text{ MeV}$  [5]. The data set consists of 31 data points, cross section results for the  $\sigma_{TT}$ ,  $\sigma_{LT}$ ,  $\sigma_0$ ,  $\sigma_{E2}$  and the polarized beam cross section  $\sigma_{LT0}$ . An  $L_{cut}=5$  value was chosen, so that a sufficiently large number of background amplitudes are included in the computational exploration. Results are derived by uniformly varying the real and imaginary part of the input amplitudes of the model in the  $\pi^0$  charge-channel after a reiterative selection of the phase volume to be explored and are shown in Figure 1. The allowed region for partial cross sections for the same data is shown in the shaded area (bands) of Figure 2. These bands are defined through the result of the AMIAS solution for the Bates/Mainz data set. The shaded band shows the envelope that accommodates all possible solutions that are compatible with the experimental data with  $1\sigma$  (68%) confidence level. These uncertainty bands are model independent.

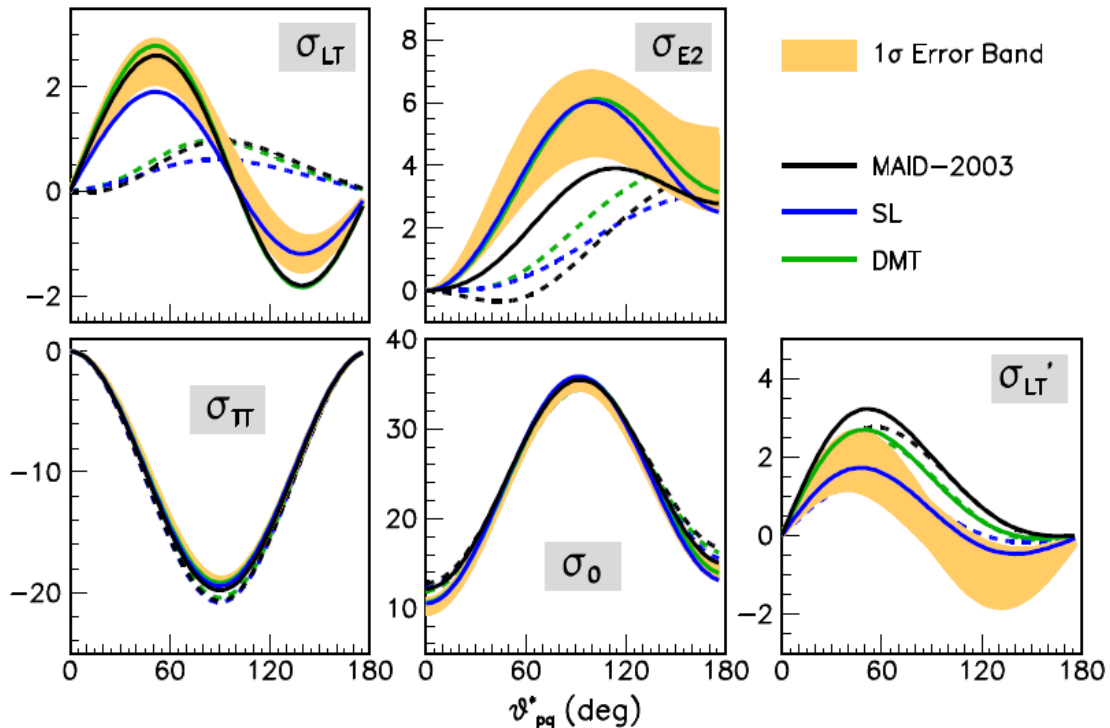


**Figure 2:** The experimentally allowed region for the partial cross sections for  $Q^2 = 0.127 \text{ GeV}^2/c^2$  and  $W = 1232 \text{ MeV}$ , as determined by the analysis of the Bates/Mainz data by AMIAS: the orange (shaded) bands depict the allowed region with  $1\sigma$  confidence. The solid curves show the model predictions while the dashed curves show the "spherical" solutions of the same models.

## Conclusions and Future Work

In summary, AMIAS is shown to offer significant advantages over existing methods in determining physical parameters from experimental data, providing model independent answers with maximal precision in terms of the derived Probability Distribution Function for each parameter. Further re-analysis of response functions for a variety of JLab Data at  $Q^2=1.000 \text{ (GeV/c)}^2$  and  $W$  values across the  $\Delta$  Resonance is in progress.

## References

1. C. N. Papanicolas, Eur. Phys. J. A **18**, 141 (2003).
2. E. Stiliaris and C.N. Papanicolas, AIP Vol. **904**, 257 (2007).
3. C.N. Papanicolas and E. Stiliaris, submitted for publication, <http://arxiv.org/abs/1205.6505v1>.
4. E. Amaldi, S. Fubini and G. Furlan: *Pion-Electroproduction*, Springer Tracts in Modern Physics, Vol. 83, Springer Verlag (1979).
5. N.F. Sparveris *et al.*, PRL **94** 022003 (2005) and Phys. Lett. **B 651** 102 (2007).

# Production of neutron-rich nuclei toward the r-process path in peripheral heavy-ion collisions at low energies

George A. Souliotis

*Laboratory of Physical Chemistry, Department of Chemistry and HINP,  
National and Kapodistrian University of Athens, Athens 15771, Greece  
soulioti@chem.uoa.gr*

## Abstract

*The production cross sections of projectile-like fragments from collisions of 15 MeV/nucleon  $^{86}\text{Kr}$  with  $^{64,58}\text{Ni}$  and  $^{124,112}\text{Sn}$  were measured using a magnetic separator with emphasis on the neutron-rich isotopes. Neutron pick-up isotopes (with 6-8 neutrons picked-up from the target) were observed with large cross sections. The present results were also compared with our data of the same reactions at 25 MeV/nucleon and show enhanced production of neutron-rich isotopes near the projectile. These reactions involving nucleon exchange offer a novel route to neutron-rich isotopes toward the astrophysical r-process path and the neutron-drip line.*

## Introduction

The investigation of the nuclear landscape toward the astrophysical r-process path and the neutron drip-line have recently received a lot of attention by the nuclear physics community. Intimately related to this endeavor is the efficient production of very neutron-rich nuclides which constitutes a central issue in current and future rare isotope beam facilities. Neutron-rich nuclides are produced by spallation, fission and projectile fragmentation. In addition, reactions of nucleon exchange prevailing at beam energies from the Coulomb barrier to the Fermi energy (20–40 MeV/nucleon) [1] can lead to very neutron rich products. Detailed experimental data in this energy range are scarce, mostly due to the complex procedure of identification and separation. Our previous studies of projectile fragments from the reactions of 25 MeV/nucleon  $^{86}\text{Kr}$  on  $^{64}\text{Ni}$  [2] and  $^{124}\text{Sn}$  [3] indicated substantial production of neutron-rich fragments. To advance our understanding of the reaction mechanisms and, furthermore, motivated by recent developments at several facilities, we undertook experimental studies at 15 MeV/nucleon [4] outlined in this contribution.

## Experimental results

We performed mass spectrometric measurements of production cross sections of neutron-rich projectile fragments from the reactions of a 15 MeV/nucleon  $^{86}\text{Kr}$  beam with  $^{64}\text{Ni}$ ,  $^{58}\text{Ni}$  and  $^{124}\text{Sn}$ ,  $^{112}\text{Sn}$  targets [4] (and references therein). In Fig. 1, we present the mass distributions of elements  $Z=35-30$  from the present data (closed circles) of  $^{86}\text{Kr}$  (15 MeV/nucleon) +  $^{64}\text{Ni}$ . We also com-

pare the data with our work [2] on the same reaction at 25 MeV/nucleon (closed diamonds). We also show the cross sections that correspond to high-energy projectile fragmentation of  $^{86}\text{Kr}$  on  $^{64}\text{Ni}$  as predicted by the parametrization EPAX [5]. We observe that the reaction at 15 MeV/nucleon results

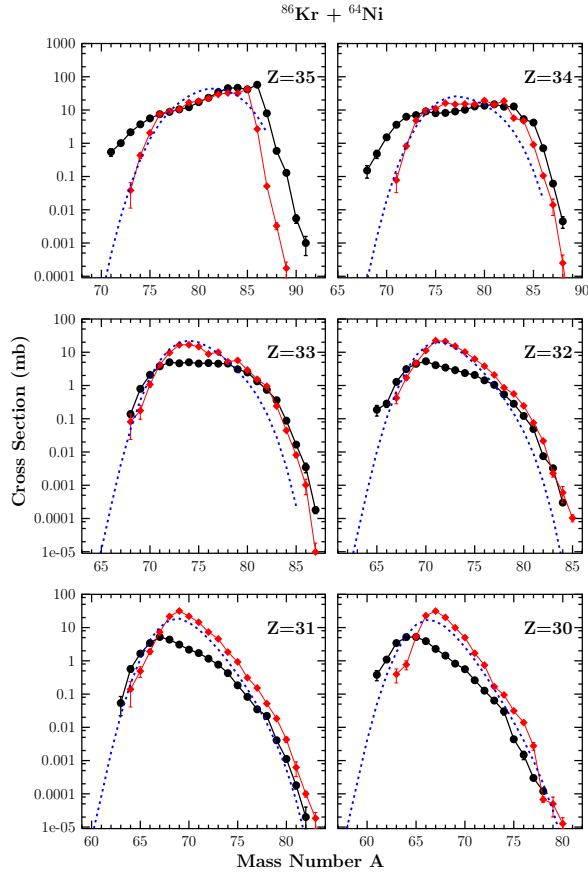


Fig. 1. Mass distributions of elements  $Z=35-30$  from the reaction  $^{86}\text{Kr}$  (15 MeV/nucleon) +  $^{64}\text{Ni}$  of this work (circles) and comparison with those of our previous work [2] at 25 MeV/nucleon (diamonds). Dotted lines: EPAX [5].

in much larger cross sections for products close to the projectile. For, e.g., Br ( $Z=35$ ), the most neutron-rich neutron-pickup isotopes are by a factor of 10 (or larger) more abundantly produced at 15 MeV/nucleon than at 25 MeV/nucleon. As we move further from the projectile (to lower  $Z$ ), the cross sections of the most neutron-rich products appear to be nearly similar between the two energies. Even if a quantitative interpretation effort is ongoing, qualitatively we can say that for the reactions at 15 MeV/nucleon, lower excitation energies of the primary fragments and larger interaction times for the most peripheral collisions may be responsible for the production and survival of residues with a large number of neutrons picked up from the target.

A comprehensive presentation of the production cross sections of the projectile-like fragments from the 15 MeV/nucleon reaction  $^{86}\text{Kr} + ^{64}\text{Ni}$  on the  $Z$  vs  $N$  plane is given in Fig. 2. We observe that the neutron pickup products from

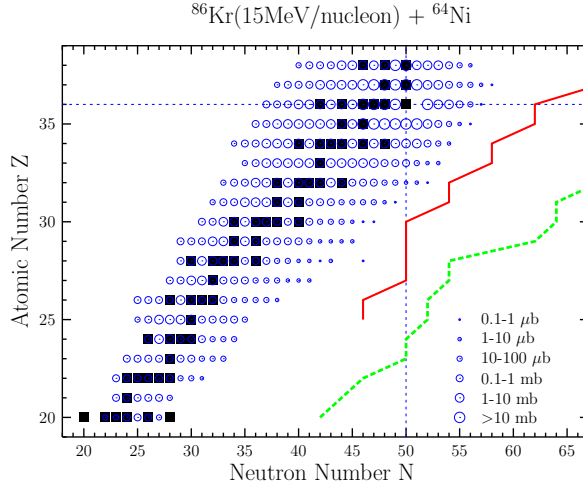


Fig. 2. Representation of the production cross sections of projectile fragments from the reaction  $^{86}\text{Kr}$  (15 MeV/nucleon) +  $^{64}\text{Ni}$  on the  $Z$ - $N$  plane. The cross section ranges are shown by open circles according to the key. The closed squares show the stable isotopes. The solid line shows the astrophysical  $r$ -process path and the dashed line shows the neutron drip-line [6]. The horizontal and vertical dashed lines indicate, respectively, the proton and neutron number of the  $^{86}\text{Kr}$  projectile.

the  $^{86}\text{Kr}$  projectile approach the path of the  $r$ -process near  $Z=32$ – $34$ . We can expect that an increase of the production rates by about  $10^3$  (by a factor of 100–200 in beam intensity and 5–10 in target thickness) may allow accessing the  $r$ -process path nuclei in the region  $Z=30$ – $36$ . From a practical standpoint, we may conclude that the large production cross section of neutron-rich nuclides, and, especially, the multi-neutron pick-up possibility can render these reactions a promising route to produce extremely neutron-rich nuclides near and beyond the  $r$ -process path.

The author wishes to thank M. Veselsky, A. Keksis, B.C. Stein, S. Galanopoulos, M. Jandel, D.V. Shetty and S.J. Yennello for the help and support on the experimental work at 15–25 MeV/nucleon at Texas A&M.

## References

- [1] M. Veselsky and G. A. Souliotis, Nucl. Phys. **A 872**, 1 (2011).
- [2] G. A. Souliotis et al., Phys. Lett. B **543**, 163 (2002).
- [3] G. A. Souliotis et al., Phys. Rev. Lett. **91**, 022701 (2003).
- [4] G. A. Souliotis et al., Phys. Rev. C **84**, 064607 (2011).
- [5] K. Summerer, B. Blank, Phys. Rev. C **61**, 034607 (2000).
- [6] P. Moller, J.R. Nix and K.L. Kratz, At. Data Nucl. Data Tables **66**, 131 (1997).

## Transfer reactions at REX-ISOLDE: The $^{66}\text{Ni}(d,p)^{67}\text{Ni}$ experiment.

N. Patronis<sup>1</sup>, J. Diriken<sup>2</sup>, A. Andreyev<sup>3</sup>, S. Antalic<sup>4</sup>, V. Bildstein<sup>5</sup>, A. Blazhev<sup>6</sup>, Y. Blumenfeld<sup>7</sup>, B. Bruyneel<sup>6</sup>, I.G. Darby<sup>2</sup>, H. De Witte<sup>2</sup>, J. Elseviers<sup>2</sup>, M. Eriksson<sup>7</sup>, V. Fedosseev<sup>7</sup>, T. Georgiev<sup>8</sup>, R. Gernhauser<sup>5</sup>, A. Herlert<sup>7</sup>, M. Huyse<sup>2</sup>, J. Jolie<sup>6</sup>, T. Kroell<sup>9</sup>, R. Krucken<sup>5</sup>, R. Lutter<sup>10</sup>, B.A. Marsh<sup>7</sup>, T. Mertzimekis<sup>11</sup>, D. Mucher<sup>5,6</sup>, R. Orlandi<sup>3</sup>, A. Pakou<sup>1</sup>, E. Piselli<sup>7</sup>, R. Raabe<sup>1</sup>, P. Reiter<sup>6</sup>, T. Roger<sup>1</sup>, M. Seidlitz<sup>6</sup>, M. Seliverstov<sup>2,7</sup>, E. Siesling<sup>7</sup>, T. Stora<sup>7</sup>, H. Tornqvist<sup>8</sup>, J. Van de Walle<sup>7</sup>, P. Van Duppen<sup>2,7</sup>, D. Voulot<sup>7</sup>, N. Warr<sup>6</sup>, F. Wenander<sup>7</sup> and K. Wimmer<sup>5,12</sup>

<sup>1</sup>Department of Physics and HINP, The University of Ioannina, Ioannina, Greece

<sup>2</sup>Instituut voor Kern-en Stralingsfysica, K.U. Leuven, Celestijnenlaan200D, B-3001 Leuven, Belgium

<sup>3</sup>School of Engineering, University of the West of Scotland, Paisley, PA1 2BE, United Kingdom

<sup>4</sup>Department of Nuclear Physics and Biophysics, Comenius University, Bratislava, SK-84248, Slovakia

<sup>5</sup>Technische Universität München, James-Frank-Str., D-85748 Garching, Germany

<sup>6</sup>Institut für Kernphysik, Zülpicher Straße 77, 50937 Köln, Germany

<sup>7</sup>ISOLDE, CERN, CH-1211 Geneva 23, Switzerland

<sup>8</sup>CSNSM-IN2P3-CNRS, Université Paris-Sud 11, 91405 Orsay, France

<sup>9</sup>Institut für Kernphysik, Technische Universität Darmstadt, Germany

<sup>10</sup>Fakultät für Physik, Ludwig-Maximilians-Universität München, 85748 Garching, Germany

<sup>11</sup>Institute of Nuclear Physics, N.C.S.R. "Demokritos", GR-15310, Athens, Greece

<sup>12</sup>National Superconducting Cyclotron Laboratory, Michigan State University, East Lansing, Michigan 48824, USA

### Abstract

*First results from the  $^{66}\text{Ni}(d,p)^{67}\text{Ni}$  experiment performed at REX-ISOLDE - CERN are presented. In this experiment, the newly built T-REX particle detection system was successfully coupled to the  $\gamma$ -ray MINIBALL detector array towards a better understanding and studying of the single particle character of the neutron rich Ni isotopes.*

### Introduction

Theoretical studies indicate that the size of shell gaps can alter when changing the N/Z ratio leading to changes in magic numbers when going away from the line of stability. One of the most interesting regions of the chart of nuclides is around  $^{68}\text{Ni}$ . The observation of the high excitation energy of the first  $2^+$  state of this nucleus [1], in combination with the minimum in the systematics of  $B(E2; 2^+ \rightarrow 0^+)$  [2,3], has led to interpretations in terms of a harmonic oscillator subshell closure. On the other hand, the two-neutron separation energies in the N=40 region do not present any irregularity - characteristic of a shell closure [4,5]. In view of this controversial experimental evidence, the single particle character of the  $^{67}\text{Ni}$  has been decided to be investigated.

In the last four decades the one-nucleon transfer reactions have been proved to be the workhorse for the deduction of spectroscopic information for nuclei at or near the valley of stability. Nowadays, the development of radioactive ion beams allows access to nuclei that were previously unapproachable. Accordingly, the excitation spectrum of  $^{67}\text{Ni}$  was studied by performing the  $^{66}\text{Ni}(d,p)^{67}\text{Ni}$  reaction study in inverse kinematics with an energy of 3 MeV/u.

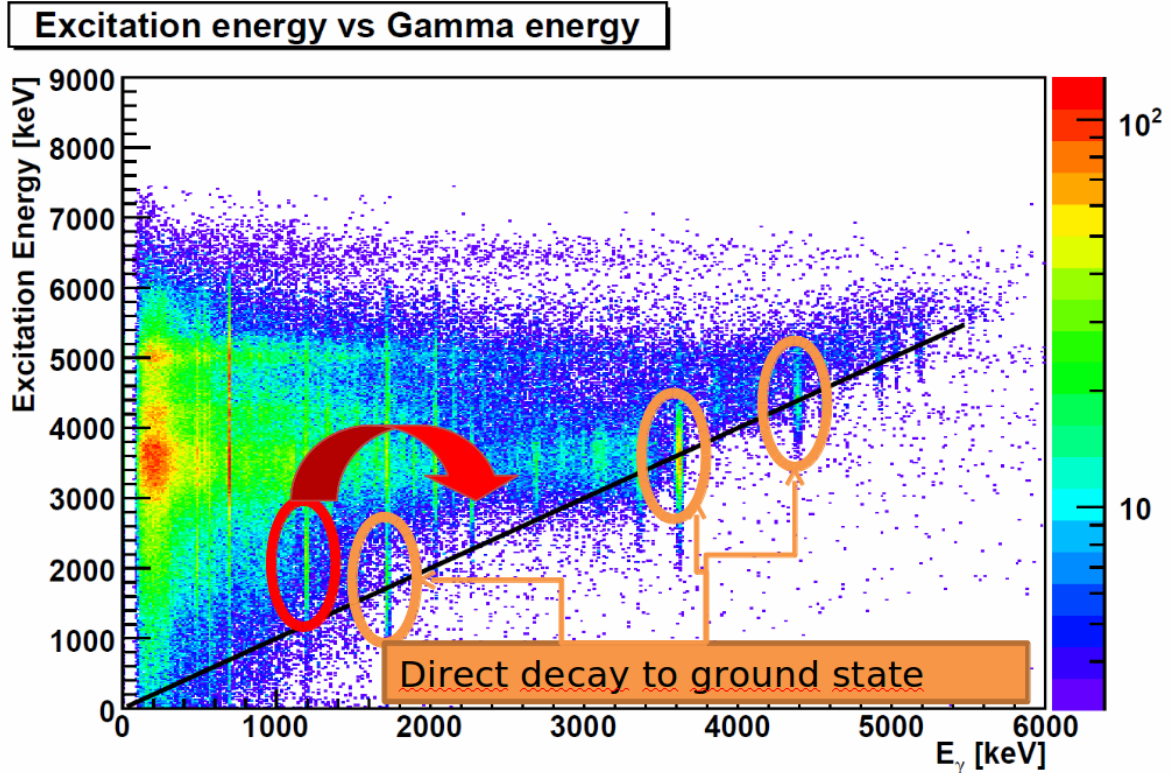


Figure 1: The excitation energy of the residual nucleus ( $^{67}\text{Ni}$ ) as deduced from the kinetic energy of the protons plotted together with the  $\gamma$ -ray energy detected in coincidence with the the protons. The transitions that de-excite directly to the ground state are lying across the diagonal (black line). Other populated levels that de-excite through an intermediate level are lying above the diagonal (e.g. the 2.2 MeV state indicated with the red circle).

### Experimental setup

The experiment was performed at REX-ISOLDE (CERN) where the  $^{66}\text{Ni}$  beam was produced by using the 1.4 GeV proton beam from the CERN PS Booster. The proton beam was impinging on an Ucx target. The produced Ni atoms were selectively ionized by using the RILIS laser ion source and accordingly were mass separated in the ISOLDE general purpose separator. The post-acceleration to 2.95 MeV/u was utilized by the REX-ISOLDE linear accelerator after bunching and charge breeding.

Afterwards, the  $^{66}\text{Ni}$  beam with intensity  $10^6$  pps was sent to the T-REX [6] transfer setup surrounded by the MINIBALL  $\gamma$ -ray detector array [7]. T-REX consists of position sensitive  $\Delta E$ - $E$  telescopes allowing for the detection and identification of the light targetlike reaction products. The solid angle coverage of T-REX amounts to 58.5% of  $4\pi$  solid angle. The thickness of the  $\text{CD}_2$  target was  $100 \mu\text{gr}/\text{cm}^2$ . The minimal thickness of the secondary target ensured the best possible energy resolution in the determination of the excitation energy of the residual nuclei.

### Results

By recording the proton kinetic energy and the  $\gamma$ -ray energies from the  $^{66}\text{Ni}(d,p)^{67}\text{Ni}$  reaction levels up to the excitation energy of 6 MeV were identified. The excitation energy of the residual nucleus was deduced from the kinetic energy of the protons. From the p- $\gamma$  coincidence

data it was possible to improve significantly the resolution of the excitation energies. This can be seen also in Fig. 1 where the coincidence data are presented in the form of excitation energy vs  $\gamma$ -ray energy. As can be seen the superior energy resolution of the detected  $\gamma$ -rays facilitated

the accurate determination of the excitation energies. From the analysis we have done so far more than 13 levels have and more than 35  $\gamma$ -ray lines been observed for the first time. Beside the previously mentioned spectroscopic information, by recording the angular distribution of the detected protons the spin and parity of the populated levels can be identified as well as the relative spectroscopic factors. This part of the analysis is still in progress.

### References:

1. R. Broda et al., **Phys. Rev. Lett.** **74**, 868 (1995).
2. O. Sorlin et al., **Phys. Rev. Lett.** **88**, 092501 (2002).
3. N. Bree et al., **Phys. Rev. C** **78**, 047301 (2008).
4. C. Guenaut et al., **Phys. Rev. C** **75**, 044303 (2007).
5. S. Rahaman et al., **Eur. Phys. J. A** **34**, 5 (2007).
6. V. Bildstein et al., **Eur. Phys. J. A** **48**, 1 (2012).
7. J. van de Walle et al., submitted to **Eur. Phys. Jour. A** (2012).

# Large Volume Spherical Proportional Counter: Development and Applications

I Savvidis<sup>1</sup>, I Giomataris<sup>2</sup>, E Bougamont<sup>2</sup>, S Aune<sup>2</sup>, M Chapelier<sup>2</sup>, Ph Charvin<sup>2</sup>, P Colas<sup>2</sup>, J Derre<sup>2</sup>, E Ferrer<sup>2</sup>, G Gerbier<sup>2</sup>, M Gros<sup>2</sup>, P Mangier<sup>2</sup>, XF Navick<sup>2</sup>, P Salin<sup>3</sup>, J D Vergados<sup>4</sup>

<sup>1</sup>Aristotle University of Thessaloniki, Greece

<sup>2</sup>IRFU, Centre d'études de Saclay, 91191 Gif sur Yvette CEDEX, France

<sup>3</sup>LSBB, Franc

<sup>4</sup>University of Ioannina, Greece

## Abstract

*A large volume (1m<sup>3</sup>) spherical proportional counter has been developed. The high voltage is applied to a small sphere 15mm in diameter, located in the center of the counter and the wall of the counter is grounded. The resolution of the detector has been measured using <sup>222</sup>Rn gas, in order to have the response of the total active volume of the detector (FWHM less than 2% at 5.5 MeV). The energy threshold has been pushed down to about 25 eV and single electrons are clearly collected and detected. The very low noise, the limited wall effect, the good resolution and the high sensitivity are some of the advantages of the detector. The above characteristics give the possibility for several applications of the spherical proportional counter a) Ultra low energy and single electron detection, b) Reactor neutrino and supernova neutrino detection, c) Relativistic atmospheric neutron detection, d) Low flux neutron detection.*

## 1. Introduction

The Spherical Proportional Counter, recently developed, is a novel concept with very promising features, among which is the possibility of easily instrumenting large target masses with good energy resolution and low energy threshold. The natural radial focusing of the spherical geometry allows collecting and amplifying the deposited charges by a simple and robust detector using a single electronic channel to read out a large gaseous volume. There is increasing interest of such massive low-background, low-energy threshold detectors in particle astrophysics for searching the origin of Dark Matter in our universe or studying low-energy neutrino physics [1,2,3]. The detector can successfully measure very low neutron fluxes ( $10^{-6}$  n/cm<sup>2</sup>/s, for thermal neutrons), providing the neutron energy spectrum from thermal up to several MeV at ground and underground level. The large spherical geometry drift (1m<sup>3</sup>), the very good energy resolution (<2% at 5.5 MeV alpha particles) and the simple electronics (one channel reading) are some of the advantages of the detector. Other potential applications requiring large volume of about 10 m in radius are described in detail in reference [4,5]

## 2. The detector

The detector consist of a copper sphere, 1.3 m in diameter and 6mm thick (figure 1). The spherical vessel is well pumped (up to  $10^{-8}$  mbar) and then is filled with a gas mixture at a pressure from several hundreds of mbars up to 5 bars. Out gassing in the order of  $10^{-9}$  mbars/s is necessary for the amplification stability, because the present of the O<sub>2</sub> in the drift volume changes the detector characteristics.

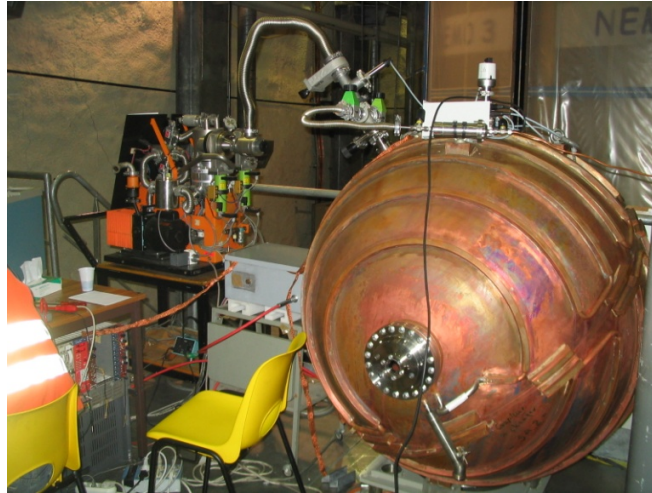


*Figure 1. A photograph of the spherical vessel*

A small stainless ball of 14 centimeter in diameter fixed in the center of the spherical vessel by a stainless steel rod, acts as an electrode with positive high voltage and as a proportional amplification counter. The detector was operated with positive bias applied to the anode (inner sphere) while the cathode (external sphere) remained at ground potential

### 3. The energy resolution

The energy resolution of the detector has been tested using  $^{222}\text{Rn}$  gas and detecting the alpha particles from  $^{222}\text{Rn}$  and  $^{222}\text{Rn}$  daughters. The gas mixture consist of Ar (98%) and  $\text{CH}_4$ (2%) at pressures, from 150 mbars up to 1 bar. The high voltage vary from 1.5 kV up to 5 kV depending on the gas pressure.

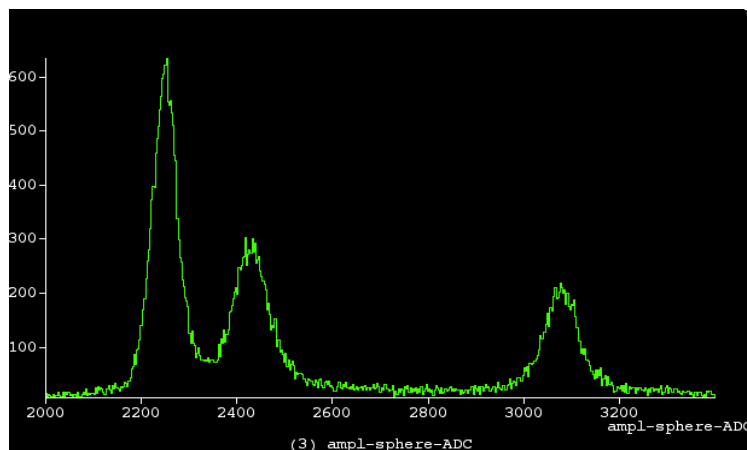


*Figure 2. The peaks observed from a  $^{222}\text{Rn}$  radioactive source. From left to right we observe the  $^{222}\text{Rn}$  peak at 5.5 MeV, the  $^{218}\text{Po}$  and  $^{214}\text{Po}$  at 6.0 MeV and 7.7 MeV respectively.*

In the figure 2 is shown the peaks observed from a  $^{222}\text{Rn}$  radioactive source. From left to right we observe the  $^{222}\text{Rn}$  peak at 5.5 MeV, the  $^{218}\text{Po}$  and  $^{214}\text{Po}$  at 6.0 MeV and 7.7 MeV respectively. The energy resolution was 2% FWHM at 200 mbar gas pressure and 2.8 kV High Voltage.

### 3. Low energy calibration and results

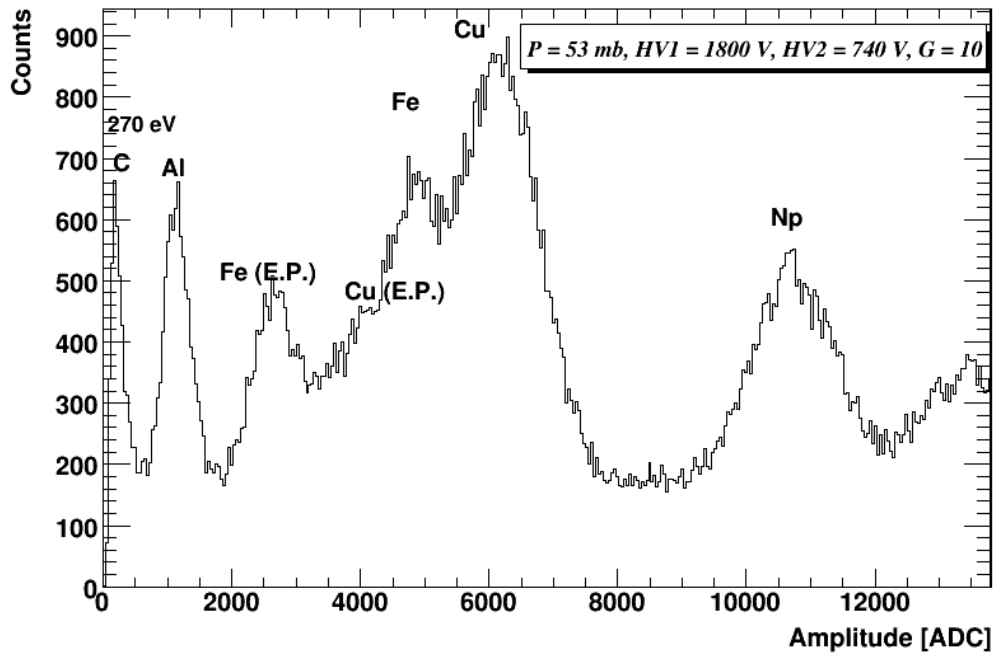


**Figure 3.** Peaks observed from the  $^{241}\text{Am}$  radioactive source through aluminium and polypropylene foil. On the left the Carbon (270 eV) peak is shown, followed by the Aluminium peak (1.45 keV), the escape peak (E.P.) of Iron in Argon (3.3 keV), the escape peak of Copper in Argon (5 keV), the Iron peak (6.4 keV), the Copper peak (8 keV) and the Neptunium peak (13.93keV) .

In order to create lower energy Xrays we have used an  $^{241}\text{Am}$  source in contact a 20  $\mu\text{m}$  thick aluminum foil. We were able to fluoresce the K Xrays ranging from Aluminium whose K electron has a binding energy of 1.56 keV, to Cu whose K electron has a binding energy of 8.98 keV. In order to obtain even lower energy calibration lines we replaced the aluminum foil by a thinner 10  $\mu\text{m}$  one and we attached a 20  $\mu\text{m}$  polypropylene foil (figure 3).

#### References:

1. Giomataris I and Vergados J D **Nucl.Instrum.Meth.A** **530** 330-58(2004)
2. Giomataris I and Vergados J D **AIP Conf.Proc.** **847** 140-6(2006)
3. Giomataris I and Vergados J D **Phys.Lett.B** **634** 23-9(2006)
4. I. Giomataris *et al.* **Nucl.Phys.Proc.Suppl.****150**:208-213(2006)
5. S. Aune *et al.*, **AIP Conf.Proc.****785**:110-118(2005)

## **CASTOR: A Calorimeter for Heavy Ions at LHC.**

X. Aslanoglou, for the CMS/CASTOR group.

*Department of Physics, The University of Ioannina, Ioannina, Greece.*

### **Abstract**

In the search for Strange Quark Matter (SQM) and Exotic objects in Heavy Ion collisions at high energy, a new Electromagnetic - Hadronic calorimeter, the CASTOR (Centaurus And Strange Objects Research) calorimeter has been constructed and is now in operation at the experiment CMS, at the LHC collider at CERN. The detector is designed for the detection of Strange and Exotic objects at heavy ion collisions and has been taking data since 2009.

### **Introduction**

Heavy Ion collisions at high energies have attracted the interest of Nuclear Physicists for the last twenty years. A new community has been formed in Physics, the Heavy Ion community, served by both Nuclear and High Energy Physicists. The most powerful collider, the Large Hadron Collider, has been constructed at CERN and has been operating since 2009. Having a circumference of 27 Km and crossing the borders between Switzerland and France (in what used to be the LEP collider tunnel), it accelerates protons to an energy  $T=7$  TeV per beam, or heavy ions to the equivalent energy of 5.5 TeV/A. The scheduled time for proton to heavy ion beams is eleven months per year to one.

Four experiments, ATLAS, CMS, ALICE and LHCb, will run in different crossing points of the beams. Three of these experiments will mainly run p-p beams for High Energy Physics research, while the fourth (ALICE) is dedicated in heavy ion collisions. Even so, the experiment CMS (Compact Muon Solenoid) has an active heavy ion group, which will operate during the corresponding beam time.

### **Heavy Ion Collisions – QGP.**

The main physics phenomenon under investigation at ultra relativistic heavy ion collisions is the achievement of a state of deconfined quarks and gluons, the Quark Gluon Plasma (QGP). This is a phase transition between nuclear matter state, in which quarks are confined into hadrons (Hadronic state) and a state, in which the quarks are deconfined in a volume of nuclear size. The achievement of this state depends on the baryonic density and the temperature.

This process has all the characteristics of a usual phase transition: as energy is added to the system, the temperature rises. When the transition begins, the temperature stays constant until all the quarks are deconfined, and then the temperature rises again. This state will only live for about  $10^{-22}$  s and then the hadronization follows, in which the quarks are bound in hadrons again and the system cools down to nuclear matter.

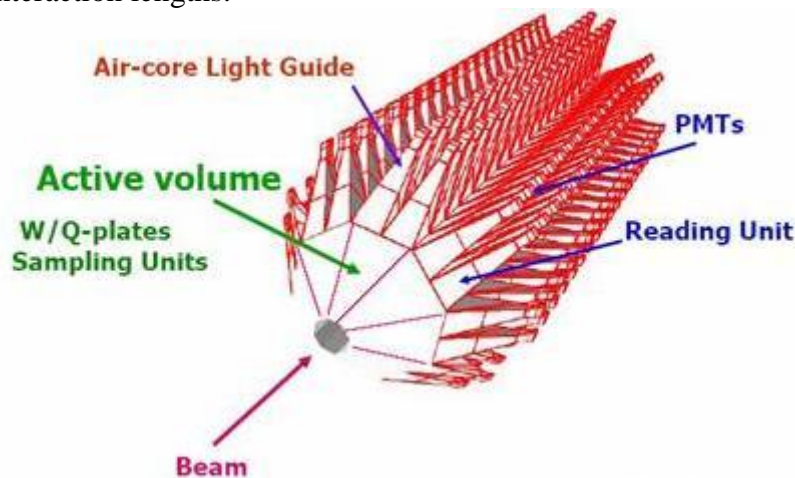
Although the phenomenology of the QGP formation and decay is very rich, the formation of Strange Quark Matter (SQM) is thought to be a unique signature of the phase transition. In the recombination process, a final state consisting of more than three quarks with enhanced strangeness, could be formed.

## The CASTOR calorimeter

The CASTOR calorimeter (CentauRO And Strange Object Research) was conceived and proposed for the H. I. Physics Program at the LHC. It is designed for potential discovery of “New Physics” such as “CentauRO” and “Strangelets”, in addition to “mainstream” Physics. It has been adopted for very forward pp Physics studies.

The calorimeter uses Tungsten ( $d=19 \text{ g/cm}^3$ ) as absorber and the active material which produces the measured light, are Quartz plates (Q). Since electrons and gamma rays lose their energy faster than hadrons, the first part serves as Electromagnetic calorimeter and the rest serves as Hadronic.

The W plates have a thickness of 5 mm each, followed by a Q-plate of thickness 2 mm. A high energy particle hitting the W plate loses energy by creating a shower of electrons. These electrons of relativistic energy interact with the subsequent Q-plate, thus creating Cherenkov radiation. Both the W and Q plates are divided in eight octants. Because the maximum light output of the Cherenkov radiation occurs at angle  $45^\circ$  with respect to the incoming particle, the plates, with trapezoidal shape, are inclined by  $45^\circ$  with respect to the impinging particles. Every seven W and Q plates are bunched together in a reading unit in which, the light created at this part of the calorimeter is measured by Photomultipliers (PMT) via two air-core light guides (Fig. 1). There are 12 rows of reading units in the Hadronic section plus 2 in the EM section, making the total number channels 448 and the total length 13.62 m, or 10 interaction lengths.



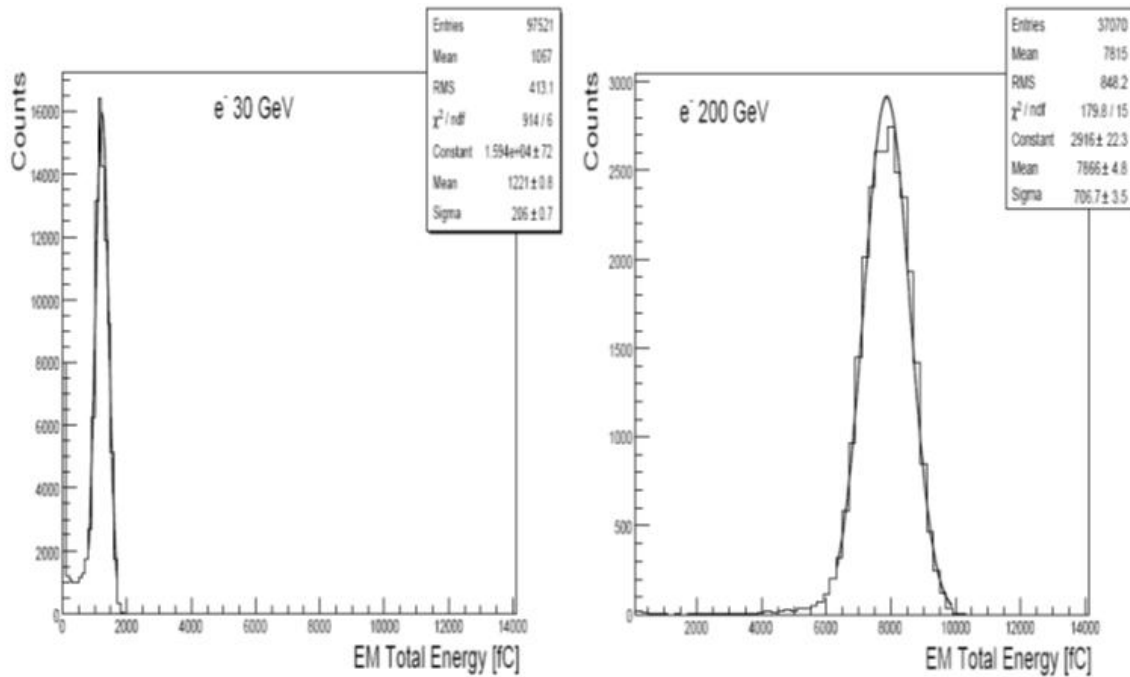
The CASTOR calorimeter

According to a model for strangelet production, we expect the emission of these particles to come from the baryon rich region of the QGP fireball. Monte Carlo simulations of the Baryonic number distribution showed that strange particles are emitted within about two units of pseudorapidity ( $5.3 < \eta < 7.3$ ). This range corresponds to an angular range  $0.08^\circ$  to  $0.57^\circ$ . Thus, CASTOR is placed at a distance 14.4 m from the interaction point and in order to cover that pseudorapidity range.

## CASTOR beam tests

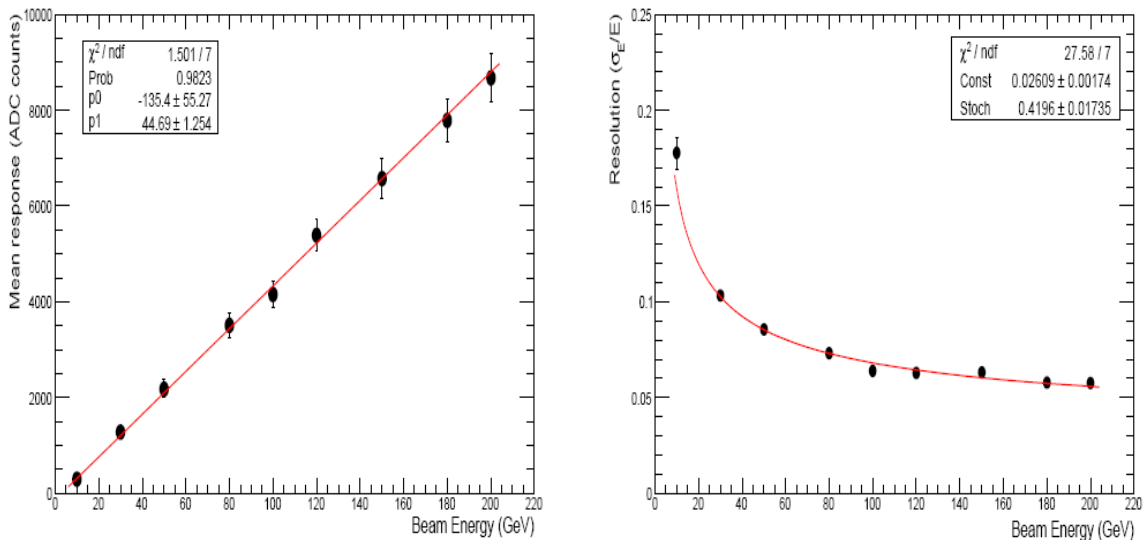
Successive beam tests were performed for different CASTOR prototypes to test the performance of the system under electron and hadron beams, in the years 2003, 2004, 2007 and 2009. All beam tests were performed at the accelerator SPS at CERN, by utilizing electron

beams of energy from T=20 to 220 GeV and pion beams of energy from from T=50 to T=180 GeV.



Energy spectrum of 30 GeV and 200 GeV electrons

The beam test data showed a good behavior of the instrument in both kind of particles, with good resolution and linear response.



Energy dependence of the light response and the resolution for electrons

The CASTOR calorimeter was integrated in the CMS experiment in fall 2009, and is taking both pp and heavy ion data since. The HI data are still under analysis.

# Optical Potential and Relevant Reaction Mechanisms at near barrier energies

Athena Pakou

*Department of Physics and HINP, The University of Ioannina, Ioannina, Greece*

## Abstract

*The present work provides a short survey of a comprehensive study on  ${}^{6,7}\text{Li} + {}^{28}\text{Si}$  performed the last ten years by the NPL-Ioannina group and in collaboration with researchers from Saclay, INFN-Italy-Warsaw University and Catania. The experimental work was hosted mainly at NSCR Demokritos and partly at LNS-Catania and includes elastic scattering angular distribution and elastic backscattering studies as well as studies on the reaction mechanisms involved (breakup-transfer-fusion) at near barrier energies. Selected results are discussed.*

When studying elastic scattering between two stable ions at energies well above the Coulomb barrier, it is adequate to ignore specific effects due to couplings to other reaction channels. It is then plausible to describe scattering by phenomenological or folding potentials which vary slowly with energy. This picture no longer remains valid when approaching the vicinity of the Coulomb barrier. Couplings between various channels increase in importance and in describing elastic scattering, either these couplings have to be taken into account through coupled channel theories, or the energy dependence of the various optical model parameters has to be considered explicitly. For weakly bound systems coupling effects due to breakup and/or transfer are expected to be intense, while the energy dependence of the optical potential parameters should differ strongly from parameters associated with well bound systems. Therefore to probe the potential at near- and sub-barrier energies interpreting elastic scattering and fusion cross sections, the full knowledge of all mechanisms involved is necessary. In this respect, during the last 10 years the systems  ${}^{6,7}\text{Li}+{}^{28}\text{Si}$  have been thoroughly investigated and elastic scattering, transfer, breakup and fusion cross sections as a function of energy were measured. Recently the elastic backscattering technique was proposed by our group as a valuable complementary tool to the conventional elastic scattering angular distribution technique for probing the optical potential even at energies below the barrier. Our experimental results, although supported to some extent by the theoreticians collaborating with our group, mainly Krzysztof Rusek and partly by Nick Keeley from the Warsaw University and the Soltan Nuclear Reaction Institute, are open to the community and offer a valuable playground for applying a self-consistent theoretical approach able to interpret all appearing phenomena. The light even-even target of silicon with its moderately simple structure can facilitate this approach, as inelastic couplings are not expected to modify in a large extend the results and breakup and transfer could be isolated and tested as the major contributors to coupling effects. This work was supported financially by two programs – PUTHAGORAS I and HRAKLEITOS II and enriched our scientific profile with 15 publications (Pakou et al.<sup>1</sup>, Zerva et al.<sup>2</sup> )

The following major conclusions have been obtained from this research:

1. The optical potential threshold anomaly is different for weakly bound nuclei than the well bound ones with an imaginary potential which persists till very low sub-barrier energies, but it evolves in a different way for the  ${}^6\text{Li}$  and  ${}^7\text{Li}$  projectiles.

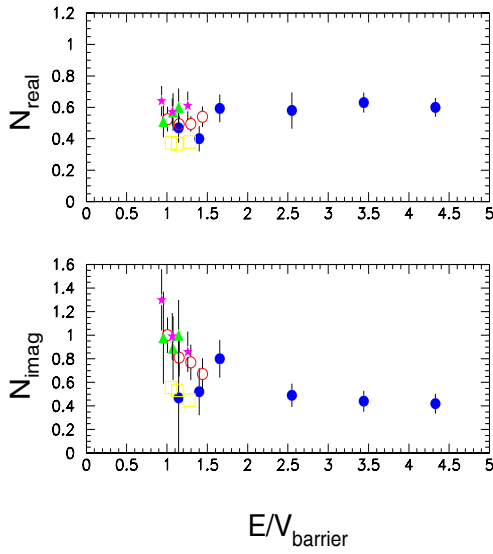


Figure 1: The energy dependence of the real (top) and imaginary (bottom) optical potential for  ${}^6\text{Li}$  on various projectiles as appears in PLB556(2003)26.

2. The validity of the dispersion relation in the phenomenological description of the potential at near barrier energies is questioned.
3. The fusion of light weakly bound nuclei at near and sub-barrier energies follows simple one barrier tunneling probability rules.
4. Transfer of weakly bound nuclei is a strong mechanism at near and sub-barrier energies but should compete with breakup in a “destructive” way giving to the energy dependence of the potential a smooth evolution.

As it can be seen from Figure 1, where the energy dependence of the optical potential for  ${}^6\text{Li}$  on various targets is presented, at barrier the behaviour of the potential is very different from the well known for well bound

projectiles. The real potential develops in a smooth way at, and below, barrier where for well bound nuclei a bump appears, and the imaginary part presents an increasing trend approaching the barrier where for the well bound ones a drop to zero occurs. Backscattering measurements, to be described by Zerva et al. in these proceedings have shown that if the dispersion relation connecting the real and imaginary part persists then the bump appears at very low energies (Figure 2 right). This should then be connected with the increasing behavior of the transfer as predicted by Continuum Discretized Coupled Channel (CDCC)

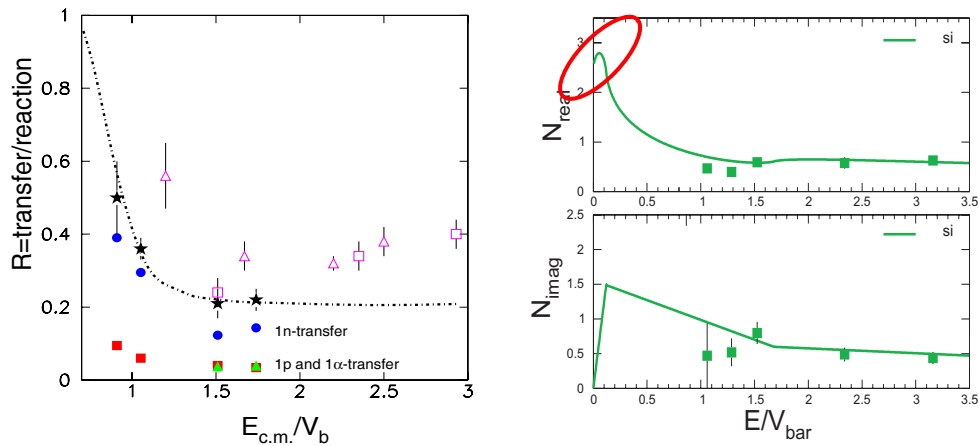


Figure 2 : (Left) Ratios of transfer versus total reaction cross sections as a function of energy for  ${}^6\text{Li}+{}^{28}\text{Si}$  as appears in the internal report [http://physics.npl/preprints/internal\\_NPL08\\_1.pdf](http://physics.npl/preprints/internal_NPL08_1.pdf). The line is due to CDCC calculations.

(Right) The energy dependence of the  ${}^6\text{Li}+{}^{28}\text{Si}$  potential as appears in EPJA 48 ,102(2012).

calculations shown in Figure 2 at the left. However it is hard to believe that at those low energies transfer channels are open, therefore we turn to conclude that the dispersion relation

may not be valid for weakly bound nuclei in these phenomenological descriptions. Similar conclusions are drawn for the  ${}^7\text{Li}+{}^{28}\text{Si}$  system. The absence of the conventional threshold anomaly for weakly bound nuclei and the validity of the dispersion relation was questioned several years ago by G. R. Satchler<sup>3</sup>. After 20 years of the Satchler report and 10 years work in this laboratory, we are in a position to support these theories experimentally. However, despite all the existing data, an open question related with the reaction mechanisms and their involvement in the optical potential anomaly persists. Although we know without doubt from the point of view of experiment (see figure 2) that transfer is the strongest reaction mechanism at the barrier and we know well from the theoretical point of view that couplings to continuum can adequately describe elastic scattering data, we have do not have yet obtained a concrete theory to describe quantitatively the “mixing” between a strong transfer channel and a weaker breakup channel which lead to the new phenomenon of anomalies for weakly bound nuclei concerning variations between different projectiles and variations with the conventional threshold anomaly.

## References

1. A. Pakou et al., **Phys. Lett. B556**, 21 (2003).
2. A. Pakou et al., **Phys. Rev. Lett. 90**, 202701 (2003).
3. A. Pakou et al., **Phys. Rev. C 69**,057602 (2004).
4. A. Pakou et al., **Phys. Rev. C 69**,054602 (2004).
5. A. Pakou et al., **Phys. Rev. C 71**,014603 (2005).
6. A. Pakou et al., **Journal of Phys. G 31**,S1723 (2005).
7. A. Pakou et al., **Phys. Rev. C 73**, 051603 (2006.)
8. A. Pakou et al., **Phys. Lett. B633**, 691 (2006).
9. A. Pakou et al., **Nucl. Phys. A784**, 13 (2007).
10. A. Pakou et al., **Phys. Rev. C 76**, 054601 (2007)
11. A. Pakou et al., **Phys. Rev. C 78**, 067601 (2008)
12. A. Pakou et al., **Eur. Phys. Journal A39**, 187 (2009).
13. K. Zerva et al., **Phys. Rev. C 80**, 017601 (2009)
14. K. Zerva et al, **Phys. Rev. C**, 044607 (2010)
15. K. Zerva et al, **Eur. Phys. Journal 48**, 102 (2012).
16. G. R. Satchler, **Phys. Rep. 199**, 147 (1991).

## Fusion Cross Sections of ${}^8\text{B}+{}^{28}\text{Si}$ at near barrier energies

A. Pakou<sup>1</sup>, E. Stiliaris<sup>2</sup>, D. Pierroutsakou<sup>3</sup>, M. Mazzocco<sup>4</sup>, N. Alamanos<sup>5</sup>, A. Boiano<sup>3</sup>, C. Boiano<sup>6</sup>, D. Filipescu<sup>7</sup>, T. Glodariu<sup>7</sup>, J. Grebosz<sup>8</sup>, A. Guglielmetti<sup>9</sup>, M. La Commara<sup>10</sup>, C. Parascandolo<sup>11</sup>, A. M. Sanchez-Benitez<sup>12</sup>, C. Signorini<sup>4</sup>, R. Silvestri<sup>10</sup>, O. Sgouros<sup>1</sup>, F. Soramel<sup>4</sup>, E. Strano<sup>4</sup>, L. Stroe<sup>7</sup>, V. Soukeras<sup>1</sup>, D. Toressi<sup>4</sup>, K. Zerva<sup>1</sup>

*1 Department of Physics and HINP, The University of Ioannina, 45110 Ioannina, Greece*

*2 Institute of Accelerating Systems and Applications and Department of Physics, University of Athens, Greece*

*3 INFN - Sezione di Napoli, via Cinthia, I-80126 Napoli, Italy*

*4 Dipartimento di Fisica and INFN - Sezione di Padova, via F. Marzolo 8, I-35131 Padova, Italy*

*5 CEA-Saclay, DAPNIA-SPhN, Gif-sur-Yvette, France*

*6 Universita' degli Studi di Milano and INFN - Sezione di Milano, via Celoria 16, I-20133 Milano, Italy*

*7 "Horia Hulubei" National Institute of Physics and Nuclear Engineering, Romania*

*8 IFJ-PAN, Krakow, Poland*

*9 Universita' degli Studi di Milano and INFN - Sezione di Milano, via Celoria 16, I-20133 Milano, Italy*

*10 Dipartimento di Scienze Fisiche and INFN - Sezione di Napoli, via Cinthia, I-80126 Napoli, Italy*

*11 Dipartimento di Fisica and INFN - Sezione di Padova, via F. Marzolo 8, I-35131 Padova, Italy*

*12 Departamento de Física Aplicada, Universidad de Huelva, Huelva, Spain*

*Fusion cross sections were measured for  ${}^8\text{B} + {}^{28}\text{Si}$  at near barrier energies by detecting the alpha particles produced in the evaporation process. Preliminary results and comparisons with cross sections obtained by other weakly bound projectiles on various targets are discussed.*

Fusion of nuclei, this important process for energy production and the synthesis of the world can in principle be understood as a quantum tunneling effect of two structureless objects in a potential depending only on the distance between their centers. Under this scenario it can be described by one barrier penetration models (BPM)<sup>1</sup>. However at near barrier energies and for complex nuclei, the influence of static and dynamic effects, relevant to the detailed structure of both projectile and target nuclei and the reaction mechanisms involved, strongly alter this image and fusion cross sections below and near barrier energies can be interpreted via coupled-channel formalisms<sup>2</sup>. More pronounced effects are expected for halo nuclei –static effects due to halo and dynamical effects due to their weakly bound nature. While our knowledge on fusion with neutron rich light projectiles starts to build up<sup>3</sup> studies with proton rich nuclei are scarce. Only one fusion measurement at sub - barrier energies on  ${}^8\text{B}+{}^{58}\text{Ni}$  was recently reported<sup>4</sup>.

${}^8\text{B}$  is a proton drip line beta decaying nucleus, attracting a strong interest due to its role in the production of high energy neutrinos in the sun and its unusual structure with a possible proton halo. The last issue is still in an exploratory stage since the Coulomb force may prevent the growth of the halo and push the proton inside the Coulomb barrier. Therefore it is interesting to test the behavior of this nucleus in a fusion process and compare it with the one presented by other weakly bound nuclei on various targets. It should be noted that the first fusion measurement of  ${}^8\text{B}$  on nickel reports for sub- and near- barrier energies very large fusion cross sections compatible with a BPM prediction only after an elongation of the interaction radius by 26%. This experimental finding should be also confronted for other targets.

Due to the very low counting rate of the beam produced at Legnaro as a cocktail of  ${}^8\text{B}$ ,  ${}^7\text{Be}$  and  ${}^6\text{Li}$  nuclei (similar beams are produced at Riken and Notre Dame), special tools had to be invoked to perform a fusion measurement. For that we have adopted the idea of total reaction cross section measurements, where a silicon detector is used as an active target and

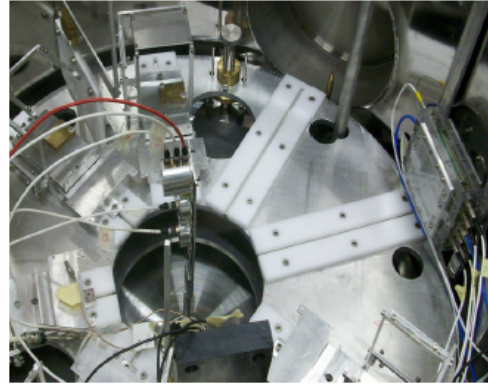
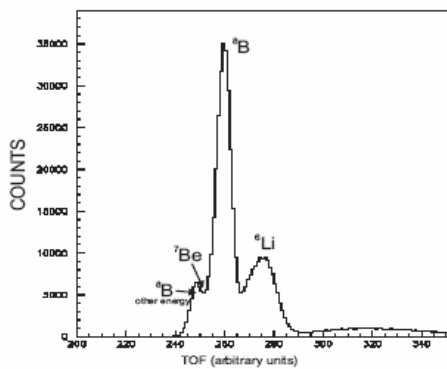


Figure 1: (Left) TOF spectrum between a beam profiler before the entrance of the chamber in a distance of 1.2m and the first stage of the target-detector. (Right) An experimental setup photo. In the middle is seen the triple telescope-target and at the right one of the two beam profilers.

the detector itself acts as a calorimeter. This active target technique was used in this study for a fusion measurement, taking into consideration that during the collision of  $^8\text{B}$  with silicon, neither the breakup nor a transfer process can produce alpha particles, but an evaporation process. The transfer of 3 protons and a neutron to silicon is considered highly improbable and in any case the high  $Q$  value of the reaction of 12.3 MeV could have given the opportunity of discrimination between alpha's from a transfer and alphas from fusion, kinematically. By using a stack of three detectors instead of one, the discrimination of alpha particles was possible via a conventional  $\Delta E$ - $E$  technique, which also prevents any contribution from frame scattering, a usual problem in this type of measurements. For the pileup rejection, special techniques were adopted and will be described in a forthcoming paper.

Our experimental setup is shown in the photo of Figure 1. Two beam profilers allowed the reconstruction of the beam and its beam spot on the target-detector. For our data reduction, two dimensional plots were formed for the alpha particle identification  $E_1 \% E_2+E_3$  ( $E_1 \sim 45\mu\text{m}$ ,  $E_2 \sim 45\mu\text{m}$ ,  $E_3 \sim 2000\mu\text{m}$ ). Alphas were integrated with a contour in the bidimensional spectrum, a TOF window on boron projectiles (see Figure 1 to the right) and a contour on the beam spot on the target. A small contamination in the TOF window of the boron beam from lithium projectiles was estimated to give only a  $\sim 0.25\%$  contribution on the produced alpha's due to lithium collisions while the contribution due to beryllium collisions even much smaller. Alpha's were normalized to the boron beam particles and evaporation reaction probabilities relevant to the alpha channels at each projectile energy  $E$ , were formed by dividing the alphas with the elastic boron particles. The reduction of the data for the determination of integrated cross sections and then to the reaction cross section of the alpha particles via recursion relations are described in detail in our previous publication on total reaction cross sections<sup>5</sup>. Our fusion cross sections are compared in Figure 2-left- with Cascade and Wong calculations. Finally these results with the appropriate reduction according to the prescription reported by Canto et al.<sup>6</sup> are compared with previous results of stable and radioactive weakly bound projectiles on various targets (Figure 2 –right). The observed suppression at the higher energies could be attributed, to coupled channel effects and or to incomplete fusion. Our results are not compatible with previous results on  $^8\text{B}+^{58}\text{Ni}$  in the overlapping energy region and therefore to a large fusion radius as the ones reported for the nickel target. The large cross sections obtained in these data below and above the barrier are explained by the authors via a model based on an angular momentum limit. It is not straight forward however the differences seen between the two targets and this fact need further

investigation. As a general comment we can point out the remarkable fact that most of the data present an excellent compatibility between their selves and the uff curve, that is results of

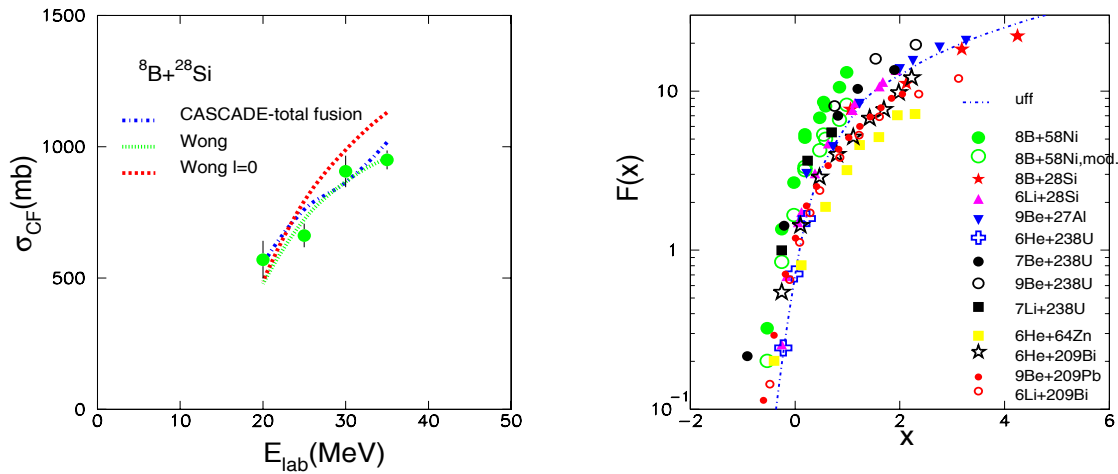


Figure 2: (Left) Fusion cross sections for  ${}^8B+{}^{28}Si$ , designated with the green circles are compared with CASCADE and WONG calculations. (Right) Fusion functions of the present data as a function of reduced energies according to the prescription of Canto et al.<sup>6</sup> are compared with previous data<sup>3,7</sup> with various targets and projectiles and the universal fusion function *uff*.

weakly bound but stable projectiles, weakly bound and radioactive and well bound. Some of the data like  ${}^8B+{}^{58}Ni$  and the  ${}^6He+{}^{64}Zn$  scatter above and below the *uff* curve creating a deviation band of 60%. These deviations need further investigation, while they may have been caused due to special features of such hard measurements. For all data, small deviations between their selves and the *uff* curve could be attributed to coupled channel effects not considered in this study.

## References

1. C. Y. Wong, *Phys. Rev. Lett.* **31**, 766 (1973).
2. C. H. Dasso, S. Landowne, A. Winther; *Nucl. Phys. A* **405**, 381(1983); D. Castro-Rizzo and N. Alamanos, *Nucl. Phys.* **443**, 525 (1985).
3. A. Yoshida et al., *Phys. Lett. B* **389**, 457(1996); J. J. Kolata et al., *Phys. Rev. Lett.* **81**, 4580(1998); C. Signorini et al., *Nucl. Phys. A* **735**, 329 (2004); R. Raabe et al., *Nature* **431**, 823 (2004); A. Di Pietro et al., *Phys. Rev. C* **68**, 044613 (2004); A. Lemasson et al., *Phys. Rev. Lett.* **103**, 232701 (2009).
4. E. F. Aguilera et al., *Phys. Rev. Lett.* **107**, 092701 (2011).
5. A. Pakou, A. Musumarra, D. Pierroutsakou et al., *Nucl. Phys. A* **784**, 13 (2008).
6. L. F. Canto, P. R. S. Gomes, J. Lubian, L. C. Chamon, E. Crema, *Nucl. Phys. A* **821**, 51 (2009).
7. A. Pakou et al., *Eur. Phys. J A* **39**, 187 (2009); G. V. Marti et al., *Phys. Rev C* **71**, 027602 (2005).

**Acknowledgement:** The research leading to these results has received funding from the European Union Seventh Framework Program FP7/2007- 2013 under Grant Agreement nB° 262010 - ENSAR. The EC is not liable for any use that can be made on the information contained herein.

# Elastic backscattering measurements and optical potential analysis for the systems ${}^{6,7}\text{Li} + {}^{58}\text{Ni}$ , ${}^{116,120}\text{Sn}$ , ${}^{208}\text{Pb}$ at sub- and near-barrier energies

K. Zerva<sup>1</sup>, A. Pakou<sup>1</sup>, N. Patronis<sup>1</sup>, N. Alamanos<sup>2</sup>, A. Di Pietro<sup>3</sup>, P. Figuera<sup>3</sup>, M. Fisichella<sup>3</sup>, T. Glodariu<sup>4</sup>, N. Keeley<sup>5</sup>, M. La Commara<sup>6</sup>, M. Mattuada<sup>3</sup>, M. Mazzocco<sup>7</sup>, A. Musumarra<sup>3</sup>, A. Sanchez Benitez<sup>8</sup>, V. Scuderi<sup>3</sup>, E. Strano<sup>3</sup>, M.G. Pellegriti<sup>3</sup>, D. Pieroutsakou<sup>6</sup>, K. Rusek<sup>9</sup>

<sup>1</sup> Department of Physics, The University of Ioannina, Greece

<sup>2</sup> DSM/IRFU/SPhN CEA SACLAY, 91191 Gif-sur-Yvette, France

<sup>3</sup> INFN-LNS, Catania, Italy

<sup>4</sup> National Institute for Physics and Nuclear Engineering (NIPNE), Romania

<sup>5</sup> The Andrzej Soltan Institute for Nuclear Studies and Warsaw University, Poland

<sup>6</sup> Dipartimento di Scienze Fisiche and INFN, Università di Napoli, Italy

<sup>7</sup> Dipartimento di Fisica and INFN, Università di Padova, Italy

<sup>8</sup> University of Huelva, Spain

<sup>9</sup> Heavy Ion Laboratory, University of Warsaw and The Andrzej Soltan Institute for Nuclear Studies and Warsaw University, Poland

## Abstract

We have performed elastic backscattering measurements for the weakly bound nuclei  ${}^{6,7}\text{Li}$  on medium and heavy mass targets  ${}^{58}\text{Ni}$ ,  ${}^{116,120}\text{Sn}$  and  ${}^{208}\text{Pb}$  for  $E_{c.m.}/V_{bar.} = 0.6$  to  $1.3$ . Excitation functions of elastic scattering cross-sections have been measured at  $\pm 160^\circ$  and  $\pm 170^\circ$  and the corresponding ratios to Rutherford scattering and relevant barrier distributions have been extracted.

## Introduction

Over the last decade, considerable interest has been focused on the energy dependence of the optical potential at sub- and near-barrier energies for reactions involving weakly bound nuclei [1–7]. Our efforts should be intensified in order to determine the potential till very low energies. The elastic backscattering, as a tool for probing the energy dependence of the potential was first applied to the weakly bound nuclei  ${}^6\text{Li}$  and  ${}^7\text{Li}$  scattered by the light target  ${}^{28}\text{Si}$  [8, 9]. Our goal in this work is to systematically probe the potential and the importance of coupling effects at near barrier energies by extending our backscattering measurements to medium and heavy targets  ${}^{58}\text{Ni}$ ,  ${}^{116,120}\text{Sn}$ ,  ${}^{208}\text{Pb}$ .

## Experimental details and data reduction

Beams of  ${}^{6,7}\text{Li}$  were delivered by the SMP Tandem accelerator of LNS in Catania in the energy range  $0.6$  to  $1.3 V_{bar.}$  The beams impinged on  $\sim 200 \mu\text{g}/\text{cm}^2$  thick  ${}^{58}\text{Ni}$ ,  ${}^{116,120}\text{Sn}$ ,  ${}^{208}\text{Pb}$  targets. The overall normalization was estimated via a measurement of the Rutherford scattering in two silicon detectors set at  $\pm 20^\circ$ . Excitation functions of (quasi-)elastic backscattering events were recorded in four telescopes, set at  $\pm 160^\circ$  and  $\pm 170^\circ$ .

Ratios of the (quasi-)elastic cross-sections to Rutherford were formed as follows:

$$\frac{\sigma_{el}(160^\circ)}{\sigma_{Ruth}} = \frac{N_{160^\circ}}{N_{20^\circ}} \frac{\sigma_{Ruth}(20^\circ)}{\sigma_{Ruth}(160^\circ)} \frac{\Omega_{20^\circ}}{\Omega_{160^\circ}}$$

where  $N_{20}$ ,  $N_{160}$  are the (quasi-)elastic scattering total counts in the forward and backward detectors and  $\Omega_{20}$ ,  $\Omega_{160}$  are their respective solid angles. Ratios at  $170^\circ$ , were also deduced and mean ratios between  $160^\circ$  and  $170^\circ$  were formed. The corresponding barrier distributions were determined by the following relation using a point-difference formula [10] for extracting

the derivative:  $D_{el}(E) = -\frac{d}{dE} \left[ \sqrt{\frac{d\sigma_{el}}{d\sigma_{Ruth}}(E)} \right]$

## Optical model analysis

The linear segment model for the imaginary part of the optical potential,  $W(E)$ , was applied according to G.R. Satchler [11]. The starting point is the imaginary potential, which is

described in the following by lines drawn from higher to lower energies. The real potential is calculated via dispersion relations. In the case of the  ${}^7\text{Li}$  projectile, trials were also performed with a flat real potential not obeying the dispersion relations. In order to systematically probe the optical potential of all systems we followed the same standard procedure:

1. Draw a straight line to define the imaginary potential above the Coulomb barrier, consistent with previous experimental data extracted via an optical-potential analysis of angular distribution data
2. Define the energy point where a second line should be drawn with positive or negative slope.
3. Define the slope of the second line which is drawn down to very low energies close to zero, changing it from negative slopes (conventional threshold anomaly) to more positive ones.
4. Define the last energy point, where the imaginary potential drops to zero, changing it from higher to lower energies up to a point beyond which the fit is not any more sensitive to potential changes.
5. (If the final fit is not satisfactory.) Iterate between 1 to 4, changing the first point, the slope, the second point or even the height of the first flat line until we have the best  $\chi^2$ .

On figures 1, 2 we present some of the trial potentials and the corresponding barrier distributions for the systems  ${}^6,7\text{Li}$  at  ${}^{58}\text{Ni}$ ,  ${}^{116,120}\text{Sn}$  and  ${}^{208}\text{Pb}$  targets. In all cases the thick black line corresponds to the best fit.

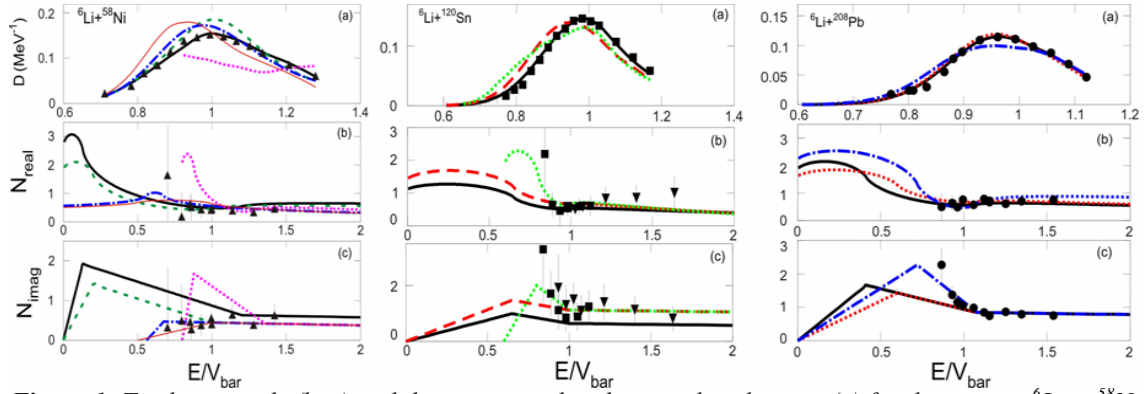


**Figure 1:** Trial potentials (b, c) and the corresponding barrier distributions (a) for the systems  ${}^6\text{Li}$  at  ${}^{58}\text{Ni}$ ,  ${}^{116,120}\text{Sn}$  and  ${}^{208}\text{Pb}$

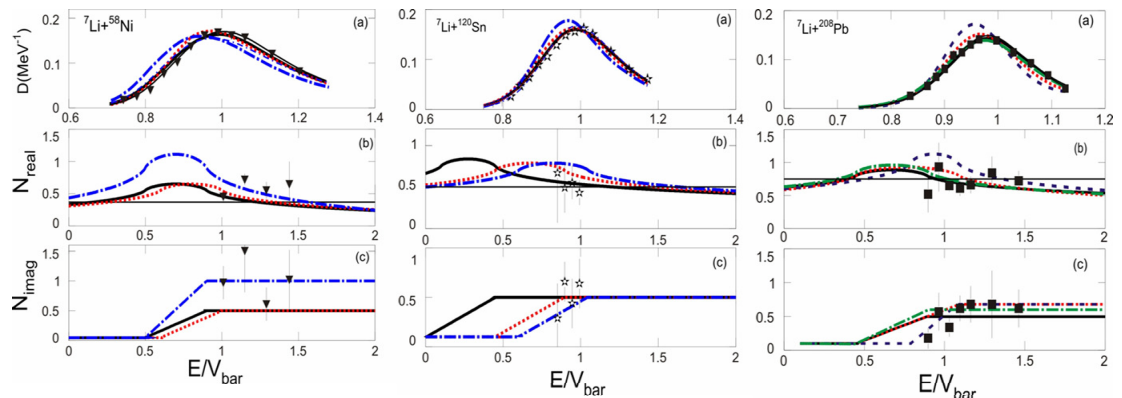


**Figure 2:** Trial potentials (b, c) and the corresponding barrier distributions (a) for the systems  ${}^7\text{Li}$  at  ${}^{58}\text{Ni}$ ,  ${}^{116,120}\text{Sn}$  and  ${}^{208}\text{Pb}$

## Reaction mechanisms

In this work we have performed Continuum Discretized Coupled Channel (CDCC) calculations for  ${}^6,7\text{Li} + {}^{58}\text{Ni}$ ,  ${}^{120}\text{Sn}$  and  ${}^{208}\text{Pb}$ . It was assumed that the nucleus  ${}^6\text{Li}$  ( ${}^7\text{Li}$ ) has a two-body  $\alpha+d$  ( $\alpha+t$ ) cluster structure. Couplings between resonant and non-resonant cluster

states were included. The backscattering results are presented in figure 3 and are compared with the CDCC calculations. It is seen that for all cases coupling to the continuum improves the description of the barrier distributions.

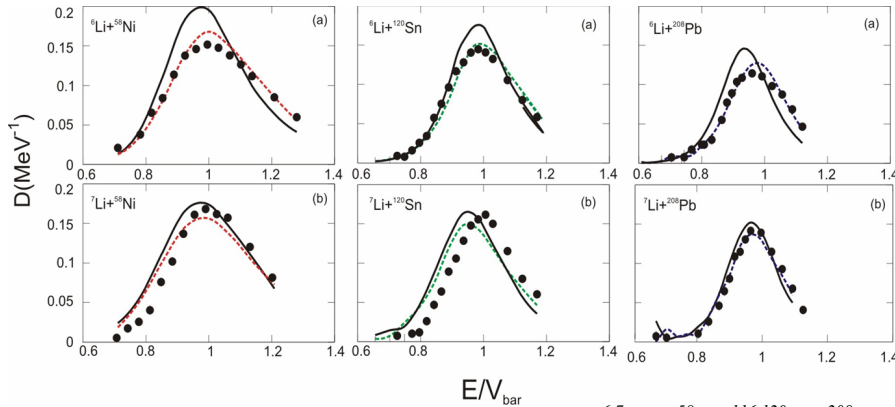


**Figure 3:** Experimental data of barrier distributions for the systems  ${}^6,{}^7\text{Li} + {}^{58}\text{Ni}$ ,  ${}^{116,120}\text{Sn}$ ,  ${}^{208}\text{Pb}$  are compared with fresco CDCC calculations. Solid lines refer to uncoupled calculation while the dashed lines represent coupling channel calculations to continuum.

## Conclusions

The backscattering technique is a valuable tool for predicting in a complementary way, the optical potential at sub-barrier energies. For weakly bound nuclei the imaginary potential persists either with an increasing trend ( ${}^6\text{Li}$ ) or a flat behaviour ( ${}^7\text{Li}$ ) to sub-barrier energies. For  ${}^6\text{Li}$  the rising part has the largest slope for the heavier targets and the smallest slope for the lighter ones, possibly indicating in a qualitative interpretation that the competition between breakup and transfer or some compound procedure at energies at the barrier is in favour of breakup. The energy where the imaginary potential drops to zero is not located at the barrier but at sub-barrier energies. This behaviour raises some questions about the validity of the dispersion relation because the bump at the real potential occurs at very low sub-barrier energies, around  $0.1\text{-}0.2 V_{\text{bar}}$ . It is hardly credible that at these energies such an enormous real dynamical polarization potential can be generated. For  ${}^7\text{Li}$ , while the backscattering technique also proves to be a valuable tool for predicting the potential at very low sub-barrier energies, it is not sensitive enough to distinguish between a potential obeying the dispersion relation and one which does not, although the trend is in favour of the second scenario.

## References:

1. N. Rowley et al., **Phys. Lett. B** **373**, 23 (1996).
2. K. Washiyawa, K. Hagino, M. Dasgupta, **Phys. Rev. C** **73**, 034607 (2006).
3. M. Dasgupta, D. Hinde, N. Rowley, A. Stefanini, **Annu. Rev. Nucl. Part. Sci.** **48**, 401 (1998).
4. L.F. Canto, P.R.S. Gomes, R. Donangelo, M.S. Hussein, **Phys. Rep.** **424**, 1 (2006).
5. N. Keeley, R. Raabe, N. Alamanos, J.L. Sida, **Prog. Part. Nucl. Phys.** **59**, 579 (2007).
6. N. Keeley, N. Alamanos, K.W. Kemper, K. Rusek, **Prog. Part. Nucl. Phys.** **63**, 396 (2009).
7. N. Rowley, G.R. Satchler, P.H. Stelson, **Phys. Lett. B** **254**, 25 (1991).
8. K. Zerva et al., **Phys. Rev. C** **80**, 017601 (2009).
9. K. Zerva et al., **Phys. Rev. C** **82**, 044607 (2010).
10. E. Piasecki et al., **Phys. Rev. C** **65**, 054611 (2002).
11. G.R. Satchler, **Phys. Rep.** **199**, 147 (1991).

## Acknowledgments:

*This research has been co-financed by the European Union (European Social Fund – ESF) and Greek national funds through the Operational Program "Education and Lifelong Learning" of the National Strategic Reference Framework (NSRF) - Research Funding Program: Heracleitus II. Investing in knowledge society through the European Social Fund.*

## Study of the reaction $^{20}\text{Ne}+^{28}\text{Si}$ : Elastic scattering at near barrier energies

V. Soukeras<sup>1</sup>, O. Sgouros<sup>1</sup>, A. Pakou<sup>1</sup>, I. Strojek<sup>2</sup>, A. Trzcinska<sup>2</sup>, N. Alamanos<sup>3</sup>, N. Keeley<sup>4</sup>, M. Mazzocco<sup>5</sup>, N. Patronis<sup>1</sup>, E. Piasecki<sup>2</sup>, K. Rusek<sup>2,4</sup>, E. Stiliaris<sup>6</sup>, K. Zerva<sup>1</sup>.

<sup>1</sup> Department of Physics and HINP, The University of Ioannina, 45110 Ioannina, Greece

<sup>2</sup> Heavy Ion Laboratory, University of Warsaw, Warsaw, Poland

<sup>3</sup> CEA-Saclay, DAPNIA-SPhN, Gif-sur-Yvette, France

<sup>4</sup> The Andrzej Soltan Institute for Nuclear Studies, Warsaw, Poland

<sup>5</sup> Dipartimento di Fisica and INFN - Sezione di Padova, Padova, Italy

<sup>6</sup> Institute of Accelerating Systems and Applications and Department of Physics, University of Athens, Greece

### Abstract

Elastic scattering angular distributions have been measured for the reaction  $^{20}\text{Ne}+^{28}\text{Si}$  at near barrier energies of 42.5, 52.3, 70 MeV. The results were analyzed in optical model framework by using the code ECIS. The basic conclusion was the existence of an anomalous increase of cross section at backward angles.

Elastic scattering of heavy ions is the main tool for investigating the optical model potential. For projectiles like  $^{12}\text{C}$  and  $^{16}\text{O}$ , due to alpha clustering, coupling effects to the elastic scattering are significant and appear as an increase in cross sections at backward angles, which for projectiles with a simple structure is not observable<sup>1-4</sup>. Coupling effects due to  $\alpha$  clustering structure of the target are also significant. In that case, it is known that there is a limit on  $Z$  where this anomaly stops to exist. So, the question is if the increase of cross section at backward angles is persistent for heavier projectiles. Taking into consideration all the above, angular distribution measurements of elastic scattering for the system  $^{20}\text{Ne}+^{28}\text{Si}$  were performed at 3 near barrier energies.

The experimental setup was visualized in ICARE facility of the Heavy Ion Laboratory in Warsaw. ICARE consists of a big chamber with various facilities for setting up numerous detectors. The schematic setup of the experiment is shown in Fig.1. All the detectors, except the 3 telescopes and S1 were fixed. Rotating the telescopes we performed an angular distribution in steps of 5 degrees, while we were able to discriminate elastic scattering from reaction channels via  $dE-E$  technique.

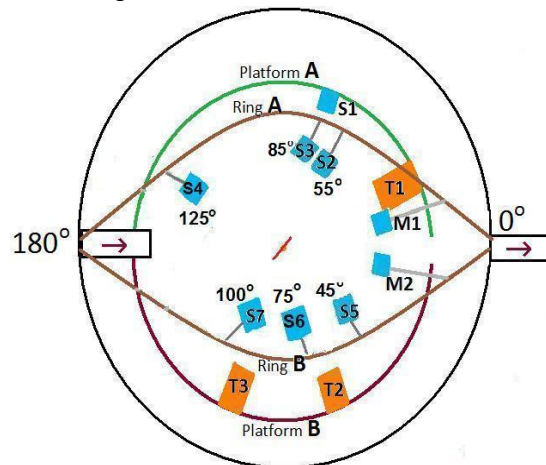


*Fig. 1: The schematic setup of the experiment.*

The cross section is calculated via the following formula (1):

$$\sigma = \frac{N}{(D\Phi)\Omega} \quad (1)$$

where N is the number of counts, D are the scattering centers,  $\Phi$  is the flux of the beam and  $\Omega$  is the solid angle. The  $D\Phi$  quantity is calculated via monitors' information by the known Rutherford scattering using the formula (2):

$$(D\Phi) = \frac{N_{\text{monitor}}}{\sigma_{\text{Ruth}}\Omega_{\text{monitor}}} \quad (2)$$

where the  $N_{\text{monitor}}$  is the number of counts of the monitor,  $\sigma_{\text{Ruth}}$  is the Rutherford scattering cross section and  $\Omega_{\text{monitor}}$  is the solid angle of the monitor. The  $D\Phi$  quantity is determined with a low error because at  $20^\circ$  where the monitors were placed, the statistical errors were not significant. Also, to minimize the error due to the asymmetry of the beam two monitors were used in symmetrical positions. The  $\Omega$  quantity was calculated by the known activity of  $^{241}\text{Am}$  source.

Angular distribution measurements were performed at the low energy of 42.5 MeV, where no increase of cross section is expected at backward angles, to determine the bare potential (Set1 – Fig.2). The elastic scattering data of  $^{20}\text{Ne} + ^{28}\text{Si}$  at energy of 52.3 MeV are presented in Fig. 2, where it is obvious an increase in cross section at backward angles. ECIS calculations were performed to determine a phenomenological optical potential. The obtain parameters in this fitting procedure adopting a Woods-Saxon potential are presented in Fig.2 as Sets 2-3. The parameters of Set 2 were obtained in a free fit using as initial parameters the parameters of Set 1. The Set 3 is a set taking into account a Christensen potential as a real part while a Woods – Saxon imaginary part was fitted to the data<sup>5</sup>. Trials with a surface term were also performed but no important impact at the calculation at our angular range was observed. Similar fits were performed for the data at 70 MeV with no conclusive results. Perhaps, the problem for the 70MeV data rises due to a resonance contribution and may need more elaborated calculations.

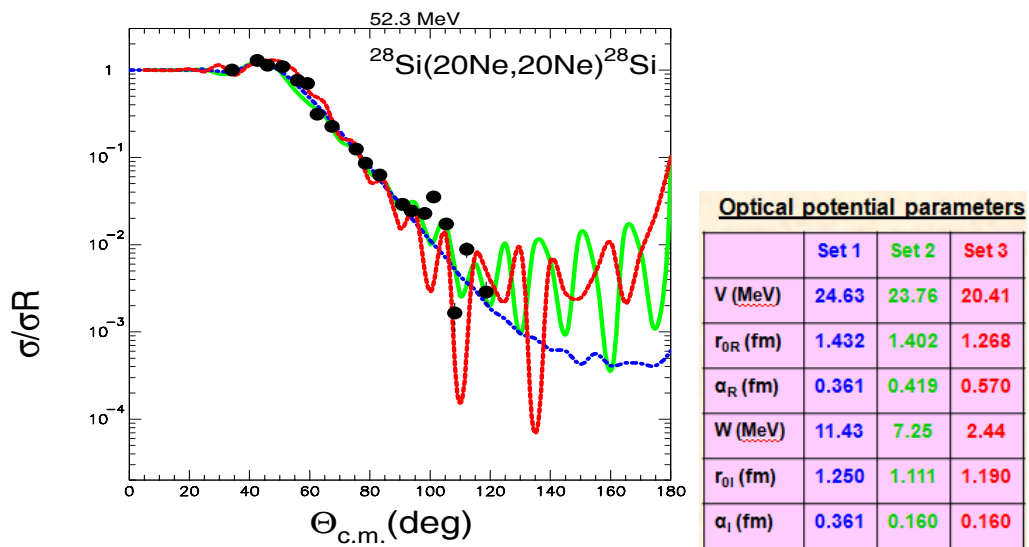


Fig. 2: Present  $^{20}\text{Ne} + ^{28}\text{Si}$  elastic scattering angular distribution data, measured at 52.3 MeV. A prediction with a bare potential is presented with the blue dotted-dashed line (Set 1 at the table). The green solid and red dotted lines are optical model calculations with our best fitted Woods - Saxon potentials (Set 2 and Set 3 at the table). Details for these calculations are included in the text.

These data were also considered in an advanced theoretical context by Nick Keeley for explaining the oscillations through coupling mechanisms<sup>6</sup>. According to these calculations, the backward anomaly cannot be explained by 2 sequential alphas transferred from the target to projectile, but assuming a transfer of a whole  $^8\text{Be}$  between  $^{20}\text{Ne}$  and  $^{28}\text{Si}$ . These calculations are still in progress.

In summary, from the study of the elastic scattering of  $^{20}\text{Ne} + ^{28}\text{Si}$  at energies of 42.5, 52.3 and 70MeV, the following conclusions can be drawn:

1. First of all, the cross section at backward angles and at near barrier energies appear an anomalous increase, as the lighter projectiles  $^{12}\text{C}$  and  $^{16}\text{O}$  do.
2. This increase can be explained by assuming elastic transfer of a  $^8\text{Be}$  cluster between  $^{20}\text{Ne}$  and  $^{28}\text{Si}$ .
3. Phenomenological Woods-Saxon potentials were determined for the lower energies.
4. On the other hand, we can't ignore the fact that: the statistical errors were significant and the angular distribution was limited to a selected angular range. So, it is necessary a further investigation of that system principally at backward angles, using inverse kinematics to increase the cross section.

## References

1. G. S. Mallick et al., **Phys. Rev. C** **73**, 054606 (2006).
2. P. Braun - Munzinger and J. Barrette, **Phys. Reports** **87**, 209 (1982).
3. A. M. Kobos and G. R. Satchler, **Nucl. Phys. A** **427**, 589 (1984).
4. P. Braun - Munzinger et al., **Phys. Rev. C** **24**, 1010 (1981).
5. P.R.Christensen and A.Winther, **Phys. Lett.** **65B**, 19 (1976).
6. N.Keeley, private contact.

## Acknowledgments

This work was performed as a part of the postgraduate program that has been co-financed as a part of the «Scholarship Program by the National Scholarship Foundation, academic year 2011-2012» by funds of the Operation Program “Education and Lifelong Learning” of the European Social Fund and the National Strategic Reference Framework (NSRF).

## Study of the system $^{20}\text{Ne}+^{28}\text{Si}$ : Transfer reactions at near barrier energies

O. Sgouros<sup>1</sup>, V. Soukeras<sup>1</sup>, A. Pakou<sup>1</sup>, I. Strojek<sup>2</sup>, A. Trzcinska<sup>2</sup>, N. Alamanos<sup>3</sup>, N. Keeley<sup>4</sup>, M. Mazzocco<sup>5</sup>, N. Patronis<sup>1</sup>, E. Piasecki<sup>2</sup>, K. Rusek<sup>2,4</sup>, E. Stiliaris<sup>6</sup>, K. Zerva<sup>1</sup>.

<sup>1</sup> Department of Physics and HINP, The University of Ioannina, 45110 Ioannina, Greece

<sup>2</sup> Heavy Ion Laboratory, University of Warsaw, Warsaw, Poland

<sup>3</sup> CEA-Saclay, DAPNIA-SPhN, Gif-sur-Yvette, France

<sup>4</sup> The Andrzej Soltan Institute for Nuclear Studies, Warsaw, Poland

<sup>5</sup> Dipartimento di Fisica and INFN - Sezione di Padova, Padova, Italy

<sup>6</sup> Institute of Accelerating Systems and Applications and Department of Physics, University of Athens, Greece

### Abstract

Angular distribution measurements of one-alpha and two-alpha transfer reactions for the system  $^{20}\text{Ne}+^{28}\text{Si}$  at two near barrier energies, at 53 and 71 MeV, were performed at the HIL laboratory of the University of Warsaw. The results were analyzed in a simple DWBA framework with the code FRESKO, by using as entrance potential the empirical one, suggested from a parallel analysis of the elastic scattering results. The agreement with the data is good for both energies, indicating the validity of the proposed potential.

Transfer calculations are strongly dependent from the entrance potential. Therefore the investigation of transfer reactions, gives us the possibility to validate the proposed optical potential from the analysis of the elastic scattering results. In this respect, angular distribution measurements of one and two alpha transfer reactions for the system  $^{20}\text{Ne}+^{28}\text{Si}$  can be studied as a complementary tool to the elastic scattering, in order to deduce the optical potential. The relevant experiment took place at the Heavy Ion Laboratory of University of Warsaw. In Figure 1, a photo presents ICARE facility which consists of a big chamber with two platforms and several rings that allow someone to place many detectors. In addition, Figure 2 presents a schematical plan of ICARE chamber with the present setup. The two monitors, M1 and M2 were used for normalization purposes while the three telescopes T1, T2 and T3 were the main tool in order to perform the angular distribution and also to discriminate the different reaction products by the standard  $\Delta E$ -E technique.



Figure 1: ICARE chamber

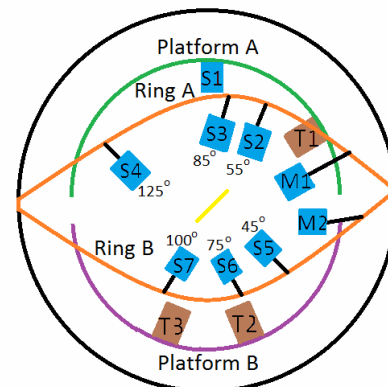


Figure 2: Schematical plan of ICARE chamber with the present setup

In figure 3 we can see a typical two dimensional  $\Delta E$ -E spectrum where apart from the elastic contour ( $Z=10$ ), we can also see the  $^{24}\text{Mg}$  contour ( $Z=12$ ), the  $^{16}\text{O}$  contour ( $Z=8$ ) and even lower the  $^{12}\text{C}$  contour ( $Z=6$ ). The circled areas represent the transfer reaction products. In the  $^{16}\text{O}$  contour the green area represents the one alpha transfer reaction product. In this case an alpha particle is transferred from the projectile to the target. Figure 4 shows a projection on E axis for the  $^{16}\text{O}$  contour. The oxygen peak is well pronounced but the statistics is low. The other pronounced peak is due to oxygen contamination on the target.

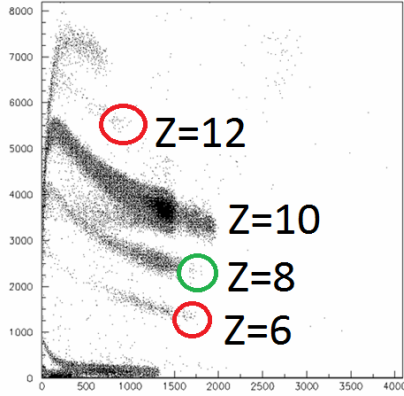


Figure 3: Typical 2-D spectrum, T1 at 33 deg, Ebeam= 53 MeV

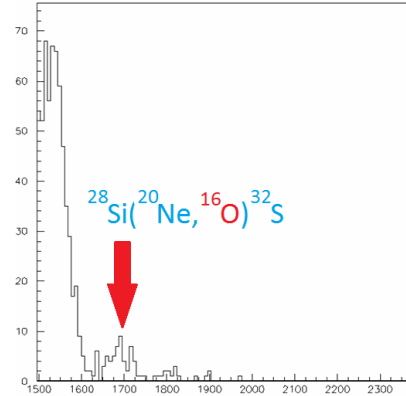


Figure 4: 1-D spectrum, projection on E axis, T1 at 33 deg, Ebeam= 53 MeV

For each reaction channel, cross sections were calculated using the following formula:

$$\sigma = \frac{N}{(D\Phi)\Omega}$$

where N is the number of counts, D is the scattering centers,  $\Phi$  is the flux of the beam and  $\Omega$  is the solid angle.

The  $(D\Phi)$  quantity was calculated via Rutherford scattering as:

$$D\Phi = \frac{N_{monitor}}{\sigma_{Ruth}\Omega_{monitor}}$$

Finally, the solid angle for each detector was calculated by the known activity of  $^{241}\text{Am}$  source.

The data were analyzed in a DWBA<sup>1</sup> framework using code FRESCO<sup>2</sup>. We have assumed the simplest cluster structure for the projectile the  $^{20}\text{Ne}$  nucleus was modeled as an  $^{16}\text{O}$  core and a valence alpha particle. Therefore, our calculations include the binding potential between the  $^{16}\text{O}$  and the alpha<sup>3</sup>, the potential between the  $^{16}\text{O}$  and the  $^{28}\text{Si}$ <sup>4</sup> and the potential between the alpha and the  $^{28}\text{Si}$ <sup>5</sup>. It was also considered the valence particle to be a pure single particle state. That means that only one combination of the core and the target gives the composite nucleus ( $^{20}\text{Ne}$ ). In a more advanced calculation, we have to take into account couplings between the valence and all the possible core states. Such advanced calculations are in progress and they are performed by Dr. Nick Keelay<sup>6</sup>.

In figure 5 we present a simple DWBA calculation for the one alpha transfer reaction  $^{28}\text{Si} (^{20}\text{Ne}, ^{16}\text{O}) ^{32}\text{S}$  at 52.3 MeV. Results using as an entrance potential a Lee-Chan<sup>7</sup> one are denoted we the red solid line, while a prediction with a bare potential as an entrance potential

is denoted with the blue dashed line. It is obvious how sensitive is the transfer calculation while we change the entrance potential. In a similar way, DWBA calculations were performed for the rest of the reactions.

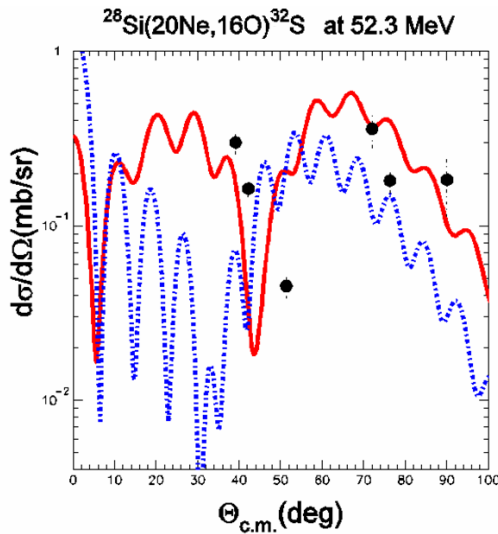


Figure 5: Present angular distribution data for the transfer reaction  $^{28}\text{Si} (^{20}\text{Ne}, ^{16}\text{O}) ^{32}\text{S}$ , measured at 52.3 MeV are compared with simple DWBA calculations. The red and blue lines represent calculations with entrance potentials extracted from best fits to elastic scattering data (Figure 6)

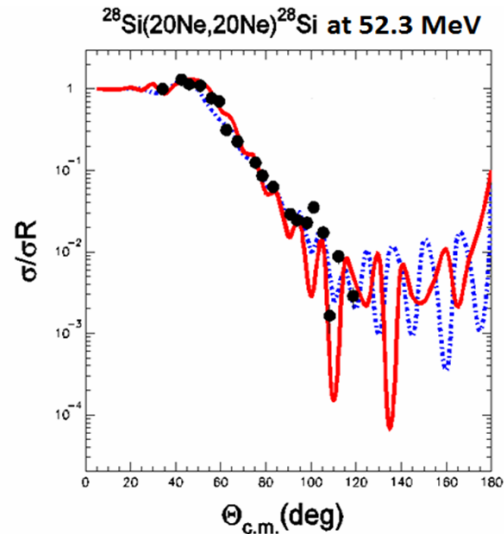


Figure 6: Present angular distribution data for the  $^{20}\text{Ne}+^{28}\text{Si}$  elastic scattering measured at 52.3 MeV. A prediction with a bare potential is denoted with the blue line. The red line represents an optical model calculation with our best fitted wood-Saxon potential

In summary, angular distribution measurements of one-alpha and two-alpha transfer reactions for the system  $^{20}\text{Ne}+^{28}\text{Si}$  were performed at near barrier energies. One and two alpha transfer reaction products were observed and the relevant data were analyzed in a DWBA framework. The agreement with the data is good for both energies, and that indicates the validity of the proposed optical potential.

At this point I should mention that more accurate experimental data and at a larger angular range are necessary in order to extract more useful conclusions.

## References

1. G.R. Satcher, Introduction to Nuclear Reactions, second edition (1990).
2. I.J. Thomson, **Comput.Phys.Rep.** 7, K. Rusek: Private contact.
3. R. Jahn et al, **Phys. Lett.** 65B, (1976).
4. I. Tserruya et al, **Nucl. Phys.** A242, 345 (1976).
5. H. Wojciechowski, **Phys. Rev. C** 72, 044601 (2005).
6. Nick Keelay: Private contact.
7. S.K. Agarwalla et al., **J Phys.G: Nucl.Phys.**32,165 (2006)

## Acknowledgments

This work was performed as a part of the postgraduate program that has been co-financed as a part of the «Scholarship Program by the National Scholarship Foundation, academic year 2011-2012» by funds of the Operation Program “Education and Lifelong Learning” of the European Social Fund and the National Strategic Reference Framework (NSRF).

**Research in the years of the economic crisis: A short review of the recent research activity of the Radiochemical Laboratory of the Aristotle University of Thessaloniki.**

P. Misaelides, F. Noli

*Department of Chemistry, Aristotle University, 54124 Thessaloniki, Greece*

**Abstract**

*This short lecture is going to present the current research activities of the Radiochemical Laboratory of the Department of Chemistry A.U.Th., which can be summarized as:*

- 1. Study of low-energy nuclear reactions of analytical interest.*
- 2. Application of ion beam analysis techniques to the characterization and study of thin near-surface layers of materials.*
- 3. Investigation of the interactions of radionuclides and heavy metals with natural and synthetic sorbents.*
- 4. Measurements of natural radioactivity.*

*The presentation will include examples and references to recent publications of the Laboratory.*

## **Radionuclides in the environment and their applications**

A. Ioannidou, S. Stoulos, M. Manolopoulou, C. Papastefanou

*Aristotle University of Thessalonik, Physics Department Nuclear Physics & Elementary Particle Physics Division,  
Radiation Physics Group, Thessaloniki 54124, Greece  
[anta@physics.auth.gr](mailto:anta@physics.auth.gr)*

### **Abstract**

*The main research activities of Radiation Physics Group of the Nuclear Physics Laboratory, Physics Department, Aristotle University of Thessaloniki (AUTH) are: Environmental radioactivity - radioecology. Natural and man-made radionuclides in the environment. Environmental radioactivity from Chernobyl and Fukushima accident. Escaping Radioactivity from Coal Power Plants. Radioactivity of building materials. Radon exposure in dwellings and caves. Radon soil gas variations due to seismic activity. Uranium in groundwater. Radioactive aerosols. In the present work main emphasis is given in the research activity on radioactive aerosols.*

*The group has more than 30 years of experience in environmental radiation studies, more than 120 publications in scientific journals and more than 500 references and has an experience in participating in more than 20 Research Programs. All group members have active collaborations with Universities and Institutes from Greece and abroad.*

*There is a full infrastructure for environmental radioactivity studies, with four Ge detectors, one alpha system, a complete radon system for measurements in soil, water, air and a number of air samplers and aerosol impactors as well as a full access in a sub-critical reactor with  $10^5 \text{ n cm}^{-2} \text{ s}^{-1}$ , which belongs to the Nuclear Physics Laboratory and it is used for educational and research activities.*

*Information of the above research activities are given in [www.physics.auth.gr](http://www.physics.auth.gr) site of the Physics Department of Faculty of Science, AUTH, Greece, and with more details at <http://users.auth.gr/~metaxia/RadiationPhysics/default.html>.*

### **1. Radioactive aerosols**

The aerosol particles in the atmosphere are liquid or solid particles. Their sizes range from a fraction of a micron to several hundreds of microns ( $\mu\text{m}$ ). They might disappear from the atmosphere and settle on some surfaces which act as a sink. The residence times of aerosol particles in the atmosphere vary from some days near the earth's surface in the troposphere to a year or more in the stratosphere.

Radioactive nuclides of  $^7\text{Be}$  are formed continuously by the interaction of cosmic-ray particles with matter (atmosphere). Beryllium-7 is a cosmogenic radionuclide ( $t_{1/2} = 53.3 \text{ d}$ ) with an important fraction of its production taking place in the upper troposphere. Soon after its formation  $^7\text{Be}$  is attached to atmospheric aerosol particles and participates in the formation and growth of the accumulation mode (from 0.07 to  $2 \mu\text{m}$ ) aerosols [1].

### **2. Radioactive aerosols as an index of air pollutant conditions**

The activity size distribution of ambient aerosols of  $^7\text{Be}$  might shift to large particle sizes in the presence of pollutants [2]. This has been detailed examined for first time in an experiment

that has been done in collaboration between the Radiation Physics Group of Nuclear Physics Lab. of Aristotle University of Thessaloniki and INFN, Università degli Studi di Milano, Physics Department, Milano Italy. More specifically the activity size distribution of radioactive nuclide  $^7\text{Be}$  has been examined at different locations in the suburban area of the city of Milano and during the four seasons of the year under different meteorological conditions. All measurements have been carried out with a parallel measurement at a reference station with two compatible cascade impactors of 1 ACFM, an instrument that has been designed as a substitute of human respiratory system.

The first results of the investigation gave that

- Similar Activity Median Aerodynamic Diameter (AMAD) values are defined in similar polluted environments
- In the most polluted environments the AMAD values are greater
- During summer the greatest AMAD values were observed in clean environments with high humidity

An anti-correlation between AMAD values and activity concentrations of  $^7\text{Be}$  aerosols was defined. It seems that during high relative humidity conditions, condensation processes become more intense, resulting in increased particle sizes of atmospheric aerosols (Fig. 1). But, greater aerosol particle sizes means higher scavenging rates of aerosols and as a result lower activity concentration of  $^7\text{Be}$  in the atmosphere (Fig. 2).

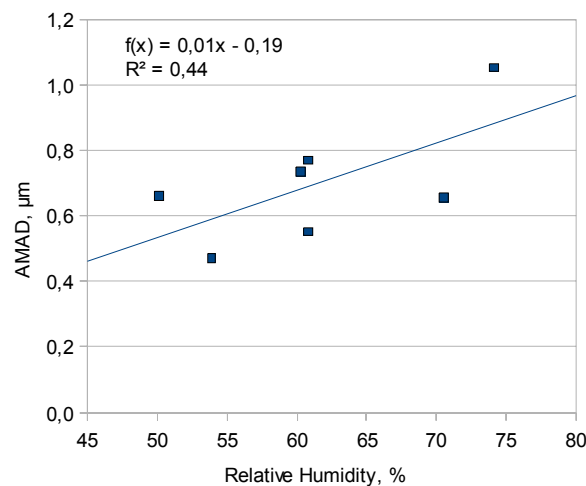


Figure 1: The AMAD values are correlated with relative humidity

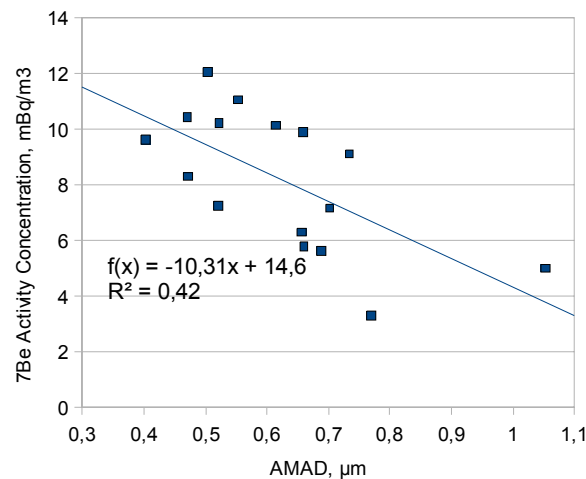


Figure 2: The AMAD values are anticorrelated with  $^7\text{Be}$  activity concentrations

### 3. Radioactive aerosols in the arctic atmosphere

The activity size distributions of the natural radionuclide tracer  $^7\text{Be}$  in different inhalable fractions ( $<0.39\ \mu\text{m}$ ,  $0.391\text{-}0.69\ \mu\text{m}$ ,  $0.69\text{-}1.3\ \mu\text{m}$ ,  $1.3\text{-}2.1\ \mu\text{m}$ ,  $2.1\text{-}4.2\ \mu\text{m}$ ,  $4.2\text{-}10.2\ \mu\text{m}$  and  $>10.2\ \mu\text{m}$ ) were determined in the boreal atmosphere in the Arctic Research Centre of the Finnish Meteorological Institute (FMI) at Sodankylä, Finland ( $67^\circ22'\ \text{N}$ ,  $26^\circ38'\ \text{E}$ ,  $180\text{m asl}$ ) [3]. The activity median aerodynamic diameter (AMAD) ranged from  $0.54\ \mu\text{m}$  to  $1.05\ \mu\text{m}$ . More than 75% of the  $^7\text{Be}$  activity was found to be associated with particles smaller than  $1.3\ \mu\text{m}$ . An anticorrelation was observed between the AMAD values and  $^7\text{Be}$  activities. The observed correlation between the AMAD values and RH% can be due to the intense condensation process during high RH% conditions resulting in increased particle sizes. But this associated with possibly higher scavenging rates of aerosols does not necessarily alone explain the anticorrelation between the AMAD and the  $^7\text{Be}$  activities. The air mass origin associated with synoptic scale weather phenomena may contribute to that too. To study this, an analysis of air mass back-trajectories was performed.

As an example, during the summer period high  $^7\text{Be}$  activity concentrations with higher than average AMAD value were observed (27 July 2010,  $6.88\ \text{mBq m}^{-3}$ ). The air masses came from south-east (Fig. 3). High  $^7\text{Be}$  concentration levels are often encountered with these air masses. These situations, as in this case too, are associated with high-pressure systems, in which the downward motion of the air masses brings  $^7\text{Be}$  from the upper troposphere to the surface. Also the moisture content of these continental air masses is low, and the lack of precipitation prevents the removal of  $^7\text{Be}$  by wet deposition. On the other hand, as the removal rate of these aerosol particles is low the particles have had time to grow with various atmospheric coagulation and condensation processes.

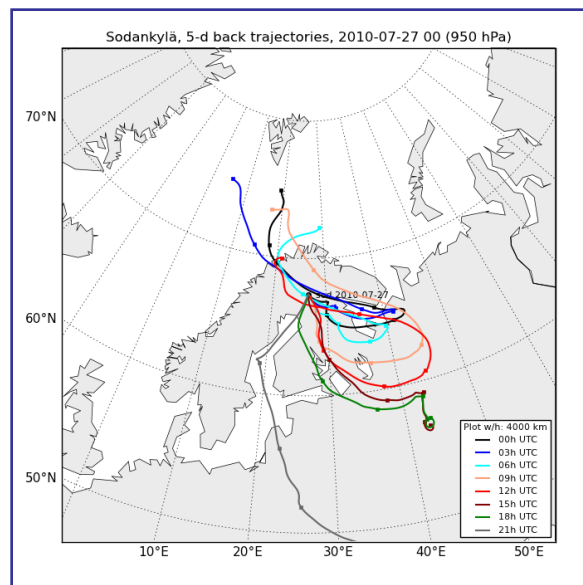


Figure 3. Five-day long air mass back trajectories, arrival to Sodankylä 27 July 2010, 950 hPa pressure level, arrival times 00, 03, 06, 09, 12, 15 18, and 21 UTC

#### References:

- 1 C. Papastefanou and A. Ioannidou, **J. Environ. Radioact.**, 26(3) (1995)
- 2 A. Ioannidou, **Atm. Environm.**, 45(6) (2011).
- 3 A. Ioannidou and J. Paatero, **Proceedings - 7th International Conference on Natural Computation, ICNC 2011**, Vol. 4 (2011).

# **Application of ion beam and radiochemical techniques in materials science and environment**

Fotini Noli

*Radiochemical laboratory, Department of Chemistry, Aristotle University of Thessaloniki*

## **Abstract**

*The research activities of the radiochemical laboratory (Department of Chemistry AUTH) involve the use of nuclear and radiochemical techniques. Techniques based on nuclear interactions, as nuclear reaction analysis-NRA and Rutherford backscattering spectroscopy-RBS, applied for the characterization of near surface layers of materials for industrial applications and investigation of their resistance to oxidation and corrosion whereas the corrosion resistance and the biocompatibility of biomaterials is also studied.*

*Examples of the measurement of natural radioactivity and determination of radionuclides in environmental samples using  $\gamma$ - and  $\alpha$ - ray spectroscopy as well as neutron activation analysis will be also presented.*

## **An introduction to selected Applied Nuclear Physics activities at Ioannina**

K. G. Ioannides<sup>1</sup>, C. Papachristodoulou<sup>2</sup> and K. Stamoulis<sup>3</sup>

<sup>1</sup>*Nuclear Physics Laboratory, The University of Ioannina, 451 10 Ioannina, Greece  
kioannid@cc.uoi.gr*

<sup>2</sup>*XRD and XRF units, Horizontal Labs Network of The University of Ioannina, 451 10 Ioannina, Greece*

<sup>3</sup>*The Archeometry Center, Horizontal Labs Network of The University of Ioannina, 451 10 Ioannina, Greece*

### **Abstract**

*A brief introduction on some of the applied nuclear physics activities at Ioannina is presented. The activities, which will be described, are in the fields of environmental radioactivity including radon research and applications, energy dispersive X ray fluorescence, radiochronology and dosimetry.*

### **Introduction**

Historically, Applied Nuclear Physics at Ioannina started right after the Chernobyl accident in 1986 in the field of Environmental Radioactivity measurements. Soon, this field was broadened by the addition of research in countermeasures following a nuclear accident and the modeling of radionuclides transfer to environmental components and Man. Today our laboratory facilities complemented by a radiochemistry laboratory allow us to perform most of environmental radioactivity analyses, including alpha radiation measurements (silicon detectors), beta measurements (gas proportional counters, liquid scintillation for tritium and carbon- 14) and gamma radiation measurements (NaI and HPGe systems).

### **Environmental Radioactivity**

Most of the work in the field of Environmental radioactivity was funded by European and National programs. It is worthy to mention the work in countermeasures that was epitomized in the “Compendium of countermeasures for the management of food production systems” and the “Generic handbook for assisting in the management of contaminated food production systems in Europe following a radiological emergency” (available online at <http://www.euranos.fzk.de/index.php?action=euranos&title=products>). Also it is of interest the radioactivity measurements in water bodies, which also can be found in <http://www.ecodonet.gr/>.

The radioactivity measurements which can be performed in Ioannina cover a broad spectrum of equipment and techniques:

*Alpha activity measurements:*

- i) Alpha activity can be measured in samples with alpha spectroscopy with silicon surface barrier detectors in vacuum. With the application of special techniques the MDL can be lowered. For example, when measuring the radium content in water, radium is first absorbed in MnO<sub>2</sub>, which subsequently is measured by  $\alpha$  spectroscopy.
- ii) Total alpha activity can be measured by a Canberra proportional gas counter.
- iii) Also total alpha activity plus radon and radium concentrations can be measured using the Tricarb Liquid Scintillation Counting System (Tricarb LSA 3170 TR/SL). Uranium and thorium is planned to be measured using an anodic stripping voltammetry system.

*Beta activity measurements*

- i) Total beta activity can be measured by the Canberra proportional gas counter.

- ii) Total beta activity plus tritium and carbon 14 can be measured using can be measured using the Tricarb Liquid Scintillation Counting System (Tricarb LSA 3170 TR/SL).

At this point our recent work on the rapid screening of  $^{90}\text{Sr}$  activity in water and milk samples using Cherenkov radiation should be measured. As it is known, preceding the measurement of radiostrontium in samples, a long process of radiochemistry is needed. The application of our method saves greatly the time of sample preparation, so the screening of a large number of samples is facilitated [1].

Also the measurements of tritium in Greece are rather scarce due to lack of suitable equipment. The measurements of tritium in our laboratories can be applied in Hydrology and Meteorology. The assessment of tritium concentration in rainwater is of importance because it can be used for hydrology investigations such as the recharge mode or the vulnerability of aquifers. We have the capability of enriching our samples in tritium. Enrichment is accomplished by electrolysis and lowers the MDL.

#### *Gamma activity measurements*

- i) Gamma activity concentrations in air can be measured using high volume air samplers using glass fiber filters, which then are measured by gamma spectroscopy (Figure 1).  
 ii) Three gamma spectroscopy systems using Ge and NaI detectors are on operation.

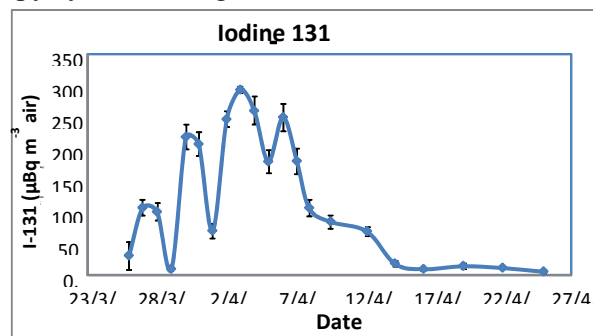


Figure 1. Iodine-131 concentrations, measured in air at Ioannina, for a month following the accident in Fukushima on 11 April 2011.

### **Radon applications**

Our Radon Group has been engaged in radon research in various fields, including indoor and outdoor radon surveys, radon studies in the Laboratory, radon and earthquake prediction, radon and geological applications.

Radon measurements are performed using both passive and continuous monitoring techniques, such as: Solid state nuclear track detectors, electret detectors and semiconductor detectors. Our recent work includes the development of computer codes (Figure 2) to automatically measure the alpha track surface density in exposed CR39 detectors and cheap monitoring systems based on PIN diodes. These were tested in a multitude of applications, including the monitoring of radon in the indoors environment, the exploration of geological faults and the study of earthquake precursor phenomena [2, 3, 4, 5].

### **Energy Dispersive X Ray Fluorescence (XRF)**

In the XRF technique, the analyzed sample is irradiated with primary X-rays and

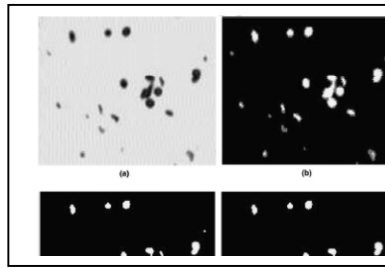


Figure 2. Analysis steps of alpha tracks surface density on SSNTDs by the TRIACII code. The code is available from the CPC library [6].

subsequently emits fluorescent X-rays, which are characteristic of the atoms present in the sample and are used for the elemental analysis. Thus, any XRF spectroscopy equipment typically consists of an X-ray source for sample excitation and a detection system for detecting the secondary fluorescent X-rays. In the XRF Unit of the University of Ioannina two home-built ED-XRF spectroscopy arrangements. The Unit maintains two home-built ED-XRF spectroscopy arrangements: 1) based on a Si(Li) semiconductor (CANBERRA, SL80175 and 2) based on a Si-PIN diode (Amptek X-123).

Amongst other applications, X-ray fluorescence spectroscopy is applied at Ioannina for the compositional characterization of ancient pottery, in studies of provenance and manufacture technology and also in environmental studies, involving heavy metals [7, 8, 9].

### Radiochronology

Our group relatively recently has acquired the Riso TL/OSL-DA-20 reader, a new HPGe system and an accompanying sample pretreatment radiochemical laboratory/ Thus, we have entered the field of radiochronology, through Thermoluminescence (TL) and Optically Stimulated Luminescence (OSL) measurements for Archeology and Geology, in cooperation with various groups in Greece and abroad. With the support of the General Secretariat for Research and Technology, a major study on Paleoseismology has started, through the dating and characterization of samples taken from seismic faults.

### Dosimetry

Studies on the dosimetric properties of material are under way. For example the properties of household materials such as tiles, bricks, roof tiles, common salt, electronic components etc. are being studied for retrospective dosimetry. Retrospective dosimetry is a new forensic analytical method applied to assess the radiological consequences of a radiological or nuclear accident.

### References

1. K.C. Stamoulis et al., **J. Env. Rad.**, **93**, 144 (2007).
2. K.G. Ioannides et al. **Appl. Rad. Isotop.** **59**, 205-213 (2003).
3. K.G. Ioannides et al. **Radioprotection**, **44** , 165 (2009).
4. C.A. Papachristodoulou et al., **Health Phys.**, **86**, 619 (2004).
5. C.A. Papachristodoulou et al., **Health Phys.**, **92**, 257 (2007).
6. D.L. Patiris et al., **Comp. Phys. Com.**, **177**, 329 (2007).
7. C. A. Papachristodoulou et al. **Anal. Chim Act.**, **573-574**, 347 (2006).
8. C. A. Papachristodoulou et al., **J. Arch. Sc.** **37**, 2146 (2010).
9. D. Karamanis et al., **Desal.**, **224**, 250 (2008).

## Dating with TL-OSL for Geology and Archaeology

K.C. Stamoulis<sup>1</sup>, K.G. Ioannides<sup>2</sup> and C. Papachristodoulou<sup>3</sup>

<sup>1</sup>*The Archaeometry Center, Horizontal Labs Network of The University of Ioannina, 45110 Ioannina, Greece*

<sup>2</sup>*Nuclear Physics Laboratory, The University of Ioannina, 45110 Ioannina, Greece*

<sup>3</sup>*XRD and XRF units, Horizontal Labs Network of The University of Ioannina, 45110 Ioannina, Greece*

### Abstract

*The Archaeometry Center belongs to the Horizontal Labs and Units Network of the University of Ioannina. It was established in 2002 and facilities of the Center are located at the Physics Department of the University of Ioannina.*

*One of its activities is in the field of Radiochronology, through Thermoluminescence (TL) and Optically Stimulated Luminescence (OSL) measurements for Archeology and Geology, in cooperation with various groups in Greece and abroad. A recently acquired Riso TL/OSL reader (2008), a new HPGe system (2010) and an accompanying sample pretreatment radiochemical laboratory are used to provide dating for a variety of samples (pottery fragments, soil, sediments etc).*

### Introduction

The Archaeometry Center supports various facilities<sup>1</sup>. One of its main facilities is the age determination of various samples, ceramics and soil from archaeological sites for dating of specific stratigraphic beds of these sites. Also soil samples are dated for geological purposes and specially for revealing paleoseismological events. The method used for these age determinations is the optically stimulated luminescence (OSL) dating. Since 2008, when a TL/OSL reader (Riso, DK) was installed, the Archaeometry Center of the University of Ioannina was involved in various archaeological and geological campaigns performing dating of samples.

Our Center is collaborating with Archaeological groups from the University of Ioannina and from the Institute of Archaeology in Tirana, Albania. Samples from Tall al-Kafrayn near the Dead Sea, in Jordan were dated as well as samples from two sites in North-East Albania at the Albanian-Greek borders, collected by an international collaboration. There is also an ongoing collaboration with archaeological groups of the University of Ioannina and samples from Ithaca, Astypalaia and Amorgos are being dated.

Radiochronological measurements are also performed in geological samples. During an extensive collaboration with a team from the Aristotle's University of Thessaloniki in cooperation with a Turkish team from Canakkale Onsekiz Mart University, samples from various places of Troy and the neighboring area were dated for sedimentation rates of the Skamadros and Simois rivers. Also samples from an archaeological site at Doxipara in the Evros area were processed for dating and for possible paleoseismological evidence. Finally, there is an ongoing collaboration aiming at the chronology of past earthquake events in various sites in Greece.

In one of these campaigns, a study of earthquake history of the wider Troy region, samples were collected from three villages-sites in the wider Troy region, Kumkale, Tvfikiye and Baliburun and soil and pottery were dated<sup>2</sup>. The purpose was to determine the ages of possible paleoseismological events detected in trenches excavated near the villages, mentioned above.

In the archaeological expedition in Jordan, at Tall al Kafrayn (near the Jordan valley), sherds and soil were collected from various archaeological sites of a hill<sup>3</sup>. The hill is in a strategic position and was inhabited as a settlement in various time periods since the Bronze Age of the

Near East. The expedition was a Hellenic research excavation project directed by T. Papadopoulos, professor emeritus of UOI.

Mikri Doxipara-Zoni, is an archaeological site in the northern part of the Evros prefecture, where cremated remains of three males and one female and five wagons with their horses were found buried<sup>4</sup>. The excavation of the site revealed a seismic fault and samples were collected in order to estimate the age of the associated paleoseismic event.

Finally, Maligrad is a small islet in the Prespa Lake at the Albanian-Greek border<sup>5,6</sup>. In this area, a joint Greek-Albanian archaeological expedition is engaged in the study of both the islet and the neighboring area along the coastline of Prespa aiming to define the life span of the area. In this case, pottery sherds from various parts of the archaeological site were dated.

### **Materials and methods**

Equipment in use in the Archaeometry Center for TL/OSL dating include a TL/OSL DA-20 reader (Riso), a Canberra  $\gamma$  detection system (model BE3825 HPGe), a Liquid Scintillation Analyzer (PerkinElmer model Tricarb, 3170 TR/SL) and a fully equipped sample preparation laboratory.

The TL/OSL Reader consists of a light detection system, a luminescence stimulation system (thermal and optical) and an irradiation source ( $^{90}\text{Sr}$ - $^{90}\text{Y}$  beta source). Two separate units are included in the system, a Reader and a Controller, while specially designed software (Sequence editor, Analysis software) is used to communicate with the individual modules of the system (PC controlled) and to perform measurement protocols and analysis.

For OSL dating, the Single Aliquot Regeneration method (SAR) is used. Multiple disks with quartz grains on one layer, are subjected to the following measurement protocol: 1. Preheating of the disks at a certain temperature (220 °C), 2. OSL signal reading at 125 °C for 40 s (natural signal), 3. Irradiation of the sample for a certain time (i.e. 60 s) with the test dose, 4. Preheating of the bleached quartz grains at 160 °C, 5. OSL signal reading at 125 °C for 40 s, 6. Commit to increasing dose (i.e. 40-60-80s), 7. Repeating 2-6 steps, 8. Constructing the growth curve. The equivalent dose is calculated by interpolation on the growth curve.

The dose rate assessment is performed by the measurement of the radioisotopes' activity ( $^{238}\text{U}$ ,  $^{235}\text{U}$ ,  $^{232}\text{Th}$  series and  $^{40}\text{K}$ ,  $^{87}\text{Rb}$ ) of surrounding soil or pottery, in Bq/kg. The radioactivity in the vicinity of the sample is transformed to dose rate in Gy/ka, using appropriate dose rate conversion factors<sup>7</sup> (Gy/ka per Bq/kg).

Age calculations are based on the equation  $\text{Age} = D_e/D_R$  in years before present (B.P.) or calendar presentation (BC or AD), where  $D_e$  is the equivalent dose in Gy and  $D_R$  is the calculated dose rate in Gy/ka. If the variation of the calculated ages is low, then an uncertainty accompanies the calculated age, otherwise the results are presented as a histogram of age vs frequency. One possible explanation for the dispersion of ages is that the sample consists of portions with different level of quartz "zeroing", thus these portions do not have the same history.

### **Results and discussion**

In the case of the study of the earthquake history of the wider Troy region, based on optically stimulated luminescence dating, two different possible seismic events were revealed, one at Baliburun at about 1200 years BP and one at Kumkale at about 3500 years BP.

Sherds and soil from Tall al Kafrayn in Jordan revealed two well separated groups. Sherds' OSL ages varied from 3400 – 4700 years BP and thus are placed in the Bronze Age of the Near East, while soil ages varied from 2700 – 3100 years BP and are placed in the Iron Age of the Near East. A possible explanation for this significant difference could be the sporadic mixing of

the soil and/or re-exposure to sunlight due to the use of the archaeological site during the history of the region.

In Mikri Doxipara-Zoni in the northern part of the Evros prefecture, OSL ages of the collected samples varied from 1450 – 41500 years BP. More recent ages coincide with the archaeological ages (1st-2nd centuries AD), while older ages reflect colluvial soils that were probably slipped over due to a paleoseismic event (about 6000 years BP).

Finally, in the case of Maligrad, OSL ages varied widely within the examined sherds. This might be due to possible mix of outer portions of the sherds (“zeroed”) with the inner ones. For this reason ages lower than 500 years BP were excluded from the calculation of the mean. Age mean values (>500 years) varied from 850-3350 years BP. In contrast, the OSL age of a headcover found in a grave is well defined at 2200 years BP.

### Conclusions

Since 2008, when the Archaeometry Center included the TL/OSL dating equipment in its facilities, numerous samples were measured and their ages were calculated using the OSL dating method. Some of the results of these studies are presented in this paper. The results show that this method is promising to archaeologists and geologists of the Greek universities and related Institutes. For more detailed presentation of the method and for results of other investigations in which our Laboratory is involved, one should follow the link of the Archaeometry Center given below<sup>1</sup>. There and also in other thereby provided links<sup>8</sup>, someone can find many more details about our involvement in environmental studies, investigations of the quality and/or the extend of heavy metal and radioactivity pollution of aquatic ecosystems (rivers, lakes, coastal zones etc.) in Epirus and other prefectures of Greece and related subjects.

### References

1. Web site of the Center <https://sites.google.com/site/archaeometrycenter/>
2. *A study of earthquake history of the wider Troy region based on optically stimulated luminescence dating*. K.C. Stamoulis and K.G.Ioannides, P. Mavrodis, A. Chatzipetros, S. Pavlides, G. S. Polymeris, S.Valkaniotis A.Kürçer, S. Zeki Tutkun, O. Ateş, S. Özden 2nd Symposium in **2<sup>nd</sup> ARCH\_RNT, Kalamata 21-23 October, 2010**.
3. *Optically Stimulated Luminescence Dating of Samples from Tall al-Kafrayn, Jordan* A. Oikonomou, K. Stamoulis, T. Papadopoulos, L. Papadopoulos, Ch. Papachristodoulou and K. Ioannides, in **39th Int. Symp. on Archaeometry 28 May - 1 June 2012**, Leuven, Belgium (poster A9)
4. *Paleoseismological study of the Doxipara archeological site (Evros-N. Greece) using optically stimulated luminescence dating*. K.Stamoulis, K.G.Ioannides, P. Mavrodis<sup>3</sup>, A. Chatzipetros, G. S. Polymeris and S. Pavlides. **2nd Symp. in ARCH\_RNT, Kalamata 21-23 October, 2010**.
5. *Optically Stimulated Luminescence Chronology and Characterisation of Pottery Sherds from Maligrad, Albania* A. Oikonomou, K. Stamoulis, P. Lera, S. Oikonomidis, A. Papayiannis, A. Tsonos, Chr. Papachristodoulou and K. Ioannides, in **39th Int. Symp. on Archaeometry 28 May - 1 June 2012**, Leuven, Belgium (poster A8)
6. *Preliminary characterization of prehistoric pottery sherds from vithkuq and maligrad, albania, by means of edxrf spectroscopy and osl chronology*. A.Oikonomou, K. Stamoulis, P. Lera, S. Oikonomidis, A. Papayiannis, A.Tsonos, C. Papachristodoulou, K. Ioannides. **3rd Symposium ARCH\_RNT, 3-6 October 2012**, Kalamata.
7. *Updating of radiation dose-rate conversion factors: a critical re-evaluation*. Liritzis I., Stamoulis K., Papachristodoulou Ch., Ioannides K. in **L.A.I.S GEOLUC, 5-7 September 2012**, Lisbon Portugal,
8. Other related websites [http://www.uoi.gr/services/lab-net/units\\_en.html](http://www.uoi.gr/services/lab-net/units_en.html), <http://omega.physics.uoi.gr/>, <http://www.ecodonet.gr/>

## The Compton Camera in the $\gamma$ -Ray Imaging

M. Mikeli<sup>1</sup>, A.-N. Rapsomanikis<sup>1</sup>, M. Zioga<sup>1</sup> and E. Stiliaris<sup>1,2</sup>

<sup>1</sup>Department of Physics, National and Kapodistrian University of Athens, Athens, GREECE  
mmikeli@phys.uoa.gr

<sup>2</sup>Institute of Accelerating Systems & Applications (IASA), Athens, GREECE

### Abstract

Based on the physical laws governing the scattering processes in the energy domain of the most commonly used radiopharmaceuticals, the Compton Effect can be utilized to detect and reconstruct gamma-ray distributions by replacing the mechanical collimation used by the typical Anger Cameras. The design and construction of a small Compton Camera prototype is investigated in this project. The system is consisted of a Double Sided Silicon Detector (DSSD), acting as scatterer, and a cylindrical, homogeneous scintillation crystal read out by a Position Sensitive PhotoMultiplier Tube (PSPMT). The sensitivity and resolution performance of the system is currently studied with GEANT4/GATE simulations by mainly varying the basic geometrical characteristics of the scatterer and the absorber.

### Introduction

Based on its ability to reconstruct a wide range of energy, the Compton Camera [1] has been used in many studies like astrophysics, industrial survey, homeland security and medical research. Its basic advantage is the absence of the mechanical collimation used in Anger Cameras [2-3], which promises low patient dose and better efficiency while tracing multiple radioisotopes. The Compton Camera consists of two detectors, called the scatterer and the absorber respectively. Its functionality relies on the Compton scattering effect. An initial photon of the source interacts with the first thin detector and then is absorbed by the second thicker one. The interaction point at each detector and the energy deposited in the absorber are detected for every single event. A conical surface (Fig.1) is formed with its vertex defined by the first interaction point and its axis determined by the two interaction locations at the scatterer and the absorber. The half-angle ( $\theta$ ) of the cone is given through the Compton kinematics equation:

$$\cos(\theta) = 1 + m_0 c^2 \left( \frac{1}{E_\gamma} - \frac{1}{E'_\gamma} \right).$$

Here,  $E_\gamma$  represents the radiopharmaceutical initial photon energy and  $E'_\gamma$  the deposited energy in the thick detector (absorber).

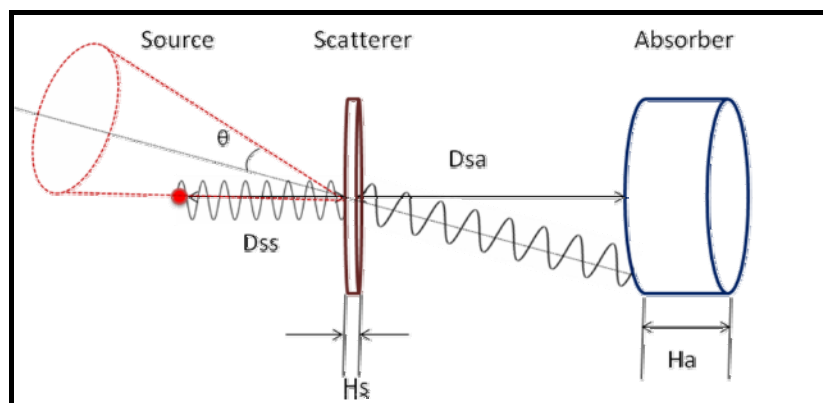
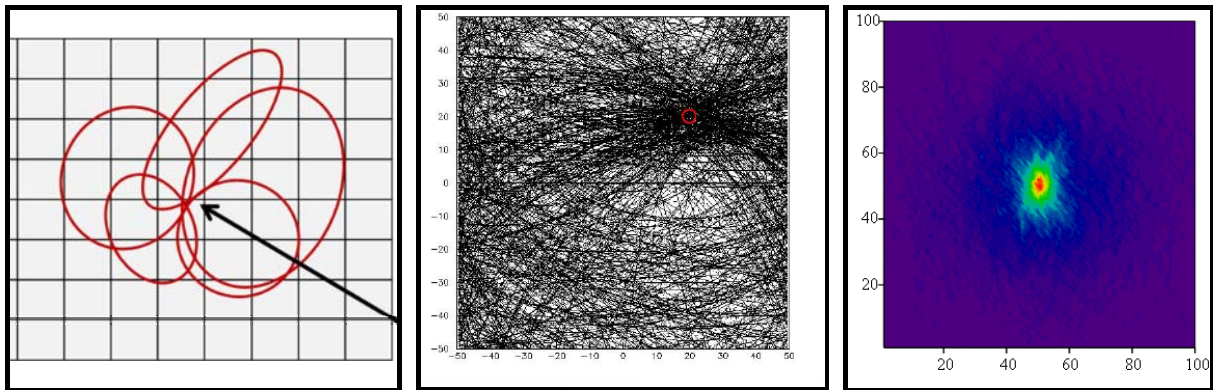


Figure 1: The principle of the Compton Camera.

## Image Reconstruction

In order to locate and reconstruct the distribution of the source, a software plane is placed vertically to the systems' axis. The locus of the conical cuts, defined for each detected event by the intersection of the cone equation and the given plane, determines the location of the source (Fig.2, left). In the praxis, the plane is appropriately segmented in pixels and the accumulated density for each pixel defines the distribution of the source. Consequently, the plane is moved along the systems' axis to form a voxelized matrix, so as to obtain a 3-D reconstructed image of the radiotracer.



**Figure 2 Left:** The conical cut with the plane introduces an ellipse for each recorded event, the locus of which determines the location of the source. **Middle:** Locus determination of a point  $^{137}\text{Cs}$  source (662 keV) on the plane. **Right:** Matrix reconstruction image of a point source in a pixelized map with simulated  $^{137}\text{Cs}$  events.

Reconstruction examples of a point  $^{137}\text{Cs}$  source with 662 keV photons are shown in Figure 2. The location of the source is defined either through the locus of the ellipses (middle) or the accumulated pixel density on the plane (right).

## GEANT4/GATE Monte Carlo Simulations

The present work includes the study of the geometrical characteristics of the system through Monte Carlo simulations using the GEANT4/GATE [4] package (Fig.3). A variety of the relative distances of the source and the detectors, the detectors' radius and depth and finally the energy of the source emitted photons are simulated, in order to achieve the optimal values for an efficient and high quality imaging device.

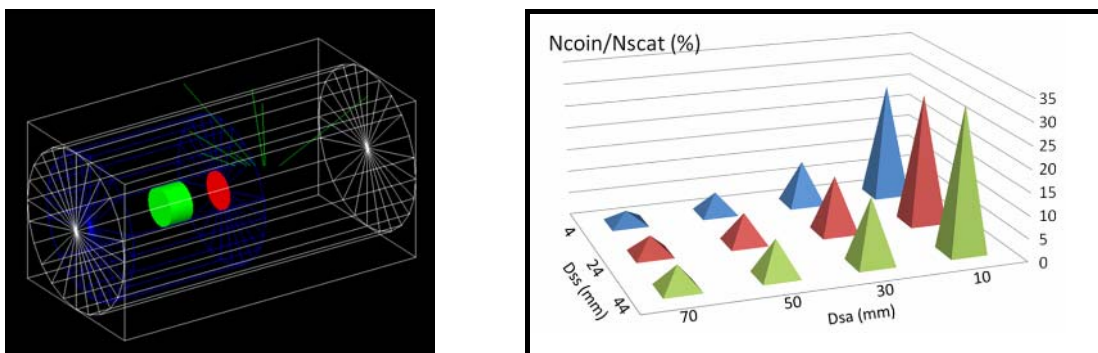


**Figure 3 Left:** The simulated system in the GEANT4/GATE environment. **Right:** The dependence of the coincidence efficiency with respect to the events detected on the scatterer for various distances.

The study of the simulated system includes characteristic physical background events, which can not be resolved in a real time experimental system. This refers to different event categories, most important of which are the following: (a) Events, where the initial photon of the

source can penetrate the scatterer and interact primarily with the absorber. (b) Missing deposited energy, where the energy of the Compton scattered photon may not be fully absorbed by the thick detector (Figure 4). A detailed study of these false events based on simulation results for a typical system's geometry leads to an efficiency reduction by almost 40%. In the praxis, both false event categories examined here are kinematically excluded in the reconstruction process.

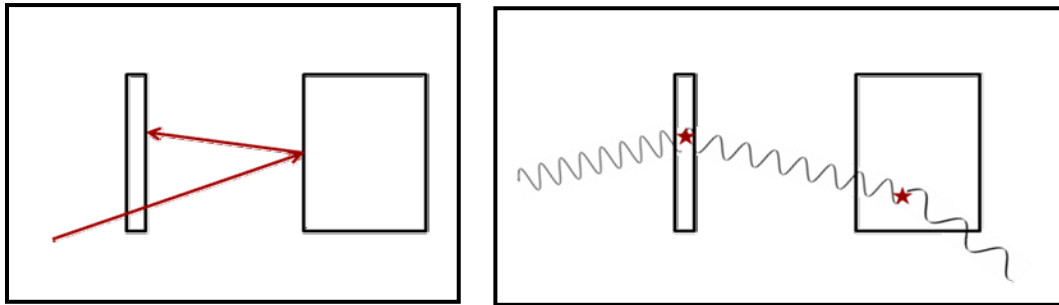


**Figure 4:** False events which contribute to the physical background. **Left:** The initial photon is interacting primarily with the absorber and then with the scatterer. **Right:** The energy of the Compton scattered photon is not fully absorbed by the thick detector.

### Future Plans

In order to improve the spatial resolution of the Compton Camera, a Double Sided Silicon Detector (DSSD) is intended to be used as scatterer in a configuration shown in Figure 5. The usage of a double-scatterer system will improve also the efficiency of the system.

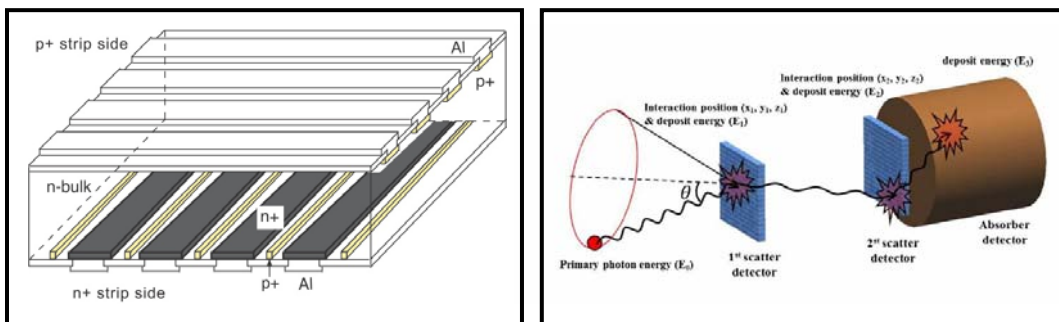


**Figure 5 Left:** The Double Sided Silicon Detector (DSSD). **Right:** A system using two separated stripped scatterers instead of one for improving the spatial resolution.

### References

1. R.W. Todd, J.M. Nightingale, D.B. Everett, Nature **251**, 132 (1974).
2. D. Thanasas *et al.* JINST **4**, P06012 (2009).
3. M. Mikeli *et al.* IEEE NSS-MIC Record **M13-369**, 3931 (2009).
4. S. Jan, G. Santin, D. Strul, S. Staelens *et al.* Phys. Med. Biol. **49**, 4543 (2004).

## Optical and Infrared Tomography in Medical Physics

A.-N. Rapsomanikis<sup>1</sup>, M. Mikeli<sup>1</sup>, M. Zioga<sup>1</sup> and E. Stiliaris<sup>1,2</sup>

<sup>(1)</sup> Department of Physics, National and Kapodistrian University of Athens, Athens, GREECE  
anrapso@phys.uoa.gr

<sup>(2)</sup> Institute of Accelerating Systems & Applications (IASA), Athens, GREECE

### Abstract

*In order to gain the necessary anatomical information of an area under examination while applying Single Photon Emission Computed Tomography (SPECT) technique, the aid of other modalities based on Optical and Infrared (IR) Tomography are imperative. The main advantage over other modalities lies on their non-ionizing nature and therefore, the absence of extra dosing loads. Our SPECT-Lab is currently developing a mobile, small-field  $\gamma$ -Camera system based on a Position Sensitive PhotoMultiplier Tube (PSPMT) which is equipped with those IR and Optical-CT modalities. The Optical CT technique is realized with infrared pulses of light, emitted by an ultra-fast LASER and a Streak Camera, acting as a fast light detector system with an extra high time resolution. The present work focuses on the experimental study using appropriately constructed <sup>99</sup>Tc, thermal and optical emission phantoms, 3D-reconstructed with various iterative algorithms.*

### Introduction

SPECT is unambiguously a powerful, low cost diagnostic technique in modern medical practice. Nonetheless, one of its major drawbacks arises from the nature of the detected ionizing radiation, which makes difficult to obtain the anatomical information of the area under investigation without the assistance of another modality (X-Ray CT, MRI). The extra load of ionizing radiation (CT), the high cost (MRI) and also the mobility of such devices make those methods superfluous. The SPECT-Lab has already developed and evaluated on a tomographic level, a small-field PSPMT  $\gamma$ -Camera system [1]. Therefore, in order to gain the necessary anatomic information two different, non invasive, non-ionizing, low cost and portable modalities are proposed in the current project. These are the Optical and Thermal Computed Tomography, both in emission processes.

### Experimental Procedure

The first step towards this attempt is the validation of the image reconstruction algorithms (Accelerated ART and MLEM) for optical and thermal radiation photons, developed and widely used in the various SPECT-Lab projects [2]. Since all the modalities were tested on the emission case, the process followed was the same for each of these modalities (SPECT, Thermal and Optical emission). A total of 24 projections with a step of  $15^\circ$  in the full angle range  $0^\circ$ – $360^\circ$  were recorded. Every projection was sliced 20-30 times along the Z- axis (vertically to the tomographic level) after taking into account energy cuts and offsets in order to reduce the background noise. This noise consists mainly of undesired Compton events and thermal or optical background. Then, by using Accelerated ART and MLEM algorithms for each slice, the tomographic images were reconstructed. Finally, all the tomograms were contour overlaid creating a 3D image using the MATLAB software environment.

### SPECT Modality

The SPECT modality has already been tested both on planar and tomographic level [1] by constructing an axially asymmetrical phantom consisting of three different cylindro-conoidal tubes and two capillaries, filled with <sup>99m</sup>Tc solution of special concentration 0.25mCi/ml. In

addition, absorption was introduced by immersing the phantom in agarose gel. The obtained spatial resolution was on planar  $\langle\sigma_x\rangle = (0.95 \pm 0.05)$  mm,  $\langle\sigma_y\rangle = (1.07 \pm 0.07)$  mm. Similarly, on the tomographic level the spatial resolution was determined to be in the order of 2 mm in X- and Y-Axis, with the smallest detectable object the capillaries volume ( $0.073\text{cm}^3$ ) for the given special activity, as shown in Figure 1.

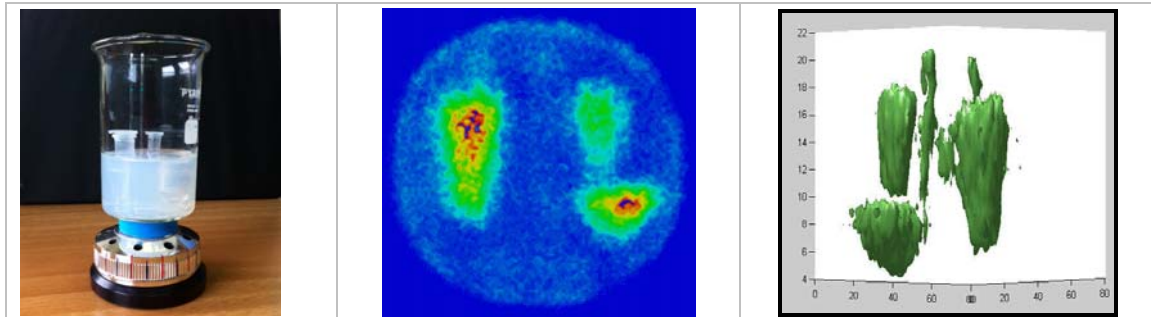


**Figure 1:** Left: A picture of the examined phantom – Middle: The planar images obtained by the  $\gamma$ -Camera - Right: The final 3D-reconstructed image.

### Thermal and Optical Modality

The capability of the developed algorithms to reconstruct also in both thermal and optical emission was then tested by using appropriate phantoms. The thermal phantom consists of alternately connected three pairs of  $100\Omega$ - $50\Omega$  resistors in line and shaped to form the letter M with the middle pair set off axis. In order to obtain the thermal planar images (Figure 2), a high resolution thermal camera was utilized (Model Thermovision ® 550, AGEMA Infrared Systems) with a built-in lens. The recorded information was in the form of high resolution

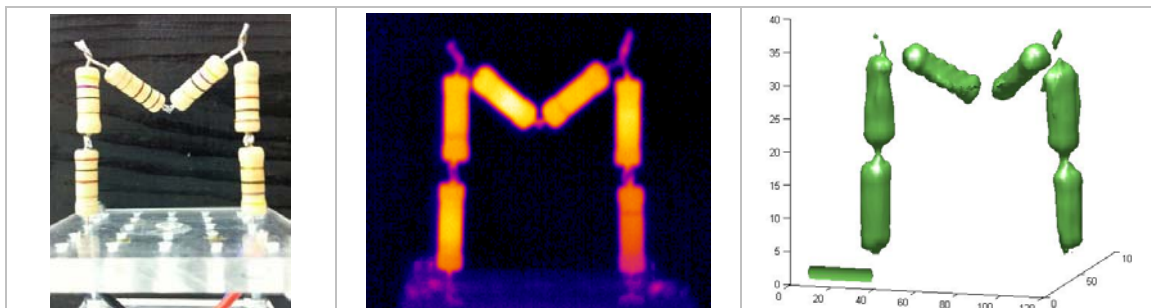


**Figure 2:** Left: A picture of the thermal resistor phantom – Middle: A planar image obtained by the IR-Camera – Right: The 3D reconstructed image of the thermal phantom.



**Figure 3:** Left: A picture of the optical phantom with fluorescent liquid (Cyalume) – Middle: A planar image obtained by the CCD-Camera – Right: The 3D reconstructed image of the optical phantom.

color images (250x188 pixels). Results of the planar and 3D reconstruction are shown in Figure 2. For the optical case, a complicated phantom with small tubes and capillaries filled with fluorescent liquid is used. Projection images (Figure 3) are taken with a simple commercial CCD camera (American Dynamics ADC733 Camera).

### Towards an Innovative Triple Modality

The proposed triple modality (SPECT with IR and Optical information, Figure 4) can provide the functional information needed to potentially detect tissue abnormalities and identify them with less or even with no use of radiotracers (thermal screenings for breast cancer). Ultimate goal of the project is its upgrade with a high precision Time-Resolved Optical Computed Tomographic system (Figure 5), utilizing an ultra-fast Infrared LASER and a Streak Camera equipped with ultra-fast photomultipliers.



Figure 4: Triple modality (SPECT, Thermal and Optical systems).

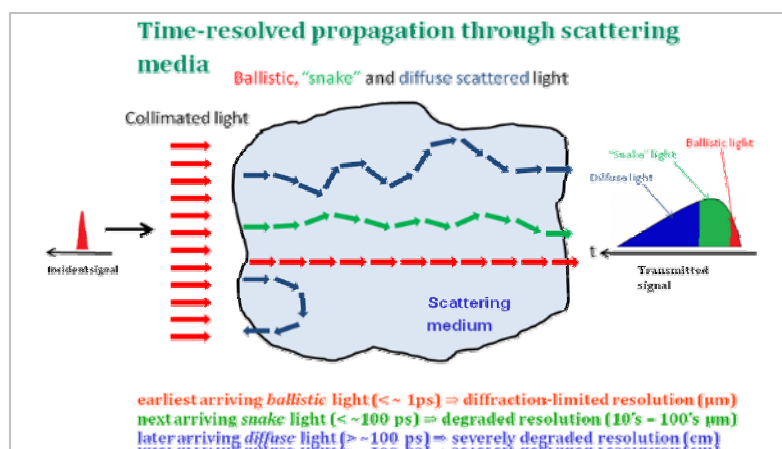


Figure 5: Principle of the Time-Resolved Optical Computed Tomography

### References

1. D. Thanasas et al. JINST **4** P0612 (2009).
2. S. Angeli and E. Stiliaris, IEEE NSS-MIC Record **M09-323** 3382 (2009).
3. AGEMA Infrared Systems: *Thermovision 550, Operating Manual*, Publ. Num. **557** (2007).
4. A.N. Rapsomanikis et al. IEEE NSS-MIC Record **M18-73** (2012).

# Construction of a High-Resolution Mobile $\gamma$ -Camera System for Mammography Study

M. Zioga<sup>1</sup>, M. Kontos<sup>2</sup>, D. Maintas<sup>3</sup>, M. Mikeli<sup>1</sup>, A.-N. Rapsomanikis<sup>1</sup> and E. Stiliaris<sup>1,4</sup>

<sup>(1)</sup> Department of Physics, National and Kapodistrian University of Athens, Athens, GREECE

[mzioga@phys.uoa.gr](mailto:mzioga@phys.uoa.gr)

<sup>(2)</sup> LAIKON Hospital, Medical School of Athens, UoA, Athens, GREECE

<sup>(3)</sup> Institute of Isotopic Studies (IIS), IATRIKON Hospital, Athens, GREECE

<sup>(4)</sup> Institute of Accelerating Systems & Applications (IASA), Athens, GREECE

## Abstract

*A small field, high resolution  $\gamma$ -Camera system based on a Position Sensitive Photomultiplier Tube (PSPMT) has been recently developed in our Laboratory. This prototype is to be engaged to clinical applications for planar imaging of <sup>99</sup>Tc-radiotracers during breast cancer operations. Among the basic requirements during data-taking operation is the absence of any distorting motion, which can drastically affect the image quality. In the present work, all necessary transformations to a clinical prototype are described. This includes the operation of the  $\gamma$ -Camera system with low voltages by utilizing a proper DC-to-DC converter in order to provide proper high voltage to the isolated head system. Camera orientation is critical during operations, thus a 3D-accelerometer will be encased in the head probe providing the necessary information for an automatic alignment of the projected image. The  $\gamma$ -Camera will be connected via a USB portal to a computer with a DAQ system, operating in a fast digitization mode.*

## Introduction

In Nuclear Medicine a general purpose  $\gamma$ -Camera device is commonly used. Since its introduction, it has become a standard choice for clinical *in vivo* tests. It provides information about the distribution of a radiotracer administered to a patient allowing noninvasive measurement of physiological functions. A general purpose  $\gamma$ -Camera shows disadvantages when used for imaging of small organs, such as breast, thyroid or sentinel lymph node, due to the large field of view and volume occupied, which affects the spatial resolution of the obtained images. For such small organ studies, the large detector of a standard commercial  $\gamma$ -Camera cannot be placed close to the organ of interest, accepting background activity from other neighbor organs and allowing only certain planar projections to be imaged. These factors imply that the general purpose  $\gamma$ -Cameras have non optimal spatial resolution and poor image contrast regarding the small organ imaging. For all the previous reasons, a dedicated, small field, high resolution portable  $\gamma$ -Camera for clinical must be manufactured.

## Portable $\gamma$ -Camera

In the past years, a prototype small field  $\gamma$ -Camera system based on the R2486 (HAMAMATSU) Position Sensitive PhotoMultiplier Tube has been developed in our laboratory [1-3]. This small field (50mm effective field of view)  $\gamma$ -Camera system utilizes the resistive chain technique in order to reduce the 16-X and 16-Y multianode wire-system to only four signals. The whole system comprises a parallel-hole Pb-collimator of hexagonal type, with a total area of 60×60 mm<sup>2</sup> and a 4 mm thick CsI(Tl) pixelated scintillation crystal. Due to the applied signal reduction technique, the Data Acquisition (DAQ) system consists of a 4-channel fast PCI-1714 Analog-to-Digital Converter (ADC) [4]. Several experimental studies with <sup>99m</sup>Tc phantoms have characterized the system as following:

- Resolution on a planar level:  $\langle\sigma_x\rangle = (0.95\pm 0.05)$  mm,  $\langle\sigma_y\rangle = (1.07\pm 0.07)$  mm
- Resolution on a tomographic level: 2 mm in both X- and Y-Axis
- Sensitivity on a tomographic level: Minimum volume which can be detected  $V=0.080\text{cm}^3$  (which corresponds to 20  $\mu\text{Ci}$  activity for a tracer solution of special activity  $0.25\text{mCi}/\text{cm}^3$ ).

In order to use this small field  $\gamma$ -Camera in a clinical environment, several adjustments must take place.

- A proper shielding is necessary to ensure the light isolation of the detector's head-system. A gun-like casing will be ideal for a comfortable operation during the surgical procedures.
- A proper DC-to-DC converter must be used to provide high voltage to the isolated head system, allowing a safe connection with the rest of the low voltage system's wiring.
- Orientation is crucial to the operator, thus a 3D-accelerometer will be encased in the head probe providing the necessary information for an automatic mapping orientation of the projected image. The  $\gamma$ -Camera will be connected via a USB portal to a computer with a DAQ system, operating in the previously described digitization mode (4-channel ADC).

Obtained data (event-by-event recording) will be automatically converted to intensity distribution images. With a proper calibration system, they will reflect the radioactive tracer distribution in real time allowing the data translation to tomographic images with off-line usage of home developed reconstruction algorithms. Energy and movement corrections will also be applied to the raw-data for image quality optimization.

### Motion Correction

The *Wii Remote* is the primary controller for Nintendo's Wii console [5]. The *Wii Remote* has the ability to sense acceleration along three axes through the use of the ADXL330 accelerometer. ADXL330 reports acceleration in the device's three dimensions ( $g_x, g_y, g_z$ ), expressed in units of the earth's gravity  $g$  with a resolution of 8 bits per axis and a 100 Hz update rate. The *Wii Remote* also features a *PixArt* optical (infrared) sensor, allowing it to determine where the *Wii Remote* is pointing. Data communication occurs over the Bluetooth protocol.

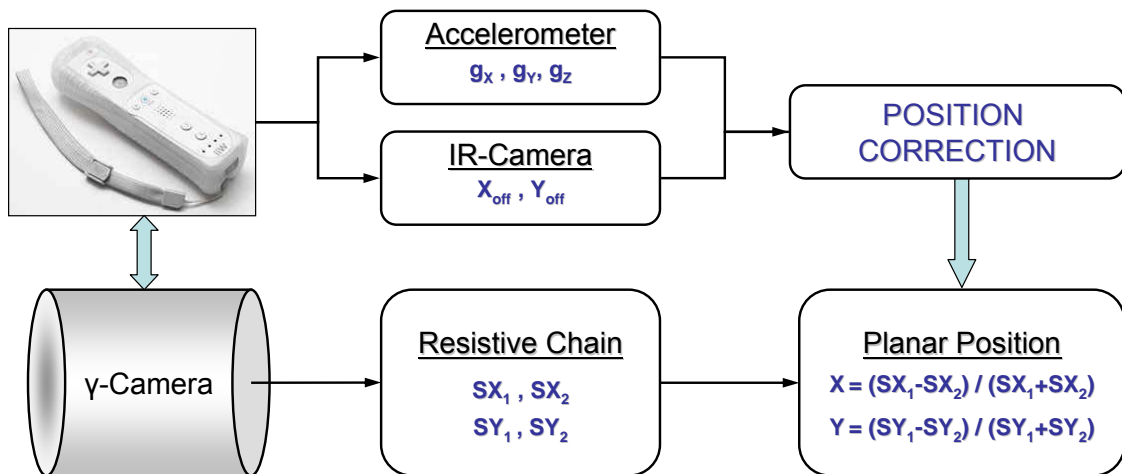


Figure 1: Flow diagram of the DAQ-recorded parameters during the operation of the portable  $\gamma$ -Camera system.

The Data Acquisition System of this portable camera has been developed on the LabVIEW environment. In addition to the four primary signals from the photomultiplier resistive chain ( $SX_1, SX_2, SY_1, SY_2$ ) the three g-components ( $g_x, g_y, g_z$ ) and the planar offset  $X_{off}$  and  $Y_{off}$  from the Wii Remote device are recorded (Fig.1).

Based on the definition of the *Euler* angles:

$$\begin{pmatrix} g_x \\ g_y \\ g_z \end{pmatrix} = \begin{pmatrix} \cos\psi \cos\varphi - \cos\theta \sin\varphi \sin\psi & \cos\psi \sin\varphi + \cos\theta \cos\varphi \sin\psi & \sin\theta \sin\psi \\ -\sin\psi \cos\varphi - \cos\theta \sin\varphi \cos\psi & -\sin\psi \sin\varphi + \cos\theta \cos\varphi \cos\psi & \sin\theta \cos\psi \\ \sin\theta \sin\psi & -\sin\theta \cos\varphi & \cos\theta \end{pmatrix} \cdot \begin{pmatrix} 0 \\ 0 \\ 1 \end{pmatrix}$$

the rotation angles  $\theta$  and  $\psi$  are calculated for any detected event. These angles, together with the planar offsets ( $X_{off}, Y_{off}$ ) recorded by the infrared-camera can be used to correct the position of the incident  $\gamma$ -photon on the planar image.

A typical example of a planar image taken with the  $\gamma$ -Camera system moving around an eccentric point inside the field-of-view is shown in Figure 2. In this example, a distant point  $^{137}\text{Cs}$ -source is used with a hole-screen in front of the system. The motion corrected image and its contour plot are shown in the same figure, where the rotation-free planar information is clearly reproduced.

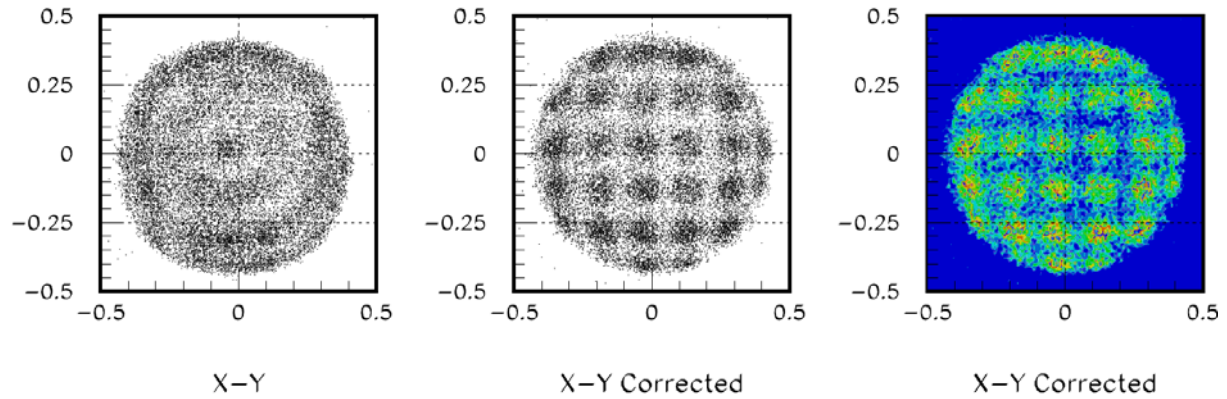


**Figure 2:** A typical planar image taken with a uniform source and a hole-screen in front of the moving  $\gamma$ -Camera system. Left: Uncorrected planar image. Center: Motion corrected image with the developed procedure. Right: Contour plot of the motion corrected image.

## References

1. M. Mikeli, D. Thanasas and E. Stiliaris, IEEE NSS-MIC Record **M13-360**, 3931 (2009).
2. D. Thanasas *et al.*, JINST **4**, P06012 (2009).
3. S. Angeli and E. Stiliaris, IEEE NSS-MIC Record **M09-323**, 3382 (2009).
4. V. Spanoudaki *et al.*, NIM A **527**, 151 (2004).
5. Chadwick A. Wingrave *et al.*, IEEE Comp. Graph. & Appl. **3/4**, 71 (2010).

## **Round Table Discussion – The Present and Future of Nuclear Physics in Greece**

Coordinators: D. Bonatsos, P. Misaelides, A. Pakou

The 1<sup>st</sup> one-day Workshop of the Hellenic Institute of Nuclear Physics (HINP) on New Aspects and Perspectives in Nuclear Physics took place in the Department of Physics of the University of Ioannina on 8 September 2012. Research activities of the member institutions, as well as of individual members, were presented in 23 oral presentations, followed by a Round Table Discussion, during which practically all present members expressed their ideas and proposals. A summary of the main points raised and suggestions made is given below.

### **1. Research directions**

There is a need to focus attention on specific directions in order to reduce multifragmentation of the efforts of the Greek nuclear physics community.

Concerning basic research, it was realized that the existing activities on nuclear structure, nuclear reactions and nuclear astrophysics should be oriented towards the emerging new era of radioactive ion beams, with detector development remaining an area in which nuclear physicists can continue making important contributions.

Regarding applications of nuclear techniques, in addition to the well-established activities related to the environment, the characterization of materials and to archaeology, increased international attention is expected within the next decade in medical applications, partially as a side-effect of the need of reorientation of a large fraction of the experimental elementary particle physics community.

Both actions on fundamental research with radioactive ion beams and applications in medical physics can find a common ground on high tech skills in hardware and computing.

It was pointed out that the description of the research area(s) of the HINP members at the HINP site is too short and should be expanded, for overlaps to be revealed.

### **2. Education – Dissemination**

The need to educate a new generation of Greek nuclear physicists was emphasized, in particular because of the expected increased demand for skilled nuclear physicists at an international level in years to come. As an example, a course on simulations could be organized through teleconferences.

Long stays (of the order of three to four months) of graduate students of Greek institutions in laboratories abroad is of utmost importance. Funds for this activity can be found through ERASMUS training programs for example. Supervisors are requested to make the appropriate arrangements with universities located close to research centers in which the students can obtain high tech education. ERASMUS programs can also be exploited for inviting teaching personnel to this effort.

The need of the nuclear physics community to approach and inform high school students was raised. One idea is the organization of a school on recent developments in nuclear physics for high school teachers, possibly in parallel with a nuclear physics conference or school, with speakers shared by the two events, as in Blagoevgrad in July 2012.

At the undergraduate or graduate level some orientation schools of about 8 weeks duration (every August-September) may be considered as good opportunities for those students who are interested to attend pure nuclear physics, courses in extreme matter and/or nuclear astrophysics (including theory and experiment) at GSI/FAIR, Darmstadt. A number of students (every year) may be funded by GSI fellowships on applying in advance the period

January/February. Note that Greece is one of the 13 member countries founded FAIR 2 years ago.

### **3. International collaborations**

Greek participation in CERN supports the involvement of Greek research groups in the n-TOF experiments, while for ISOLDE the interested groups have to secure funding from other sources, an activity which should be pursued.

Despite the fact that there is long term Greek participation in experiments at GANIL, as well as interest for carrying out Greek experiments there, no relevant MoU has been signed. In contrast, a MoU had been signed in the past with FAIR/GSI, despite the lack of expressed interest by specific Greek research teams, with no financial contribution made since then anyway.

Excellent possibilities for collaboration exist in the HH-IFIN in Bucharest, where the 9 MV Tandem has recently acquired a pelletron charging system, the RoBall gamma spectroscopy array and a plunger, while two new accelerators, a 3 MV Tandem for ion beam analysis and ion implantation and a 1 MV Tandem for accelerated mass spectrometry have been installed. In parallel, the construction of the Extreme Light Infrastructure for Nuclear Physics (ELI-NP) starts, to be completed by the end of 2016.

While we see our future mainly in Europe, we keep an eye on all other possible actions. In this spirit, the American Physical Society has expressed an interest in establishing research collaboration in the subject of nuclear physics with the Balkan region. Details should become available during the 2<sup>nd</sup> European Nuclear Physics Conference, to be held in Bucharest on 17-21 September 2012.

There is great interest for the development of experimental activities in nuclear physics and for building groups in applications of nuclear techniques taking advantage of the existing DC-60 heavy ion cyclotron in the Republic of Kazakhstan, with able funding available.

### **4. Funding**

The need was emphasized for better coordination among the members, in order to respond to funding calls by a smaller number of proposals, each containing the maximum number of members possible.

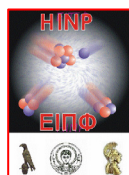
It was realized that the poor record of nuclear physics proposals in the recent "Thales" and "Excellence" calls was due to the heavy domination of the relevant committees and of the bodies appointing these committees by elementary particle physicists. It has been strongly recommended that senior members of the nuclear physics community should not avoid participation in evaluation committees, since this is equivalent to suicidal behavior.

### **5. Admission of new members**

Greek institutions hosting research activities in nuclear physics, as well as individual members of the Greek nuclear physics community interested in joining the HINP are welcome to apply, according to the by-laws of the Institute.

The HINP has in no way any role contradictory to the goals of the Hellenic Nuclear Physics Society (HNPS). The HINP has a legal status different from that of the HNPS, allowing the joint participation of several members from different institutions in research projects as a single entity. An excellent example is given by the Joint Institute for Nuclear Astrophysics (JINA), a virtual institute formed in USA by 3 member institutions and 18 associate institutions.

© 2012 by the HELLENIC INSTITUTE OF NUCLEAR PHYSICS



## PROCEEDINGS

of the 1<sup>st</sup> ONE-DAY WORKSHOP  
on New Aspects and Perspectives in Nuclear Physics

Available online at [http://www.uoi.gr/HINP/Workshop\\_2012/Workshop2012\\_proceedings.pdf](http://www.uoi.gr/HINP/Workshop_2012/Workshop2012_proceedings.pdf)